AD_____

Award Number: W81XWH-10-1-0392

TITLE: Military Vision Research Program

PRINCIPAL INVESTIGATOR: Dr. Darlene Dartt

CONTRACTING ORGANIZATION: The Schepens Eye Research Institute, Inc.
                                          Boston, MA 02114

REPORT DATE: July 2011

TYPE OF REPORT: Final

PREPARED FOR: U.S. Army Medical Research and Materiel Command
                    Fort Detrick, Maryland 21702-5012

DISTRIBUTION STATEMENT: Approved for public release; distribution unlimited

REPORT DOCUMENTATION PAGE

1. REPORT DATE (DD-MM-YYYY) 01-07-2011	2. REPORT TYPE Final	3. DATES COVERED (From - To) 25 JUN 2010 - 24 JUN 2011

4. TITLE AND SUBTITLE

Military Vision Research Program

5a. CONTRACT NUMBER

5b. GRANT NUMBER
W81XWH-10-1-0392

5c. PROGRAM ELEMENT NUMBER

6. AUTHOR(S)
Dr. Darlene Dartt

E-Mail: darlene.dartt@schepens.harvard.edu

5d. PROJECT NUMBER

5e. TASK NUMBER

5f. WORK UNIT NUMBER

7. PERFORMING ORGANIZATION NAME(S) AND ADDRESS(ES)

The Schepens Eye Research Institute, Inc.
Boston, MA 02114

8. PERFORMING ORGANIZATION REPORT NUMBER

9. SPONSORING / MONITORING AGENCY NAME(S) AND ADDRESS(ES)
U.S. Army Medical Research and Materiel Command
Fort Detrick, Maryland 21702-5012

10. SPONSOR/MONITOR'S ACRONYM(S)

11. SPONSOR/MONITOR'S REPORT NUMBER(S)

12. DISTRIBUTION / AVAILABILITY STATEMENT
Approved for Public Release; Distribution Unlimited

13. SUPPLEMENTARY NOTES

14. ABSTRACT
EYE INJURIES HAVE INCREASED IN WARFARE OVER THE PAST 200 YEARS. IN THE CURRENT CONFLICT THE EYE IS PARTICULARLY VULNERABLE TO BLAST INJURY AS WELL AS TO ENVIRONMENTAL STRESS FROM THE CURRENT THEATERS OF OPERATION. FOR CLEAR VISION, THE ENTIRE VISUAL AXIS (TEARS, CORNEA, AQUEOUS HUMOR, LENS, VITREOUS, RETINA, AND OPTIC NERVE) MUST BE TRANSPARENT, INTACT, AND HEALTHY AND EACH PART OF THIS AXIS FUNCTIONAL. EACH OF THESE STRUCTURES HAS ITS PARTICULAR VULNERABILITIES. IN THE PRESENT PROPOSAL WE HAVE DESIGNED MULTIPLE PROJECTS TO INVESTIGATE THE SPECIAL VULNERABILITIES OF THE CORNEA, RETINA, OPTIC NERVE, AND BRAIN TO MECHANICAL, LASER, INFECTIOUS, AND ENVIRONMENTAL TRAUMA AND TO DEVISE MEANS TO PREVENT, DIAGNOSE, AND REPAIR THE SEQUELAE OF THESE TRAUMAS.

15. SUBJECT TERMS
injury, laser injury, infection, angiogenesis, stem cells, dry eye, cornea, inflammation, traumatic brain injury, pain receptors, immune response

16. SECURITY CLASSIFICATION OF:			17. LIMITATION OF ABSTRACT	18. NUMBER OF PAGES	19a. NAME OF RESPONSIBLE PERSON USAMRMC
a. REPORT U	b. ABSTRACT U	c. THIS PAGE U	UU	111	19b. TELEPHONE NUMBER (include area code)

Standard Form 298 (Rev. 8-98)
Prescribed by ANSI Std. Z39.18

Table of Contents

Task 1
Meredith Gregory-Ksander, Ph.D.
Title: Using scavenger receptors to improve corneal wound healing and increase resistance to corneal infections.

INTRODUCTION:
Bacterial keratitis is an acute infection that is both rapid and aggressive, often resulting in significant corneal damage and loss of vision. Fortunately, the healthy cornea is highly resistant to infection due to the presence of multiple barriers, including the: (i) tear film, (ii) mucin layer, and (iii) epithelial tight junctions. However, when these barriers are breached due to either: ocular injury, surgery, or prolonged (or improper) contact lens use, the risk of infection increases significantly.
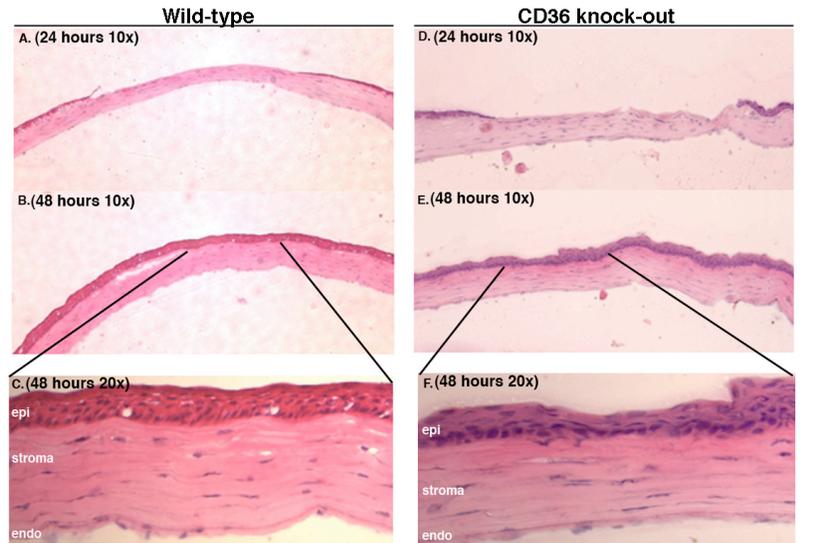
We recently identified CD36, a scavenger receptor expressed in the cornea, as a critical component of the corneal epithelial barrier to infection. In the absence of CD36, we observed that mice developed spontaneous bacterial keratitis that was preceded by the development of mild corneal defects. Histological analysis of the corneal defects revealed: a disorganized corneal epithelium, a loss of epithelial tight junctions, disruption of the protective mucin layer, and increased bacterial binding [1]. From these data we hypothesize that **CD36 is essential for maintenance of the corneal epithelial barrier to infection through regulation of (i) epithelial migration and adhesion, (ii) epithelial tight junctions, and (iii) epithelial mucin formation.** We propose that upregulation of CD36 in the wounded cornea will (i) accelerate wound healing and barrier restoration and, (ii) increase resistance to infection.

BODY:
The technical objectives of this task were twofold. The first objective was to demonstrate, using CD36KO mice, that CD36 is an essential component of the epithelial barrier to infection in the cornea. The second objective was to show that the upregulation of CD36 in a wounded cornea, through the topical application of an oxidized phospholipid, would accelerate wound healing and increase resistance to infection. These technical objectives were achieved through the following specific aims:

*Aim 1) Demonstrate that CD36 is required for proper wound healing of the corneal epithelium.*To determine whether CD36 was required for proper wound healing, we utilized a murine corneal epithelial wound model. Briefly, a 1.5 mm epithelial wound was created in the central cornea without disrupting the epithelial basement membrane using a trephine and blunt scalpel in either CD36 knockout mice or wild-type C57BL/6 mice. Wound healing was assessed via: (i) slit lamp examination, (ii) fluorescein

Figure 1. Corneal wound healing in Wild-type and CD36 knock-out mice

Wild-type | CD36 knock-out

A. (24 hours 10x) | D. (24 hours 10x)
B. (48 hours 10x) | E. (48 hours 10x)
C. (48 hours 20x) | F. (48 hours 20x)
epi, stroma, endo | epi, stroma, endo

staining, and (iii) histological analysis at multiple time points (4, 24, 48, 72, 96 hrs and day 34).

Wild-type mice displayed normal wound healing in which the cornea was re-epithelialized within 48 hrs and remained clear (**Figure 1 A-C**). By contrast, CD36 knock-out mice displayed increased inflammatory infiltrate at 24 hours (**Figure 1D**) and a disorganized re-epithelialization at 48 hours **(Figure 1 E and F).** At 48-72hrs post corneal wounding, slit-lamp examination reveals a clear cornea in wild-type mice. By contrast, persistent corneal haze and increased neovascularization is observed in the corneas of CD36 KO mice. At 34 days post corneal wounding, histological analysis reveals the presence of inflammatory infiltrate, indicating persistent inflammation. Furthermore, the corneal epithelium is very disorganized and coincides with what appears to be a disruption of the basement membrane. **(Figure 2).**

Figure 2
A. (34 days 10x)
B. (34 days 20x)
epi, stroma, endo
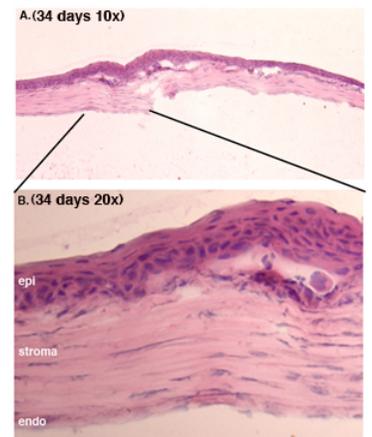
Taken together, while both wild-type and CD36 KO mice appear to re-epithelialize within 48 hours, histology reveals persistent inflammation and a disorganized epithelium in CD36 KO mice. These data indicate that CD36 is required for proper wound healing.

Development of Immortalized corneal epithelial cell lines: In the second quarter we focused on creating immortalized corneal epithelial cell lines from wild-type (WT) and CD36KO mice to further study the function of CD36 in epithelial cell adhesion and migration. Immortalized corneal epithelial cell lines were produced from WT and CD36KO mice using the E6/E7 oncogenes from human papilloma virus (HPV) type 16 (Provided by Dr. Neiderkorn, UT Southwestern). Briefly, fresh corneas were excised from euthanized mice and placed in a 6 well plate epithelial side down. After cells growing out from the explants reached approximately 60% confluence the explants were removed and

Figure 3

Isotype	AE1/AE3
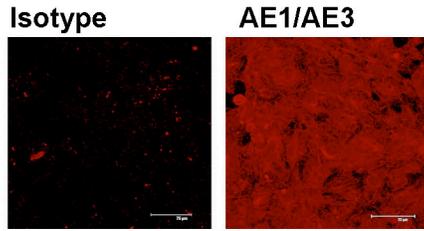
infecting media containing a retroviral construct with the E6/E7 oncogenes was added. After overnight incubation, infecting media was removed and cells were cultured in normal cell culture media for 24 hours. Subsequently, transformed cells were selected by culturing in selection media containing 800μg/mL G418 for several passages. Immortalized corneal epithelial cells were characterized by immunohistochemistry with antibodies to keratin (AE1/AE3), which are specific for epithelial cells (**Figure 3**).

Cells began to grow out from both WT and CD36KO corneal explants after 3-5 days in culture. However, the CD36KO cells (i) migrated more slowly, (ii) were much larger in size, (iii) formed an irregular ruffled leading edge, and (iv) detached and died more readily (**Fig. 4A and 4B**) Normal epithelial cells were observed in the WT culture (**Fig. 4E and 4D**). After immortalization both cell lines continued to proliferate for 3 weeks (**Fig. 4B and 4D**). Upon confluence, the cells were passaged and transferred to a larger flask (**Fig. 4C and 4F**). While the WT cells reattached to the new flask and continued to proliferate (**Fig. 4F**), the CD36KO cells never reattached and

Figure 4
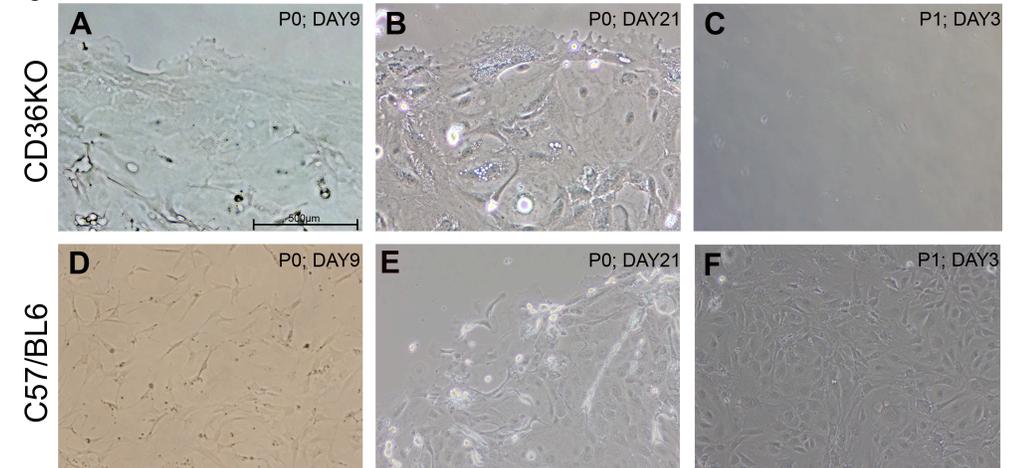
died. After three days only floating dead cells were seen in CD36KO cultures (**Fig. 4C**). These data support the hypothesis that CD36 is critical for corneal epithelial migration and adhesion. Moreover, a defect in epithelial migration and adhesion will lead to poor wound healing as observed in CD36KO mice (**Figure 1 and 2**).

Aim 2) Demonstrate an increased susceptibility to S. aureus keratitis in CD36 deficient mice.

Briefly, C57BL/6 WT and CD36KO mice were anesthetized and the cornea was wounded using a 1.5mm trephine and a blunt scalpel was used to remove the central epithelium without disrupting the basement membrane. A 10ul aliquot containing 1×10^8 CFU suspension of RN6390 *S. aureus* was applied to the wounded cornea and the development of keratitis was evaluated macroscopically and microscopically for up to 72 hours. Four groups of mice were examined in this study: **Group 1** - C57BL/6 WT (no wound + *S. aureus*); **Group 2** - C57BL/6 WT (wound + *S. aureus*); **Group 3** - CD36KO (no wound + *S. aureus*);

Group 4 - CD36KO (wound + *S. aureus*). At 72hours post infection eyes were enucleated and processed for H&E staining.

C57BL/6 WT mice are normally highly resistant to *S. aureus* induced keratitis. In both C57BL/6 WT and CD36KO mice, no keratitis was observed in unwounded corneas inoculated with *S. aureus* (**Fig. 5A** and **5C**). Moreover, no keratitis was observed in C57BL/6 WT corneas at 3 days post wounding and *S. aureus* inoculation, with only a few polymorphonuclear cells (PMNs)

Figure 5

observed in the corneal stroma (**Fig 5B**). By contrast, severe keratitis was observed in CD36KO corneas at 3 days post corneal wounding and *S. aureus* inoculation, with an intense PMN infiltration throughout the corneal stroma (**Fig. 5D**). These data demonstrate that CD36KO mice are more susceptible to *S.aureus* induced keratitis.
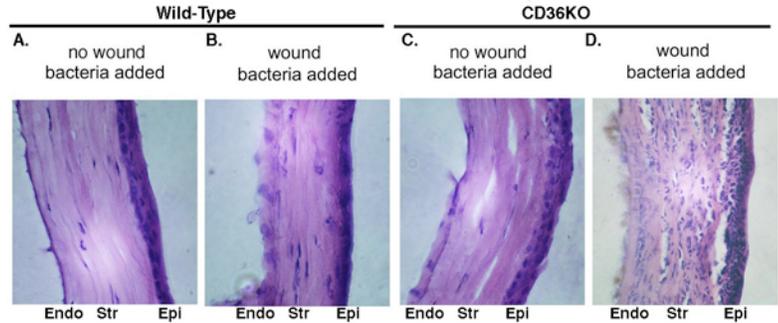
Aim 3) Demonstrate that upregulation of CD36 in the corneal epithelium accelerates wound healing and increases resistance to S. aureus keratitis.

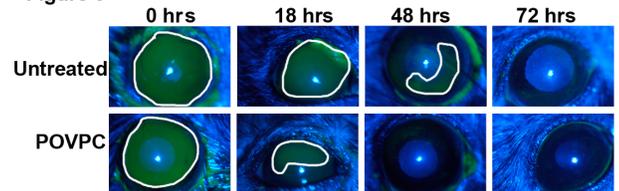Corneal epithelial wounds were performed on wild-type mice in the presence or absence of the oxidized phospholipid 1-palmitoyl 2-(5'-oxoyaleroyl) phosphatidylcholine (POVPC). Topical application of POVPC (100 ug/ml) has previously been shown to upregulate the expression of CD36 in the corneal epithelium and prevents corneal neovascularization [2]. Briefly, C57BL/6 WT mice were anesthetized and the cornea was wounded using a 2.0 mm trephine and a blunt scalpel was used to remove the central epithelium without disrupting the basement membrane. Wound healing in the different groups were monitored via corneal fluorescein staining and slit lamp microscopy at 0hr, 18hr, 48hr, and 72hrs post wounding. POVPC (100ug/ml sterile saline) was applied to the cornea by eye drop (10μl) immediately after wounding and every 12 hours for 48 hours post wounding. Corneal fluorescein staining revealed complete re-epithelialization of a 2.0 mm wound in untreated WT mice (N=3) at 72 hours post wounding (**Figure 6**). By contrast, WT corneas treated with topical POVPC (N=3) presented with accelerated wound healing and complete re-

epithelialization was observed at 48 hours (**Figure 6**). These data demonstrate that upregulation of CD36 in the wounded cornea can accelerate wound healing, thereby increasing resistance to infection. Studies are currently underway (i) to increase the animal numbers in each group and (ii) to perform quantification of wound closure using Image J software for the manuscript that is in preparation.

KEY RESEARCH ACCOMPLISHMENTS:
     (1) We demonstrate the scavenger receptor, CD36, is required for proper corneal wound

healing.

(2) We demonstrate a defect in adhesion and migration in corneal epithelial cells that lack CD36.

(3) We demonstrate that CD36KO corneas are more susceptible to *S. aureus* induced keratitis.

(4) We demonstrate that upregulation of CD36 in the wounded cornea accelerates wound healing.

REPORTABLE OUTCOMES:

(1) A manuscript describing these results is currently in preparation and will be submitted within the next couple of months.

(2) Dr. Julia Klocke, from the University of Leipzig, Germany completed her MD Thesis on this project in June 2011.

(3) An immortalized corneal epithelial cell line was successfully produced from C57BL/6 WT mice.

CONCLUSIONS:

These data demonstrate that (i) CD36 is critical in wound healing and restoration of the barrier function of the epithelium, and (ii) CD36 is an important mediator of corneal epithelial migration and adhesion. In the absence of CD36, CD36KO mice are more susceptible to *S.aureus* induced keratitis. The most clinically relevant results demonstrated that upregulation of CD36 following the topical application of an oxidized lipid (POVPC) in the wounded cornea accelerates wound healing. Taken together, these data support the critical role of CD36 in the corneal barrier to infection and suggest that topical application of POVPC could be used to accelerate closure of corneal wounds and thus reduce the risk of bacterial infections.

REFERENCES:

(1)   Klocke J, Barcia RN, Heimer S, Cario E, Zieske J, Gilmore MS, Ksander BR, Gregory M.   Spontaneous bacterial keratitis in CD36 knockout mice. *IOVS,* 2010;52(1):255-263.

(2)   Mwaikambo B, F Sennlaub, H ong, S Chemtob, P Hardy. Activation of CD36 inhibits and induces regression of inflammatory corneal neovascularization. Invest Ophthalmol Vis Sci. 47:4356-4364, 2006.

Task 2
Reza Dana, M.D., M.P.H., M.Sc.
Title: Molecular regulation of the ocular surface stem cell niche: A new paradigm for regenerative medicine

APPENDICES:

As his final report, Dr. Dana is submitting the following manuscript, of which the abstract appears below. A copy of the full manuscript appears in **Appendix 1.**

Dependence of Corneolimbal Progenitor Cells on Ocular Surface Innervation

Hiroki Ueno[1,2], Giulio Ferrari[1,2,3], Takaaki Hattori[1,2], Daniel R. Saban[1,2], Sunil K. Chauhan[1,2], and Reza Dana[1,2]

[1] Schepens Eye Research Institute, Boston, MA 02114
[2] Massachusetts Eye and Ear Infirmary, Harvard Medical School, Boston, MA 02114
[3] Bietti Eye Foundation, IRCCS Rome, Italy.

Word count: 2879

Corresponding author:
Reza Dana, M.D., M.P.H., M.Sc.
Schepens Eye Research Institute, Harvard Medical School
20 Staniford Street, Boston, MA 02114
Email: reza.dana@schepens.harvard.edu
Phone: 617-912-7401, Fax: 617-912-0117

ABSTRACT

Purpose: Neurotrophic keratopathy (NK) is a corneal degeneration associated with corneal nerve dysfunction. It can cause corneal epithelial defects, stromal thinning, and perforation. However, it is not clear if and to which extent epithelial stem cells are affected in NK. The purpose of this study was to identify the relationship between corneolimbal epithelial progenitor/stem cells and sensory nerves using a denervated mouse model of NK.

Methods: NK was induced in mice by electro-coagulation of the opthalmic branch of the trigeminal nerve. The absence of corneal nerves was confirmed with beta-III tubulin immunostaining and blink reflex test after 7 days. ABCG2, p63 and Hes1 were chosen as corneolimbal stem cell markers and assessed in denervated mice versus controls by immunofluorescent microscopy and real-time PCR. In addition, corneolimbal stem cells were detected as side population cells using flow cytometry, and colony-forming efficiency assay was performed to assess their function.

Results: ABCG2, p63 and Hes1 immunostaining were significantly decreased in denervated eyes after 7 days. Similarly, the expression levels of ABCG2, p63 and Hes1 transcripts were also significantly decreased in denervated eyes. Stem cells measured as side population from NK mice were decreased by approximately 75% compared to normals. In addition, we found a significant (p=0.038) reduction in colony-forming efficiency of stem cells harvested from denervated eyes.

Conclusions: Corneolimbal stem cells are significantly reduced after depletion of sensory nerves. Our data suggest a critical role of innervation in maintaining stem cells and/ or the stem cell niche.

Task 3
Sharmila Masli, Ph.D., Darlene Dartt, Ph.D.
Title: Regulation of conjunctival inflammation with thrombospondin

INTRODUCTION:
Thrombospondin-1 is a matrix protein expressed by various cell types including epithelia in different ocular structures iris and ciliary body, retina, cornea and conjunctiva. In avascular tissues like cornea the antiangiogenic property of TSP-1 contributes to prevention of blood vessel growth thereby avoiding inflammation. Its ability to activate latent TGFβ to its active form makes this anti-inflammatory cytokine biologically available in the environment. Thus TSP-1 potentially can regulate local inflammatory immune response indirectly by activating TGFβ. Additionally, it is now known that direct ligation of receptors on immune effectors such as antigen presenting cells by TSP-1 can prevent their inflammatory responses. We have previously reported that the absence of TSP-1 leads to inflammation in the lacrimal gland subsequently causing ocular surface inflammation. In this project we evaluate anti-inflammatory potential of TSP-1 in the conjunctiva and determine if its absence in the conjunctiva could result in inflammation that disrupts mucin secretion by goblet cells. Conjunctival epithelium contains goblet cells capable of secreting gel-forming mucin MUC5AC onto the ocular surface providing protection from damaging stimuli from the external environment. This mucin secretion is a tightly regulated process with any disturbances resulting in increased or decreased mucin secretion. We hypothesized that inflammatory responses in the conjunctiva due to absence of TSP-1 may alter the goblet cell secretion.

BODY:
To determine if inflammatory cytokine production is increased in TSP-1null conjunctiva we assessed message levels of cytokines IFN-γ, TNF-α, IL-17 and IL-6 using real-time PCR assay. We harvested conjunctiva tissue from age-matched wild-type (WT) control or TSP-1null mice at 6, 8 and 12 weeks of age. The RNA harvested from these tissues was subjected to PCR amplification using cytokine specific primer sets. As shown in figure 1, significantly increased levels of IFN-γ were detected in TSP-1null conjunctiva at the ages of 8 and 12 weeks, whereas levels of TNF-a remained undetectable until 8 weeks and were significantly increased in TSP-1null conjunctiva at 12 weeks of age. This increase in TNF-α message level coincided with increased infiltration of neutrophils in H&E stained histological sections of the conjunctiva tissue harvested from 12 weeks old TSP-1null mice as compared to age-matched WT control tissue (figure 2). The presence of neutrophils thus confirmed the significant inflammatory response detectable in the absence of TSP-1 in conjunctiva by 12 weeks of age. Expression of cytokine such as IL-17 was found elevated in TSP-1null conjunctiva at the youngest age tested of 6 weeks compared to the control tissue (figure 1), while that of IL-6 remained unaltered at this age. With increasing age, expression of both IL-17 and IL-6 was found significantly elevated compared to control conjunctiva tissue. Thus our results clearly indicated significantly increased expression of inflammatory cytokines in the conjunctiva in the absence of TSP-1.

To determine if the presence of inflammation in the conjunctiva alters mucin secretion by goblet cells we determined total mucin levels in pilocarpine-induced tears using an Enzyme-

8

Linked Lectin Assay (ELLA). Tears collected from 12 week old WT and TSP-1null mice were analyzed for their mucin content. As shown in figure 3, significantly reduced levels of mucin was detected in tears collected from TSP-1null mice compared to those collected from WT control mice. Furthermore, message levels for goblet cell associated gel-forming mucin, MUC5AC, were assessed in conjunctiva tissues of WT and TSP-1null mice (8 wks) in a real-time PCR assay. Significantly reduced level of MUC5AC expression was detectable in the absence of TSP-1 as compared to WT control (figure 3). Thus the message level of MUC5AC in the conjunctiva corresponded with the tear mucin levels in TSP-1null mice.

Our results indicate that in the absence of TSP-1 the cells in the conjunctiva express significantly elevated levels of inflammatory cytokines IFN-γ, TNF-α, IL-17 and IL-6. The presence of these cytokines in the conjunctiva coincides with reduced mucin secretion and synthesis of MUC5AC by goblet cells in the TSP-1 deficient conjunctiva.

Furthermore, to determine if the reduced mucin secretion by goblet cells in TSP-1null conjunctiva is the direct influence of inflammatory cytokines we developed mouse goblet cell cultures. An extensive characterization of cells grown in culture was completed to identify expression of goblet cell specific markers. As shown in figure 4, cultured cells showed immunoreactivity to anti- cytokeratin-7 antibody (CK-7) that identifies cytokeratin primarily expressed by goblet cells as against CK-4 expressed by other epithelial cells. Cultured cells also contained mucin that was detectable by binding of a fluorescent conjugated lectin (HPA). Moreover, upon cholinergic stimulation with carbachol, cultured cells released mucin in culture supernatants that was quantitated using ELLA (figure 5). Cultures confluent in the range of 50-60% released most mucins. Thus a culture system was optimized to study the direct effect of cytokines on mucin secretion.

KEY RESEARCH ACCOMPLISHMENTS:
- Detection of increased expression of inflammatory cytokines associated with chronic diseases in TSP-1 deficient conjunctiva.
- Detection of increased neutrophil infiltration in TSP-1null conjunctiva and its correlation with reduced mucin expression and secretion in tears.
- Establishing in vitro culture of mouse goblet cells.

REPORTABLE OUTCOMES:
Results generated in this project were presented at ARVO 2011. Experimental results of changes in mucin secretion by cultured goblet cells exposed to inflammatory cytokines are currently being processed and data is being prepared for inclusion in a manuscript for publication.

CONCLUSIONS:
Our results support our hypothesis that TSP-1 regulates inflammation in the conjunctiva and that inflammatory cytokines are likely to regulate secretory functions of goblet cells by reducing their mucin secretion. Such reduced mucin secretion may render ocular surface vulnerable to further inflammatory damage.

Task 4
Andrius Kazlauskas, Ph.D Title: The role of endogenous inhibitors of PDGF receptors in PVR

INTRODUCTION:
Proliferative vitreoretinopathy (PVR) is a serious complication that can develop in patients with retinal detachments (Campochiaro, 1997; Committee, 1983; Michels et al., 1990; Pastor, 1998). It is characterized by the formation of a fibroproliferative membrane that contracts and tears the retina from the back of the eye. PVR occurs in 5-10% of the patients who undergo retinal reattachment surgery. Of this group, nearly 20-40% have recurring episodes of PVR and partial vision loss. Military personnel who survive violent traumatic episodes are prone to severe PVR that has a particularly poor prognosis. Furthermore, certain service-related procedures, such as removal of intraocular foreign bodies, are associated with a very high incidence of PVR (Colyer et al., 2007). Aside from surgical interventions to relieve the vitreoretinal traction, there are no effective treatment options. Thus there is an acute need for pharmacological/molecular-based therapies for PVR.

BODY:
Work from several labs has shown that platelet-derived growth factor (PDGF) receptor α (PDGFRα) is essential for experimental PVR and tightly associated with PVR in patients (Lei et al., 2010). While PDGFs are abundant in vitreous, they are not required to activate PDGFRα. Instead, vitreal growth factors outside of the PDGF family (non-PDGFs) activate PDGFRα and drive experimental PVR. The duration of receptor activation is a fundamental difference between PDGF- and non-PDGF-mediated activation of PDGFRα (Lei et al., 2011). While PDGFs trigger transient activation of PDGFRα, non-PDGFs result in chronic activation. This is because PDGFs induce internalization and degradation of PDGFRα, whereas non-PDGFs do not. Since chronic activation selectively engages a series of signaling events associated with pathology, it appears that the duration of PDGFRα activation is a critical parameter in the development of experimental PVR.

When cells are stimulated with PVR vitreous, PDGFRα activation is chronic (Lei et al., 2011), even though PVR vitreous contains enough PDGF to saturate all PDGFRs (Lei et al., 2007), and thereby induce their internalization and degradation. One explanation for this observation is that vitreous contains an agent that competes with PDGF for binding to its receptor and thereby prevents PDGF-dependent degradation of PDGFRα. The results from our ongoing research support this possibility. One of the candidate PDGF competitors was vascular endothelial growth factor A (VEGF-A) (Pennock et al., 2010), which other groups have reported to be structurally similar to PDGF and bind to PDGFRα (Ball et al., 2007; Muller et al., 1997).

A PDGF competitor has the potential to contribute to pathogenesis of PVR. In PVR vitreous, where both PDGFs and non-PDGFs are present, such a PDGF inhibitor would favor activation of PDGFRα by non-PDGFs, i.e. chronic activation of PDGFRα, which is associated with the manifestation of PVR. The level of this inhibitor may be indicative of an individual's likelihood of succumbing to PVR (more inhibitor would indicate a greater risk).

Neutralizing such inhibitors should protect from PVR, and hence be an effective pharmacological option to reduce the risk of PVR in patients that undergo surgery to correct retinal detachment.

As mentioned above, we recently identified VEGF-A as one of the agents in vitreous that suppressed PDGF-dependent activation of PDGFRα (Pennock et al., 2010). In the first quarter of the grant period we determined that VEGF-A and PDGF-A had a comparable affinity for PDGFRα, and that VEGF-A accounted for a substantial fraction of the inhibitory activity present in vitreous. In the second quarter of the grant period we characterized the relationship of VEGF-A with the remaining members of the PDGF/PDGFR family. In the third quarter of the grant period we determined the level of VEGF-A and PDGFs in human specimens, and discovered that neutralizing VEGF-A influenced the ability of vitreous to promote signaling events and cellular responses intrinsic to PVR. In the fourth quarter of the grant period we investigated the mechanism by which neutralizing VEGF-A attenuated the ability of vitreous to provoke pathological signaling events and cellular responses.

As shown in lanes 1 and 2 of Fig 1, vitreous induced prolonged activation of Akt and suppression of p53, signaling events that are closely associated with PVR (Lei et al., 2011). Indirect activation of PDGFRα greatly promoted these vitreous-driven changes (Lei et al., 2011). In contrast, direct activation of PDGFRα less effectively engaged this set of pathology-associated signaling events because direct activation of PDGFRα led to rapid PDGFRα degradation (Lei et al., 2011).

These findings challenged the traditional view that PDGF in vitreous promotes PVR. PDGF may be protecting from PVR by inducing degradation of PDGFRα, and thereby reducing the amount of PDGFRα that can be activated indirectly. Indeed, we found that increasing the amount of PDGF in vitreous reduced the level of PDGFRα and mitigated vitreous-dependent pathology-associated signaling events (lanes 2 and 3 of Fig 1). Similarly, neutralizing vitreal VEGF-A boosted the bioactivity of vitreal PDGFs, and thereby attenuated vitreous-driven pathological signaling (lane 4 of Fig 1). We conclude that neutralizing vitreal VEGF-A attenuated the ability of vitreous to provoke PVR-related signaling events, and that a likely mechanism involved a PDGF-mediated reduction in the amount of PDGFRα expressed at the cell surface.
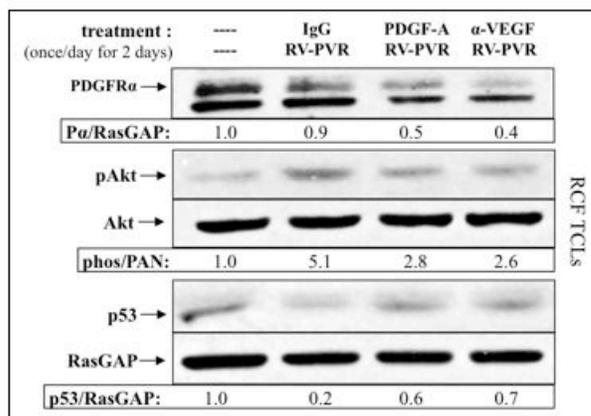
Figure 1. Vitreal VEGF-A was required to promote long-term PDGFRα-mediated pathological signaling. Serum-starved rabbit conjunctival fibroblasts (RCFs) were treated for 48 h with buffer alone (---), 200 ul of pooled rabbit PVR vitreous (RV-PVR), or 200 ul RV-PVR supplemented with either 25 ug/ml isotype control IgG (IgG), PDGF-A (0.15 nM), or 25 ug/ml VEGF-A neutralizing antibody (α-VEGF). Media was replaced, cells washed, and fresh treatment added at 24 h. Following treatment, cells were harvested, lysed and subjected to western immunoblot analysis first using anti-PDGFRα, anti-phospho-Akt, and anti-p53 antibodies, and then anti-Akt and anti-RasGAP to assess for equal loading of proteins. Immunoblot bands were quantified, normalized to RasGAP (for quantification of PDGFRα levels) or Akt (for quantification of Akt phosphorylation), and presented numerically as a fold increase over the unstimulated control. We conclude that neutralizing VEGF-A reduces the amount of PDGFRα and PDGFRα-mediated pathological signaling events.

We performed the same types of experiments and focused on cellular responses instead of signaling. As shown in Fig 2, vitreous promoted contraction of collagen gels, which is an in vitro mimic of retinal detachment. Supplementing the vitreous with agents that reduced that amount of PDGFRα (PDGF-A and anti-VEGF) attenuated the ability of vitreous to promote contraction. Thus, reducing the amount of PDGFRα suppressed both signaling events and cellular responses associated with PVR. Furthermore, direct activation of PDGFRα, which robustly activates signaling and drives many cellular responses, appears to make a negligible contribution to the types of signaling events and cellular responses that are inherent to PVR. The major, PVR-related consequence of directly activating PDGFRα appears to be reducing the amount of PDGFRα that can be activated indirectly by vitreal non-PDGFs. These observations lead to the provocative idea that vitreal PDGFs, which are high in both experimental and clinical PVR (Lei et al., 2007), act to protect instead of promote PVR.

	--- ---	--- RV-PVR	PDGF-A RV-PVR	IgG RV-PVR	α-VEGF RV-PVR
no preconditioning	140	95	85	95	67
24h preconditioning	142	78	108	90	131
48h preconditioning	143	75	105	90	135
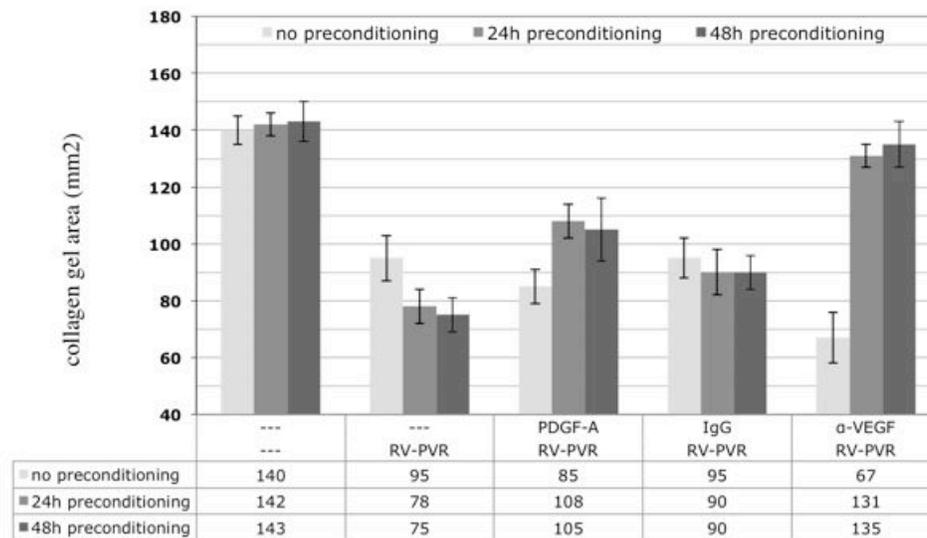
Figure 2. Neutralizing VEGF-A in the vitreous reduced vitreous-mediated contraction. Rabbit conjunctival fibroblasts (RCFs) were preconditioned for 0, 24, or 48 h in buffer alone (---), 250 ul of pooled rabbit PVR vitreous (RV-PVR), or 250 ul RV-PVR supplemented with either PDGF-A (0.15 nM), 25 ug/ml isotype control IgG (IgG), or 25 ug/ml VEGF-A neutralizing antibody (α-VEGF). Media was replaced every day and fresh treatment added. After preconditioning, cells were

suspended in collagen gels containing the same treatments that were used during the pre-treatment period. Media and treatment was replaced every day, and after 2 days, the gel area for each sample was calculated and the data presented as the mean +/- SD. These results indicate that preconditioning cells with VEGF-neutralized vitreous for at least 24 hours is required to attenuate the ability of vitreous to drive collagen gel contraction.

KEY RESEARCH ACCOMPLISHMENTS:

- Reducing the amount of PDGFRα suppressed both signaling events and cellular responses associated with PVR.
- The functional consequence of PDGF-dependent activation of PDGFRα was attenuation, rather than promotion, of PVR-related events.
- Neutralizing vitreal VEGF-A has the potential to protect from PVR.

REPORTABLE OUTCOMES:
None.

CONCLUSION:
Vitreous contains agents that both promote and attenuate signaling events and cellular responses intrinsic to PVR. Altering the composition of the vitreous is a potential approach to protect patients from developing PVR.

REFERENCES:

Ball, S.G., Shuttleworth, C.A., and Kielty, C.M. (2007). Vascular endothelial growth factor can signal through platelet-derived growth factor receptors. J Cell Biol *177*, 489-500.
Campochiaro, P.A. (1997). Mechanisms in ophthalmic disease: Pathogenic mechanisms in proliferative vitreoretinopathy. Arch Ophthalmol *115*, 237-241.
Colyer, M.H., Weber, E.D., Weichel, E.D., Dick, J.S., Bower, K.S., Ward, T.P., and Haller, J.A. (2007). Delayed intraocular foreign body removal without endophthalmitis during Operations Iraqi Freedom and Enduring Freedom. Ophthalmology *114*, 1439-1447.
Committee, T.R.S.T. (1983). The classification of retinal detachment with proliferative vitreoretinopathy. Ophthalmology *90*, 121-125.
Lei, H., Hovland, P., Velez, G., Haran, A., Gilbertson, D., Hirose, T., and Kazlauskas, A. (2007). A potential role for PDGF-C in experimental and clinical proliferative vitreoretinopathy. Invest Ophthalmol Vis Sci *48*, 2335-2342.
Lei, H., Rheaume, M.A., and Kazlauskas, A. (2010). Recent developments in our understanding of how platelet-derived growth factor (PDGF) and its receptors contribute to proliferative vitreoretinopathy. Exp Eye Res *90*, 376-381.
Lei, H., Velez, G., and Kazlauskas, A. (2011). Pathological signaling via PDGFRa involves chronic activation of Akt and suppression of p53. Molecular and Cellular Biology *In Press*.
Michels, R.G., Wilkinson, C.P., and Rice, T.A. (1990). Proliferative retinopathy (St. Louis, Mosby).
Muller, Y.A., Li, B., Christinger, H.W., Wells, J.A., Cunningham, B.C., and de Vos, A.M. (1997). Vascular endothelial growth factor: crystal structure and functional mapping of the kinase domain receptor binding site. Proc Natl Acad Sci U S A *94*, 7192-7197.
Pastor, J.C. (1998). Proliferative vitreoretinopathy: an overview. Surv Ophthalmol *43*, 3-18.
Pennock, S., Lei, H., Velez, G., and Kazlauskas, A. (2010). unpublished observations.

Task 5
Joan Stein-Streilein, Ph.D.
Title The effect of retinal laser burn on the immunosuppressive function of retinal pigmented epithelium

INTRODUCTION:
Following antigenic insult, the body responds with immune inflammatory responses that are meant to lead to repair. In rare cases, depending on the immune homeostasis of the tissue, repair may be prevented by chronic inflammation. To protect vision, the immune privilege mechanisms limit ocular inflammatory responses. Immune privilege mechanisms are made up of multiple overlapping regulatory mechanisms. Many of the cells within the eye express inhibitory ligands, (PD-L1, CD200Rand FasL) and the fluids of the eye contain soluble immunosuppressive factors, (TGFβ)

Our studies show that RLB encourages uncontrolled activation of myeloid cells in the eye. We postulate that RLB changes the immunosuppressive environment of the eye and in turn contributes to loss of the tolerogenic ability of indigenous cells. We will specifically study the changes in the inhibitory molecules on the cells and in the fluids that are induced post RLB.

BODY:
This quarter we continued our focus on Objective 2 b.2.
Objective 1. To examine the cytokine profile secreted of RPE from mice treated with RLB or not.
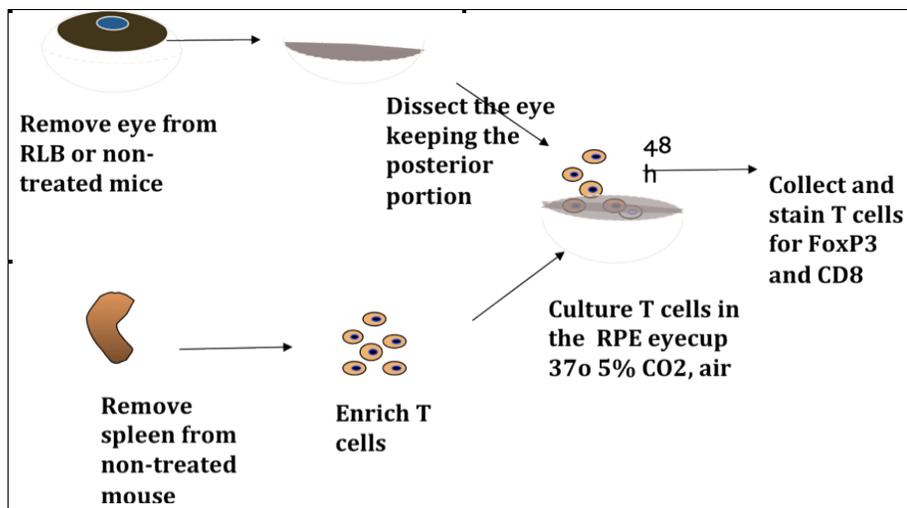

Fig. 1A. Schematic protocol analysis of RLB effect on regulating immune T cells.
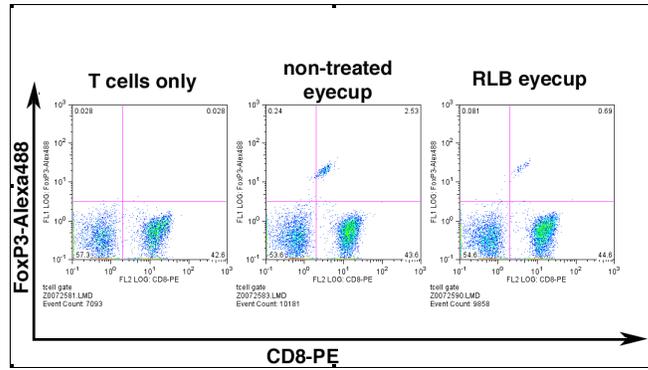
Figure 1B. Flow cytometry analysis of T cells. The Dot plot shows the number of cells that express FoxP3 post incubation with eye cups removed from untreated and RLB mice. The vertical axis is the number of FoxP3 + Cells and the horizontal axis is the number of CD8+ T cells.

CONCLUSION:

We did not evaluate the cytokine in a transwell plate because the RLB eyecup was unable to induce the FoxP3 + in the activated T cells . This suggests that if an immunosuppressive cytokine is responsible in the naïve eye cup it was absent or diminished in the RLB treated eyecup.

Objective 2: To determine if RLB damage to the RPE leads to the loss of ACAID in the contralateral eye.

2.b.1. To examine the mRNA expression level of CD200, FasL, and PD-L1 in the eye and RPE eyecups following RLB treatment or not. These molecules are known to be important in ocular immune homeostasis. Changes in regulatory surface molecules may contribute to loss of immune privilege in eyes of mice that receive RLB. CD200 is expressed on the cell membrane by stromal cells in the eye and its receptor CD200R is displayed by the ocular and peripheral cells of myeloid lineage. engagement of the receptor and ligand lead to inhibition of myeloid activation.
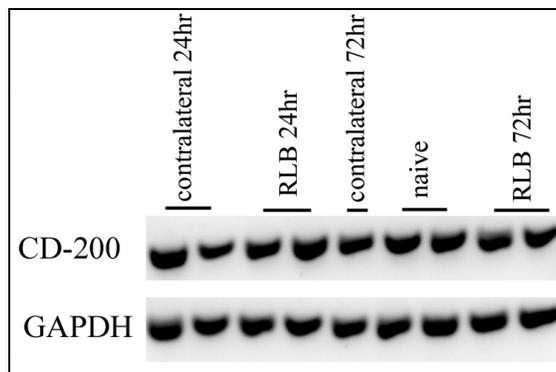

Fig. 2. RTPCR analysis of CD200 mRNA in RPE cells. Top panel: mRNA expression of CD200. Bottom panel: mRNA expression of GAPDH.

15

In brief, eyes were removed from euthanized mice that untreated or received RLB 24 and 72 hours prior to extirpation of the eye.. Ocular tissue (excluding the lens) was placed in trizol and mRNA was extracted using phenol-chloroform. After mRNA extraction, the concentration of each sample was assessed using a spectrophotometer. cDNA was produced from the mRNA. PCR analyses using primers for CD200 and GAPDH. The amount of CD200 in samples from the treated and non-treated eyes of the mice that received RLB were compared to mice that did not receive RLB. In this experiment we found that CD200 mRNA levels did not change in either eye of mice that received RLB compared to mice that did not receive RLB. These results suggest that CD200 in the eye may not change at these time points however this does not rule out the possibility that CD200R on resident or invading machrophages in the eye may change. This will be assayed in section 2.b.2.

Objective: 2.b.2. To compare the number of cells expressing CD200R, Fas, and PD-1 in the eyes of mice that received RLB treatment vs. untreated mice.

FINDINGS:
In brief, eyes were removed from euthanized naïve or RLB treated mice 4 days post RLB. The eyes were dissected and the RPE containing retina (eyecup) was kept (lens, neural retina, and anterior portion of the eye were discarded). Eyecups were than incubated with 0.25% Trypsin for 1 hour at 37˚C. RPE cells were removed from the eyecup and incubated in Complete Media for 14 days. At the end of the 14 days cells were assayed for the existence of a monolayer.

We were successful in producing a monolayer of RPE cells from naïve, or the treated and untreated eye of RLB mice. These cells were checked the expression of proteins on the RPE monolayer by flow cytometry . The cultured RPE cells were used as for Flow cytometry studies of expression of regulatory molecules.

Fig. 3. Histogram of flow cytometric analyses of FasL in RPE cells: FasL expression in RPE cells harvested from or RLB treated mice one day post RLB (Panel A) and four days post RLB (Panel B). The left histogram in both panels represents FasL expression of the RPE harvested from the ipsilateral eye that received the RLB (blue) compared to naïve eye (red). The right histogram in both panels represents FasL expression of the RPE harvested from the contralateral eye that received the RLB (green) compared to naïve eye (red).
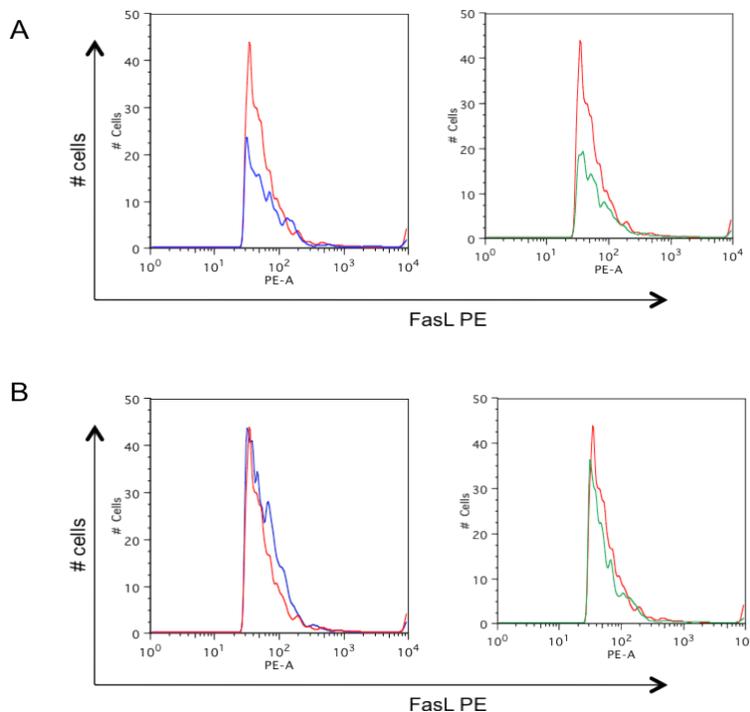
Figure 4: Histogram of flow cytometric analyses of PDL-1 on RPE cells. PDL-1 expression in RPE cells harvested from or RLB treated mice one day post RLB (Panel A) and four days post RLB (Panel B). The left histogram in both panels represents PDL-1 expression of the RPE harvested from the ipsilateral eye that received the RLB (blue) compared to naïve eye (red). The right histogram in both panels represents PDL-1expression of the RPE harvested from the contralateral eye that received the RLB (green) compared to naïve eye (red).

KEY RESEARCH ACCOMPLISHMENTS:
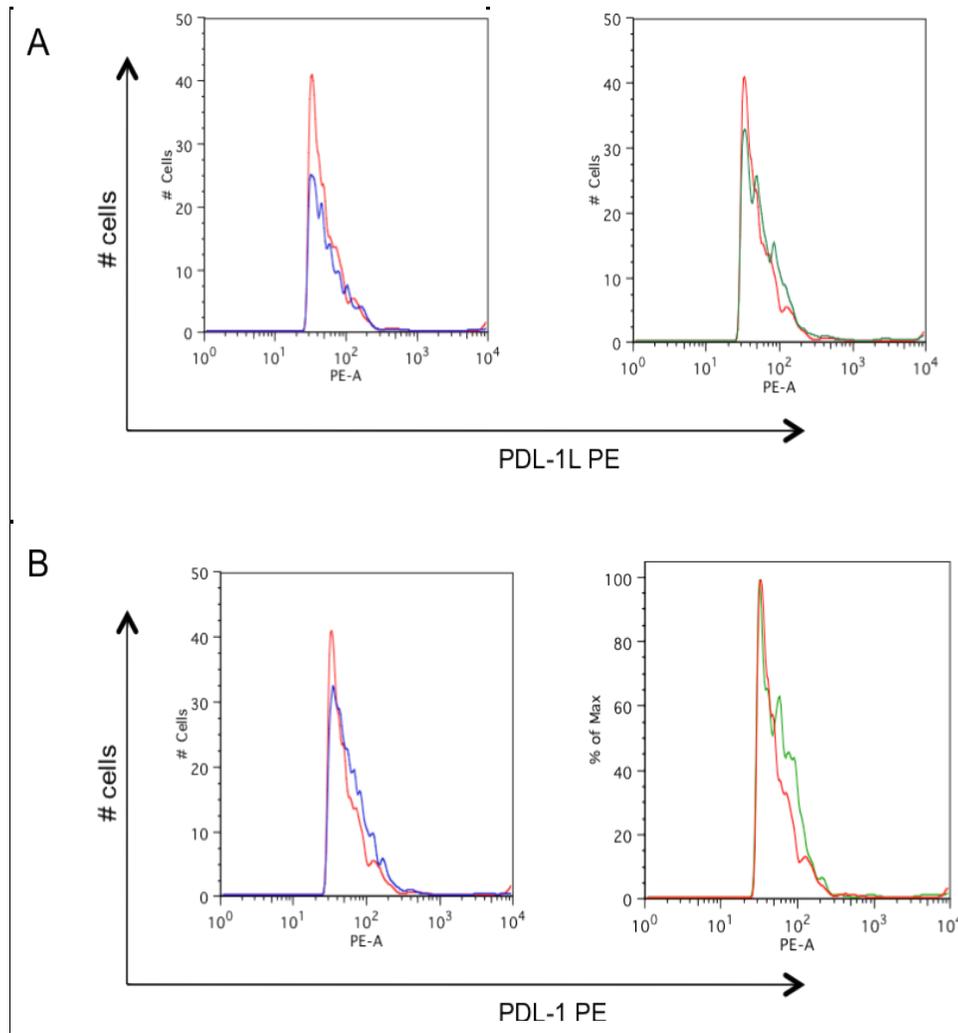- This grant period, we have successfully produced a monolayer of RPE cells from cells harvested from eyes of naïve and RLB mice.

- We observed that critical regulatory molecules expressed by the RPE cells are down regulated early post RLB

- A manuscript entitled: "*Substance P interferes with Ocular Immune Privilege post Retinal Laser Burn*" by Kenyatta Lucas, Joan Stein-Streilein is in preparation for publication

REPORTABLE OUTCOMES:
- A manuscript entitled "Retinal laser burn disrupts immune privilege in the eye" has been published in the American Journal of Pathology 2009 Feb; 174(2): 414-22.

- An abstract of this work by Kenyatta Lucas was presented as Poster at the ARVO 2011 meeting in Fort Lauderdale.

- A manuscript entitled: "*Substance P interferes with Ocular Immune Privilege post Retinal Laser Burn*" by Kenyatta Lucas, Joan Stein-Streilein is in preparation for publication

CONCLUSION:
RLB abrogates immune privilege in the burned eye in part by breaking the blood ocular barrier, allowing an influx of inflammatory cells. The reason for the loss of immune privilege in the contralateral eye is less apparent.
- This grant period, we have successfully produced a monolayer of RPE cells from cells harvested from eyes of naïve and RLB mice.

- We observed that critical regulatory molecules expressed by the RPE cells are down regulated early post RLB

APPENDICES:
- "Retinal laser burn disrupts immune privilege in the eye" has been published in the American Journal of Pathology 2009 Feb; 174(2): 414-22.
  See Appendix (2)
- An abstract of this work by Kenyatta Lucas was presented as Poster at the ARVO 2011 meeting in Fort Lauderdale.
  See Appendix (3)

We plan to continue to study the expression of the molecules of the regulatory molecules on the RPE cells. Our next approach will be to assay the mRNA of the molecules in freshly dissected RPE. This will check if what is expressed by the cells after 14 days of culture is related to what is expressed by the freshly isolated RPE cells. To relate it to the previous substance P studies, we will also check the RPE cells at various time post RLB with and the addition of a substance P antagonist given to the mice prior and

Task 6
Andrew Taylor, Ph.D.
Title: Regulation of the wound response within the retina of eyes with catastrophic injury

Dr. Taylor is no longer working at the Schepens Eye Research Institute. Funds from this project were approved to be re-budgeted toward the purchase of an electroretinography (ERG) microscope. This microscope will be utilized by Drs. Patricia D'Amore, Dong Feng Chen, and Andrius Kazlauskas.

Task 7
Bruce Ksander, Ph.D
Title: Glial regulation of neuronal damage after traumatic brain injury

INTRODUCTION:
Our studies indicate that a prolonged expression of membrane FasL (mFasL) at the site of a traumatic brain injury triggers increased neuronal damage. The aim of the current studies was to determine if this neurotoxicity was dependent upon microglia. We are focusing on microglia, since these cells are known to express FasL.

Task- Determine if prolonged expression membrane FasL on microglia triggers increased neuronal damage following a traumatic brain injury.

These studies will utilize a unique mutant knock-in mouse that produces membrane FasL (mFasL), but is unable to produce soluble FasL (sFasL). This is the first time this type of FasL knock-in mutation has been successfully produced and the first time this unique mutation will be used to study the pathogenesis of traumatic brain injury.

BODY:
During the third quarter of this project we successfully produced immortalized microglia cell lines from three types of mice: (i) wild-type, (ii) membrane FasL knock-in, and (iii) FasL knockout mice. These cell lines express the Iba-1 marker expressed on microglia. Our results indicate that all microglia cell lines (WT, mFasL-only, and FasL KO) express high levels of the Fas receptor. Membrane FasL is expressed on microglia isolated from either wild-type mice, or mFasL-only mice (but not on microglia isolated from FasL knockout mice).

We encountered two problems during the final (fourth) quarter of this project. Fortunately we were able to find solutions to these problems that will allow us to finish this project in the future. The two problems were due to limitations in the technology currently available: (i) we were unable to quantitatively determine the levels of membrane and soluble FasL on cells and tissues, and (ii) we were unable to distinguish activated microglia from infiltrating macrophages within the brain. Our work on solving these problems and the solutions are described below.

There are a variety of papers in the literature that claim to determine the levels of membrane and/or soluble FasL on tissues using a variety of techniques (western blot, flow cytometry, or

ELISA). However, when we rigorously tested these techniques using tissue from our mice that: (i) fail to express either sFasL or mFasL (FasL KO mice), and (ii) express only sFasL (mFasL only mice); we determined these techniques were not adequate and we believe that if other laboratories had used rigorous controls, they would have found similar problems quantitating FasL. One of the most important reasons for this problem is that all of the available antibodies for FasL appear to have low specificity and/or low avidity for the target protein. Therefore, we needed to develop and/or find a new technique to quantitatively track the expression of mFasL and sFasL in brain tissue of mice following a traumatic brain injury. After searching, we chose a new emerging biotechnology called sortase-mediated ligation. This approach utilizes a specific enzymatic reaction mediated via *sortase* to fuse a probe to the C terminus of FasL. In order to use this technique, we first had to construct a FasL cDNA vector that contains the sequence recognized by the sortase enzyme and then demonstrate this sequence does not interfere with the ability of FasL to bind and trigger activation of the Fas receptor. These experiments were conducted using cell lines in vitro. We are currently in the final stages of these experiments. Once we have validated the FasL-sortase cDNA sequence, we will construct a FasL-sortase knock-in mouse using the targeting vector that we used to construct the mFasL-only knock in mouse. Successful construction of the FasL-sortase knock-in mouse will allow us follow track and quantitate precisely the expression of mFasL and sFasL in brain tissue following a traumatic brain injury. This work is being done in collaboration with Dr. Hidde Ploegh at MIT, an expert in this new sortase-mediated ligation technology.

The second problem we encountered was the inability to distinguish between resident microglia and infiltrating macrophages. This is not a new problem, since it has been known for many years that there are no cell surface markers that distinguish between these two types of cells. However, for our studies it is particularly important to distinguish between these cell types, since these two populations can express FasL and are predicted (but not proven) to have separate and distinct functions. Recently, a laboratory from Brigham & Women's Hospital in Boston successfully produced a monoclonal antibody that recognizes a cell surface protein that is expressed on microglia, but not expressed on CD11b+ bone marrow derived cells. We are collaborating with this laboratory and using their antibody to differentiate resident brain microglia from infiltrating macrophages following a traumatic brain injury in wild-type and mFasL-only knock-in mice. In conclusion, using the sortase technology and the new microglia-specific antibody will allow us to rigorously study the mechanism(s) that mediate the increased neurotoxicity via membrane FasL following a brain injury.

KEY RESEARCH ACCOMPLISHMENTS:
(i) We demonstrated there was increased neurotoxicity following a traumatic brain injury in mice that were unable to produce soluble FasL, (ii) we successfully produced immortalized microglia cell lines from the brain tissue of the following mice: wild-type, mFasL knock-in, and FasL knockout.

REPORTABLE OUTCOMES:
We have descriptive data demonstrating increased neurotoxicity via membrane FasL following brain injury. We will publish this work when we have completed the experiments that determine the mechanism behind this phenomenon. This will require completing the

experiments that determine quantitatively the levels of mFasL and sFasL in vivo, along with, the experiments that separate resident microglia from infiltrating macrophages.

CONCLUSIONS:
At this time, our data support the hypothesis that expression of membrane FasL is neurotoxic following a traumatic brain injury. This implies that a new therapeutic target to reduce neuronal damage is either reduction of membrane FasL and/or an increase in soluble FasL.

Task 8
Patricia D'Amore, Ph.D.
Title: Regeneration of bruch's membrane in vitro and in vivo

INTRODUCTION:
Bruch's membrane (BrM) is an elastic lamina that separates the retinal pigment epithelium (RPE) and the choriocapillaris (CC). Though it has not been experimentally demonstrated, it is widely believed that BrM is produced by both cell populations. BrM represents both a physical and biochemical barrier to vessel growth from the CC so that a break in BrM nearly always leads to choroidal neovascularization (CNV), an element of the wet form of age-related macular degeneration (AMD) as well as in response to laser injury (experimental or accidental) to the retina. There is currently no known way to repair or restore BrM. The studies in conducted in this application are testing the hypothesis that heat treatment can induce the production of BrM components by RPE and EC in vitro and induce regeneration of BrM in vivo.

BODY:
During the last quarter we began to examine the effect of heat treatment on the production of matrix components b RPE. For heat treatment, ARPE-19 cells grown for four weeks on the transwells were cultured at 43°C for 30 min. RNA was isolated 15 min, one, two, and four hr after heat treatment and cell associated proteins were examined in cell lysates collected two and four hr after heat treatment. Proteins secreted into the culture media were collected four hr after heat treatment and analyzed. The effect of heat treatment on the levels of tropoelastin mRNA and protein were examined by real-time PCR and western blot analysis of cell lysates. Tropoelastin mRNA levels were increased by 180% at 15 min after heat treatment **(Figure 1)** and the protein levels increased by 170% at 120 min after heat treatment **(Figure 2).**
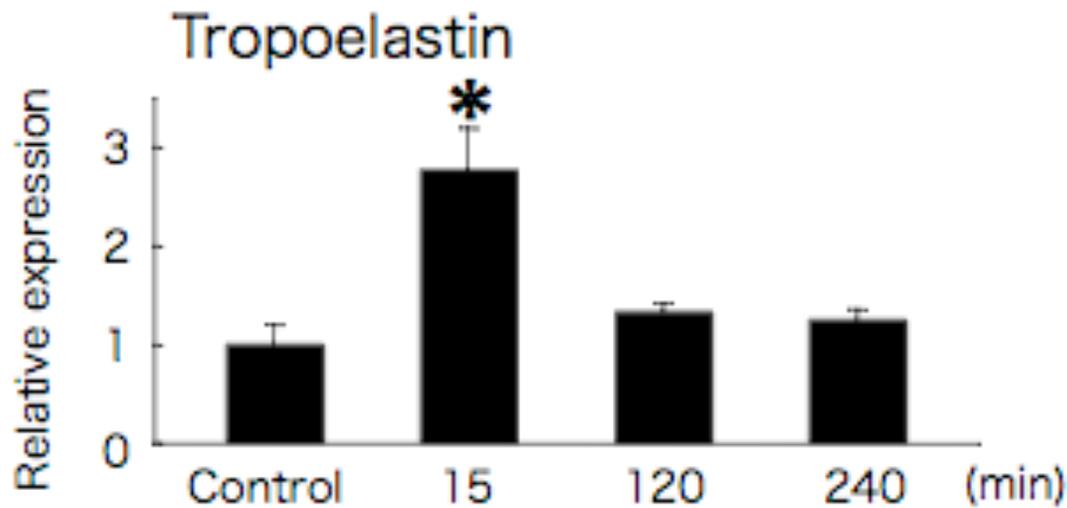
Figure 1. Heat treatment increases tropoelastin expression by ARPE-19 cells.
(A) Expression of tropoelastin mRNA by ARPE-19 cells 15, 120, and 240 min after heat treatment at 43°C for 30 min.
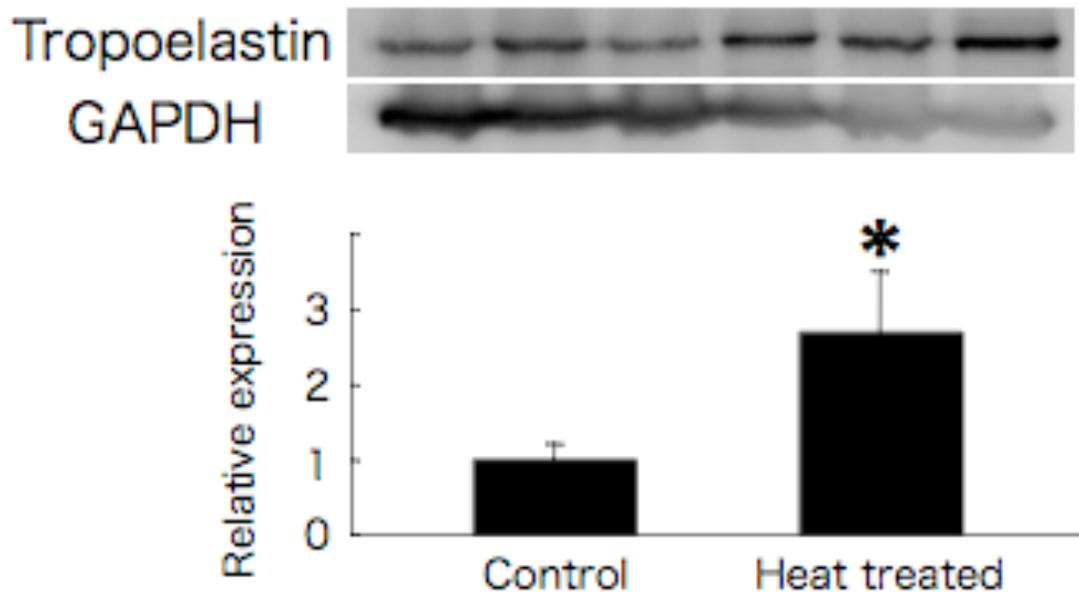
Figure 2. Heat treatment increases tropoelastin expression by ARPE-19 cells.
(B) Expression of tropoelastin protein 120 min after treatment at 43°C for 30 min. Values are means ± SE (n=3).

Next we tested whether pre-treatment with heat would affect laser-induced CNV.
To determine if heat treatment has any effect on normal retina, IDL irradiated retinal tissues were dissected and examined. . C57BL/B6J mice were anesthetized by intraperitoneal

injection of 100 mg/kg ketamine and 10 mg/kg xylazine. Pupils were dilated with 1% tropicamide. Heat from an IDL was delivered through a slit lamp (model 30 SL-M; Carl Zeiss Meditec, Oberkochen, Germany) by a trimode IDK emitting at 810 nm (Iris Medical Instrument, Inc., Mountain View, CA) at a power setting of 50 mW and a beam diameter of 1.2 mm for 60 sec. A series of four laser spots were delivered to the posterior pole of each retina at two disc-diameters from the optic nerve. Fourteen days after heat treatment, eyes were enucleated and dissected into 0.8 μm sections, which were stained with hematoxylin and eosin. The area that had been irradiated by IDL showed no visible structural abnormalities including atrophic change or fibrosis of neural retina, or recruitment of inflammatory cells **(Figure 3).**

To test the effect of heat treatment on choroidal neovascularization, one day following the heat treatment, mice were anesthetized as above and fixed on a rack connected to the slit lamp delivery system. To induce CNV, an argon laser photocoagulation burn was placed in the center of the IDL heat treatment area at a power setting of 300mW and a beam diameter of 50 μm for 0.05 sec to induce CNV. Only eyes in which a subretinal bubble was formed following each burn were included in the study. Seven days following argon photocoagulation, mice were perfused with concanavalin A lectin (20 μg/ml in PBS)(Vector Laboratories, Burlingame, CA), then the eyes were enucleated and fixed in 2% paraformaldehyde. The RPE-choroid-sclera complex was flat mounted and was imaged using a Zeiss fluorescence microscope (Univision, Carl Zeiss Meditec). The neovascular area was measured using Scion Image software (version 4.0.2; Scion Corp.). Laser-induced CNV was visualized and measured in choroidal flat mounts. The mean size of neovascular areas in heat-treated mice was only 15 % of control mice **(Figure 4).**
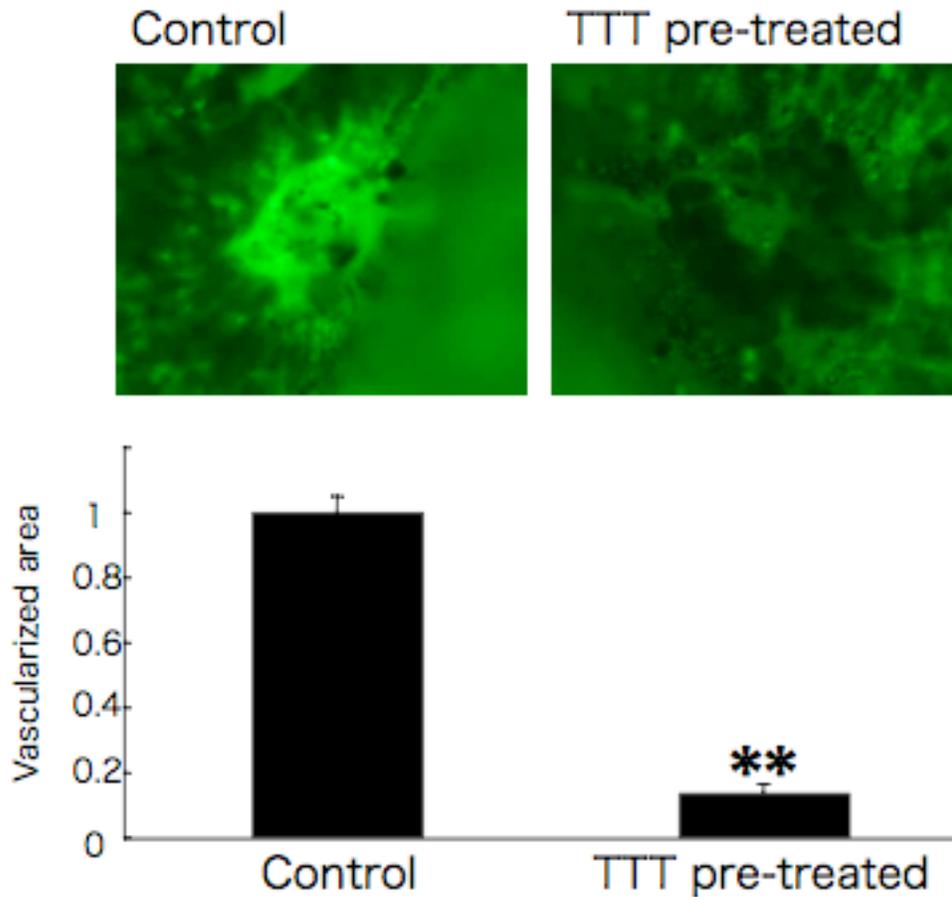
Figure 3. Pretreatment of the retina with heat reduced CNV in vivo without causing tissue damage.

(A) Representative micrographs of PC-induced CNV in retinas with no pretreatment and in retina that had been pretreated with TTT. CNV was visualized in choroidal flat mounts by fluorescein angiography. Hyperfluorescent areas were quantified. Values are means ± SE (n=6).
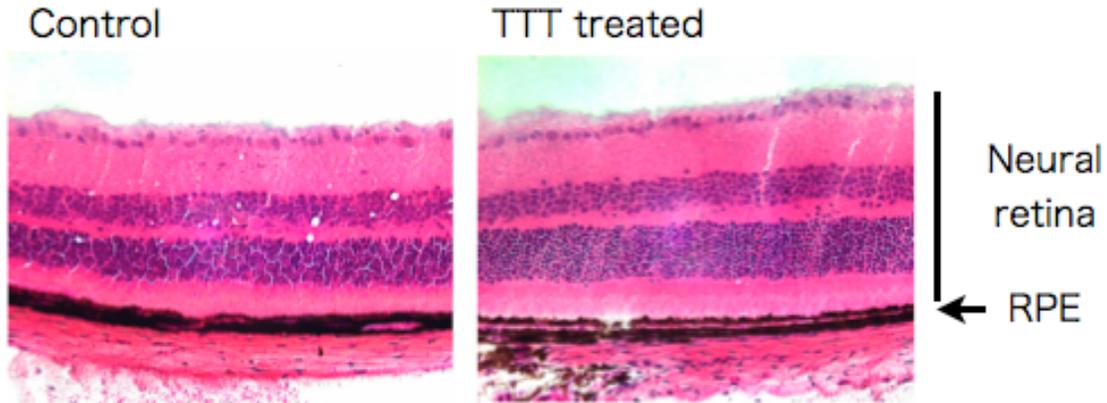
Figure 4. Pretreatment of the retina with heat reduced CNV in vivo without causing tissue damage.
(B) Untreated and TTT treated mouse retina. Fourteen days after TTT treatment, mouse retina was sectioned, and stained with hematoxylin and eosin.

KEY RESEARCH ACCOMPLISHMENTS:
• Heat treatment of RPE stimulates their production of tropoelastin mRNA and protein
• Heat treatment of the murine retina does not disturb its architecture
• Heat treatment of the murine retina reduces choroidal neovascularization following laser injury

REPORTABLE OUTCOMES:
Eiichi Sekiyama, Magali Saint-Geniez, Kazuhito Yoneda, Toshio Hisatomi, Shintaro Nakao, Tony E. Walshe, Kazuichi Maruyama, Ali Hafezi-Moghadam , Joan W. Miller , Shigeru Kinoshita, and Patricia A. D'Amore. Heat treatment of retinal pigment epithelium induces production of elastic lamina components and anti-angiogenic activity. Submitted to FASEB J.

CONCLUSION:
The use of heat treatment stimulates the production of matrix components by RPE cells in vitro and can block experimental new vessel growth in vivo. These results suggest a possible therapeutic application of heat for the treatment of choroidal neovascularization.

APPENDICES:
Manuscript:
"Heat treatment of retinal pigment epithelium induces production of elastic lamina components and anti-angiogenic activity." Submitted to FASEB J.
See Appendix (4).

Task 9
Peter Bex, Ph.D.
Title: Quantification of visual distortion in visual impairment

INTRODUCTION:
Visual distortions, termed metamorphopsia, cause recognition problems for faces, objects and text and are frequently reported by people with visual impairments following retinal or cortical insult. Metamorphopsia is typically measured qualitatively with an Amsler chart, which requires patients to report their subjective impression of distortions in a grid pattern. These subjective data have poor sensitivity and specificity and do not provide any numeric quantification that can be used to evaluate clinical intervention. Accurate quantification of the magnitude of visual distortion is important in order to monitor progression of visual impairment and to develop and assess treatment and rehabilitation outcomes. In this project, we develop and evaluate simple methods that quickly and accurately quantify visual distortions with two dichoptic (separate control of images in each eye) and one monocular method. These behavioral data will be compared with structural imaging data. These data can be used to quantify the magnitude of visual impairment and monitor progression and rehabilitation outcomes.

BODY:
Experiment 1
Visual distortions were measured across the visual field with a monocular spatial discrimination task. A pair of *standard* lines separated by a fixed interval of 0.5 degrees was presented at one of 10 locations, between 8 degrees left and 8 degrees right of fixation. A similar pair of *match* lines was presented at the same eccentricity on the opposite side of fixation. The separation between the match lines was under computer control to determine the separation between that matched that of the standard lines. The observer's task was to indicate on which side the separation was larger. An illustration of the stimuli is shown in Figure 1.1.
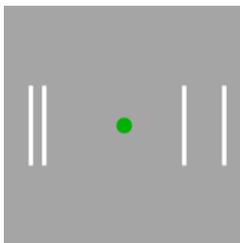

Figure 1.1: Illustration of the stimuli Employed in Experiment 1
Spatial matching data are shown in Figure 1.2 for 5 normally-sighted observers. The abscissa shows the horizontal eccentricity of the matching lines, the ordinate shows the relative separation at which the match lines appeared equally separated. A value of 1 means lines that were *physically* equally-spaced were *apparently* equally spaced. Most of the data clearly deviate from this value, therefore that unequal physical spacing was required to produce equal apparent separation. These data indicate that there are clear, idiosyncratic distortions even in the normally-sighted observers tested.
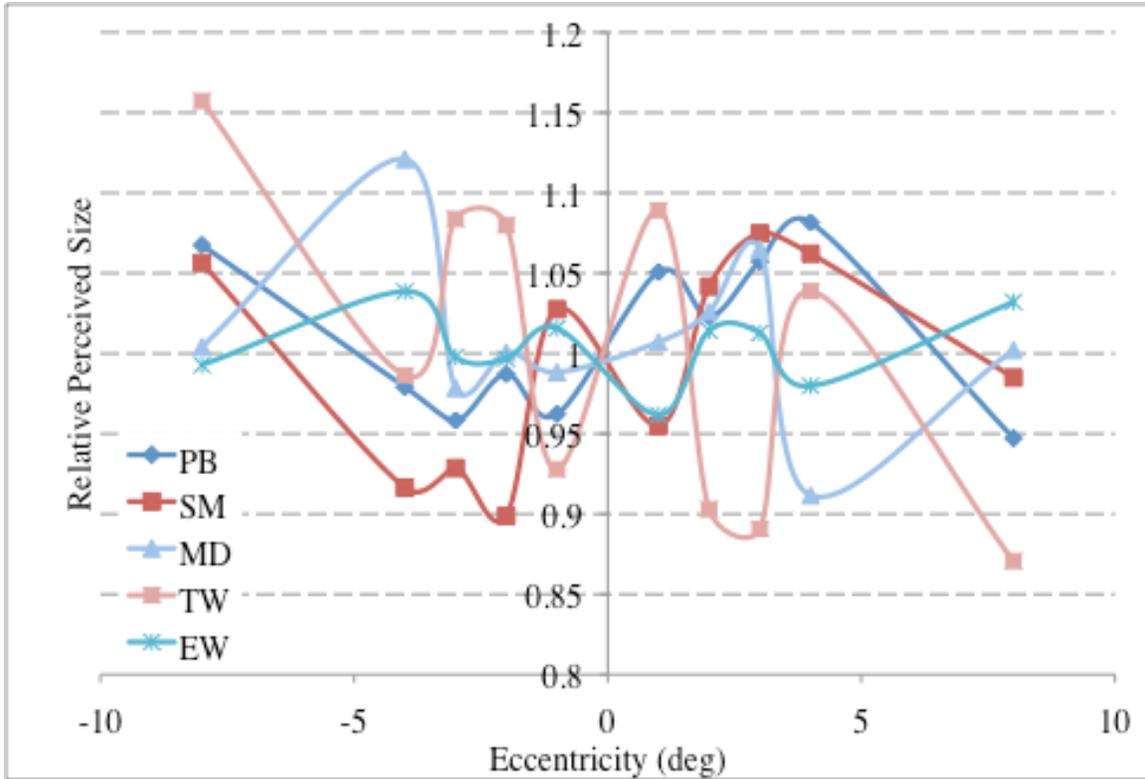
Figure 1.2: Relative Apparent Size as a function of Eccentricity for 5 subjects indicated by the caption. The abscissa shows the location of a pair of lines, separated by 0.5 degrees. The ordinate shows the relative matching separation between an identical pair of lines at the same eccentricity on the opposite side of fixation.

Experiment 2

Next, we developed a dichoptic pointing task that provides an estimate of the spatial distortion between the eyes. An illustration of the stimuli is shown in Figure 2.1 A stereo system was used to control the stimuli presented to each eye. A prominent green fixation point was presented in the center of a computer screen at all times and was visible to both eyes. During the experiment, a series of single white target dots was presented in fixed locations to one eye of each participant on a notional 8 deg by 8 deg grid. Target dots were not visible to the other eye. Figure 2.1a shows all 16 test locations, in practice each target dot was presented one at a time in random order. A cross-hair target was presented simultaneously to the 2nd eye, but was not visible to the 1st eye. The location of the cross hair marker was under the control of a computer mouse. The observer's task was to maintain fixation on the central green point at all times and to center the cross hair on the target dot by moving the computer mouse and clicking the mouse button. This process was repeated until all 16 test location had been completed and the whole procedure was repeated a minimum of 4 times for each observer.
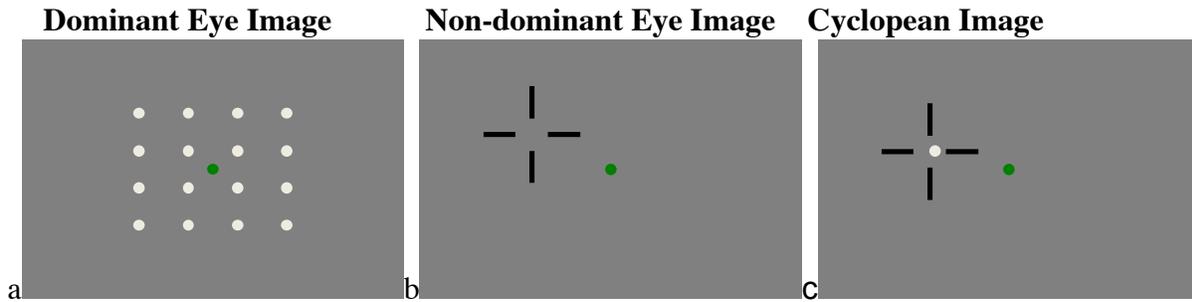
Dominant Eye Image   **Non-dominant Eye Image**   **Cyclopean Image**

Figure 2.1: Illustration of the stimuli a) 16 target dots were presented to the dominant eye, one at a time in random order and were not visible to the non-dominant eye. b) A cross hair, under the control of a computer mouse, was presented to the non-dominant eye and was not visible to the dominant eye. c) The cyclopean percept was a single screen containing a fixed white target dot and a moveable black coss hair, along with a green fixation point.

Figure 2.2 shows dichoptic alignment data for two observers, both of who had 6/6 acuity in both eyes, no ocular pathology and did not report irregularities on an Amsler chart. Blue circles show the horizontal and vertical (x,y) co-ordinates of the target, seen only by the dominant eye. Orange squares show the (x,y) coordinates of the cross hairs, seen only by the non-dominant eye, at which the cross hairs and target dot were vertically and horizontally. Differences between these points represent visual distortions between the eyes. The data are the mean of 4 repetitions of the task, error bars show ±1 standard deviation. For each observer, the mean distance between the physical and perceived location provides an overall estimate of inter-ocular distortion. Note that these distortions potentially arise from either or both eyes. It can be seen that target placement for observer S1 is much closer to the physical location of the targets than for S2. This difference can be quantified by the mean (and standard deviation) alignment error which was 0.09° (0.05°) for observer S1 and 0.45° (0.23°) for observer S2.
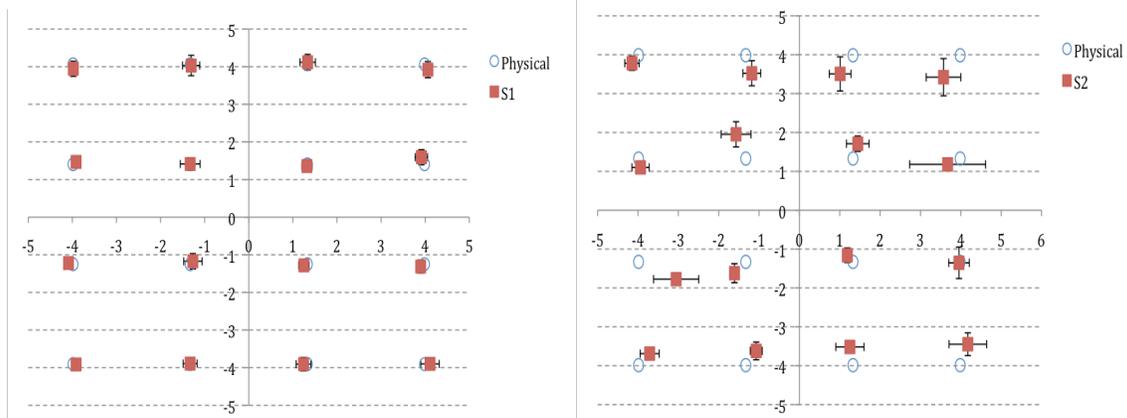
Figure 2.2: Dichoptic alignment for 2 subjects indicated by the caption. Open circles show the physical locations of target dots in the dominant eye, orange squares show the location of the cross hair in the non dominant eye producing best vertical and horizontal alignment. Error bars show the standard deviation of 4 repetitions of the alignment task.

Experiment 3

Lastly, we developed a motion-based inter-ocular alignment task. An illustration of the stimuli is shown in Figure 3.1. The stimuli and methods were similar to those in Experiment

2, except that apparent motion was induced between the eyes. One dot was presented only to the 1st eye, a 2nd dot was presented only to the 2nd eye in temporal sequence every 3 video frames (25 msec), as illustrated in Figure 3.1. When the dots are in the same perceived location, the appearance is a single, stationary dot, however, when the two dots are in non-corresponding perceived locations, the appearance is of a single dot moving back and forth (red arrow, Figure 3.1c). The observer's task was to maintain fixation on the central green point at all times and to use the up/down and left/right arrow keys on the computer keyboard to change the position of the 2nd dot to cancel any apparent motion of the dot pair. Once the apparent motion was nulled, the observer pressed the space button, which initiated the next trial. This process was repeated until all 16 test location had been completed and the whole procedure was repeated a minimum of 4 times for each observer.

Dominant Eye   **Non-dominant Eye**   **Cyclopean View**

a   b   c
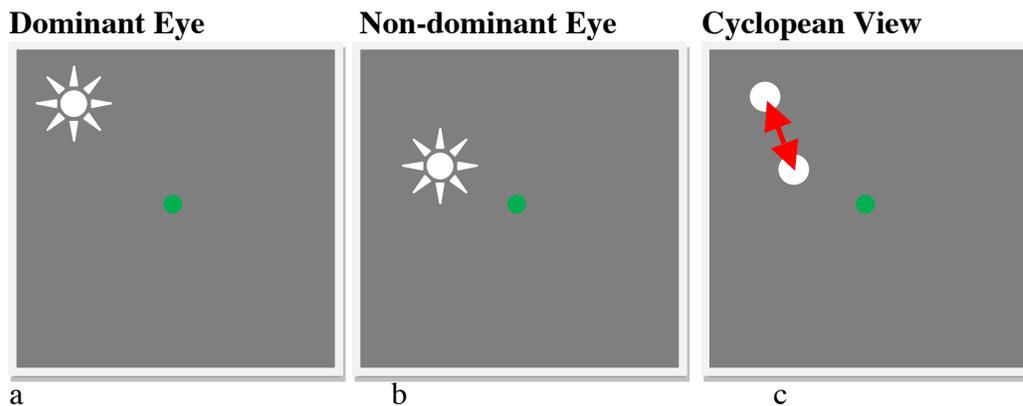
Figure 3.1: Illustration of the stimuli a) a single white dot was presented to the dominant eye in a fixed location, alternating on or off every 3 video frames (25 msec), but was not visible to the non-dominant eye. b)) a single white dot was presented to the non-dominant eye in a location that was under the observer's control. This adjustable dot alternating in anti-phase relative to the fixed dot and was not visible to the dominant eye. c) The cyclopean percept was a white dot moving back and forth, along the trajectory of the red arrow (not present in the experiment).

Figure 3.2 shows motion nulling data for 4 observers, all of whom had 6/6 acuity or better in both eyes. Red lines show the horizontal and vertical (x,y) co-ordinates of the target and motion nulling dots that cancelled dichoptic apparent motion. The length and orientation of the red lines represent visual distortions between the eyes. The data are the mean of at least 4 repetitions of the task, the blue ellipses show ±1 standard deviation along horizontal and vertical axes. For each observer, the mean vector length of the red lines location provides an overall estimate of inter-ocular distortion. Note that these distortions potentially arise in either or both eyes. It can be seen that target placement for 3 observers (LL, TW and TC) are centered on the physical locations of the targets, while observer PB (a strabismic amblyope) shows large inter-ocular distortions. Response precision is also higher in 3 observers (LL, PB and TW).

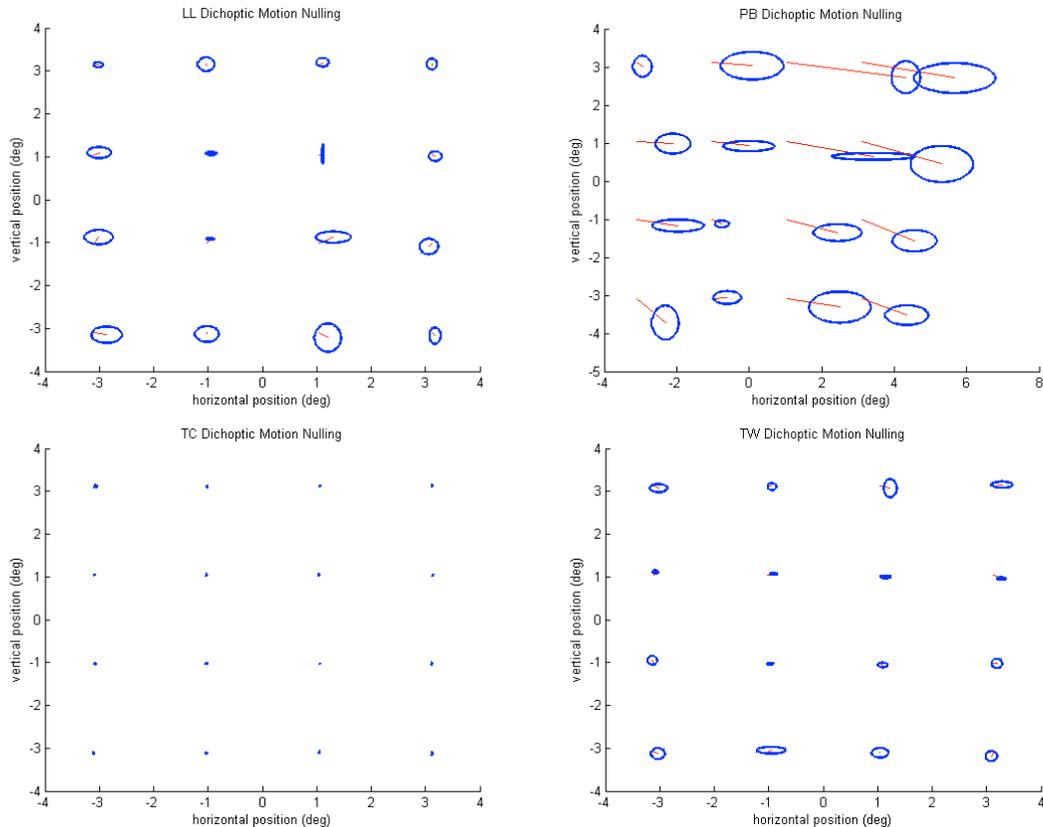**Figure 3.2**: Dichoptic Motion Nulling for 4 subjects. The origins of the red lines show the physical locations of the target dots, then end shows the locations of the motion nulling dots that canceled apparent motion of the dots. Blue ellipses show one standard deviation on the horizontal and vertical nulling location estimates from a minimum of 4 repetitions of the task.

KEY RESEARCH ACCOMPLISHMENTS:
Bulleted list of key research accomplishments emanating from this research.
- 3 novel computer-based tasks have been developed that measure visual distortions
- These tests are based on simple tasks that can be performed quickly and efficiently by normally-sighted and visually-impaired observers
- Each task provides a quantitative estimate of distortion at a local and global scale across the visual field
- Monocular visual distortions are common across the visual field of normally-sighted observers
- Interocular distortions are insignificantly small in normally-sighted observers
- Interocular distortions are large and systematic in visually-impaired observers

REPORTABLE OUTCOMES:
These results will form the basis of a report to be submitted for publication.

CONCLUSION:

- There are clear distortions in the visual field of normally sighted observers who do not report seeing any visual distortions on a standard Amsler chart.
- This result is surprising and provides novel insights into the perception of visual space in normally-sighted people
- These results provide a quantitative method to measure the presence topography and magnitude of visual distortions.
- These methods provide a basis for measuring the magnitude of visual distortions during rehabilitation therapy.

Appendix 1

Task 2
Reza Dana, M.D., M.P.H., M.Sc.
Title: Molecular regulation of the ocular surface stem cell niche: A new paradigm for regenerative medicine

Manuscript:
"Dependence of Corneolimbal Progenitor Cells on Ocular Surface Innervation"
Hiroki Ueno[1,2], Giulio Ferrari[1,2,3], Takaaki Hattori[1,2], Daniel R. Saban[1,2], Sunil K. Chauhan[1,2], and Reza Dana[1,2]

Dependence of Corneolimbal Progenitor Cells on Ocular Surface Innervation

Hiroki Ueno[1,2], Giulio Ferrari[1,2,3], Takaaki Hattori[1,2], Daniel R. Saban[1,2],

Sunil K. Chauhan[1,2], and Reza Dana[1,2]

[1] Schepens Eye Research Institute, Boston, MA 02114

[2] Massachusetts Eye and Ear Infirmary, Harvard Medical School, Boston, MA 02114

[3] Bietti Eye Foundation, IRCCS Rome, Italy.

Word count: 2879

Corresponding author:

Reza Dana, M.D., M.P.H., M.Sc.

Schepens Eye Research Institute, Harvard Medical School

20 Staniford Street, Boston, MA 02114

Email: reza.dana@schepens.harvard.edu

Phone: 617-912-7401, Fax: 617-912-0117

ABSTRACT

Purpose: Neurotrophic keratopathy (NK) is a corneal degeneration associated with corneal nerve dysfunction. It can cause corneal epithelial defects, stromal thinning, and perforation. However, it is not clear if and to which extent epithelial stem cells are affected in NK. The purpose of this study was to identify the relationship between corneolimbal epithelial progenitor/stem cells and sensory nerves using a denervated mouse model of NK.

Methods: NK was induced in mice by electro-coagulation of the opthalmic branch of the trigeminal nerve. The absence of corneal nerves was confirmed with beta-III tubulin immunostaining and blink reflex test after 7 days. ABCG2, p63 and Hes1 were chosen as corneolimbal stem cell markers and assessed in denervated mice versus controls by immunofluorescent microscopy and real-time PCR. In addition, corneolimbal stem cells were detected as side population cells using flow cytometry, and colony-forming efficiency assay was performed to assess their function.

Results: ABCG2, p63 and Hes1 immunostaining were significantly decreased in denervated eyes after 7 days. Similarly, the expression levels of ABCG2, p63 and Hes1 transcripts were also significantly decreased in denervated eyes. Stem cells measured as side population from NK mice were decreased by approximately 75% compared to normals. In addition, we found a significant (p=0.038) reduction in colony-forming efficiency of stem cells harvested from denervated eyes.

Conclusions: Corneolimbal stem cells are significantly reduced after depletion of sensory nerves. Our data suggest a critical role of innervation in maintaining stem cells and/ or the stem cell niche.

INTRODUCTION

Corneolimbal epithelial stem cells are a small subpopulation of oligopotent cells located primarily in the basal epithelial layer of the limbus. They produce undifferentiated progeny with limited proliferative potential that migrate centripetally from the periphery of the cornea to replace cells desquamating during normal life.[1-7] Corneal limbal stem cells reside primarily in the palisades of Vogt in a niche which maintains their "stemness" by producing a unique anatomical and functional milieu.[8,9] Although the exact anatomical location of the niche is thought to be the limbus in humans, it has recently been proposed that epithelial stem cells of equal potency are distributed throughout the entire ocular surface in other mammals.[10]

Detection of corneal epithelial stem cells is the object of controversy between many groups, as there is still no universal consensus over which marker(s) should be used. Side population (SP) cell detection is one of the most consistent methods to quantify these cells. Stem cells express the SP phenotype based on the ability to efflux the DNA-binding dye Hoechst 33342.[11-13] SP cells have also been identified in the hematopoietic compartments of different species, and have been isolated from various other adult tissues[12,13]. These findings suggest that the SP phenotype represents a common feature of adult tissue-specific stem cells, and the same method has been used to isolate stem cells from human, rabbit, rat and mouse limbuses.[14-17]

The cornea is the most densely innervated tissue in the body, being 400 times more sensitive than the skin.[18] Corneal nerves, in addition to their well known sensory

function, help maintain the integrity of the ocular surface by releasing epitheliotrophic substances that promote corneal surface health.[19] The limbus, where stem cells reside, is densely innervated; however, the role of these nerves is poorly understood.[20] It has been suggested that various nerve-secreted factors and neuropeptides such as nerve growth factor (NGF), substance P, acetylcholine and brain-derived neurotrophic factor (BDNF) could influence corneal stem cells, and play a role in maintaining epithelial integrity, and promote epithelial proliferation.[19] It has also been shown that human corneal stem cells express TrkA which is a high affinity receptor for NGF.[21-23] Moreover, corneal limbal stem cells grown in the presence of both epidermal growth factor (EGF) and nerve-secreted factors show the highest rate of colony expansion in vitro compared with EGF alone.[24] However, the influence of corneal denervation on epithelial stem cells has not yet been studied *in vivo*.

The purpose of the present study was to elucidate the relationship between corneal progenitor/stem cells and trigeminal nerves *in vivo* using a mouse model of denervated cornea. Herein, we hypothesize that corneal stem cell survival and/or function is dependent on intact corneal innervation. Our data demonstrate that sensory nerves deprivation of cornea affects stem cell homeostasis and lead to a significant decrease in both the frequency and the function of corneolimbal stem cells.

METHODS

Animals

Six to 8 week-old male C57BL/6 mice (Taconic Farms, Germantown, NY) were used for this study. The research protocol was approved by the Schepens Eye Research Institute Animal Care and Use Committee, and it conformed to the standards of the Association for Research in Vision and Ophthalmology Statement for the Use of Animals in Ophthalmic and Vision Research.

Experimental procedure

NK was induced in mice by electro-coagulation of the opthalmic branch of the trigeminal nerve, as previously described by Ferrari et al.[25] Briefly, animals were anesthetized with a Ketamine (100mg/ml)-Xylazine (20mg/ml) Acepromazine (15mg/ml) mixture. The animal was then mounted in the stereotactic frame and a median incision was made on the skull. The bregma (the point of conjunction of coronal and sagittal suture) was identified and chosen as a point of reference. The skull was opened with a dental drill, and a conductive electrode was lowered at 3 different locations on the ophthalmic trigeminal nerve and a 2 mA current was passed.

After removal of the electrode, the skin of the skull was sutured. In addition, a tarsorrhaphy (lid closure) was performed to reduce the risk of infection, and to assure that the effect on progenitor/stem cells is primarily due to the direct derervation but not secondary to the dryness caused by abolishment of blink reflex and loss of tears. Tarsorrhaphy was kept on for the entire length of the study until day 7. Finally antibiotic

ointment was placed on the suture and Buprenorphine (0.1mg/Kg body weight every 8-12 hours for 72 hours) and 1 ml of saline were injected subcutaneously. Corneal sensitivity using a cotton filament was recorded pre- and post-operatively comparing the blinking of the treated eye (left) with the control eye (right). The effectiveness of the procedure was confirmed by biomicroscopy of the cornea, testing blink reflex and immunostaining with β tubulin III (neural marker) at 7 days after the procedure. All the animals used for the experiments showed an abolished blink reflex. All animals were euthanized by carbon dioxide overdose followed by cervical dislocation. All the procedures were performed in the Schepens Eye Research Institute Animal Facility, following an approved protocol.

Isolation of corneal epithelial Cells

On day-7 post-experimental procedure, corneas from normal and denervated animals (n = 8 per group) were obtained by scissor dissection under an operating microscope. Corneal epithelial cells were freshly isolated from the normal and denervated eyes after ethylenediaminetetraacetic acid (EDTA) (Sigma)-mediated removal of the corneal stroma and incubated for 60 minutes at 37°C. The corneal epithelium was subjected to digestion with DNase I (Roche Diagnostics) / trypsin (Gibco)-EDTA for 45 minutes at 37°C. After incubation, the harvested cell suspension was filtrated through a nylon mesh and centrifuged for 10 minutes at 1250rpm. The pellet was resuspended in 1.0 mL of Dulbecco's Modified Eagle's Medium (DMEM) with 10% fetal calf serum (FCS), and the number of cells was determined by hemocytometry.

Immunohistochemistry

Cryostat sections of 5 μm thickness were prepared from tissue embedded in Tissue-Tek OCT compound (Sakura Finetek, USA). After fixation with cold acetone for 10 minutes, the tissues were incubated with 10% goat serum containing 0.3% Triton X-100 (room temperature (RT), 1 hour) for ATP-binding cassette subfamily G member 2 (ABCG2), and with 2% bovine serum albumin and goat serum (RT, 30 minutes) for hairy enhancer of split 1 (Hes1).[26] For ABCG2 staining, overnight incubation with a rat monoclonal antibody anti-BCRP/ABCG2 (20x) (Abcam) was performed. For Hes1 staining, rabbit anti-Hes1 polyclonal antibody (1,000x) was used (a gift from Dr. T. Sudo, Toray Industries, Japan). The sections were then incubated (RT, 1 hour) with the appropriate primary antibody and washed three times in phosphate-buffered saline (PBS) containing 0.15% Triton X-100 for 15 minutes. Antibody binding was detected by Alexa 488-conjugated secondary antibodies (Invitrogen-Molecular Probes, Germany). The slides were washed (three times) in phosphate-buffered saline (PBS) containing 0.15% Triton X-100 for 15 minutes. Nuclear counterstaining was performed with 4, 6-diamidino-2-phenylindole (DAPI, Vectashield). For p63 staining, after fixation with a cold mixture of methanol and acetone for 10minutes, we incubated with MOM mouse IgG blocking reagent (Vectashield; Vector Laboratories, Burlingame, CA,) when we used mouse mAbs (50x) (Dako, Monoclonal Mouse Anti-Human p63: RT, 1 hour). The samples were incubated overnight with the appropriate primary antibody, and were treated with biotinylated second antibody and finally with Cy3-conjugated streptavidin (Jackson Immuno Research, West Grove, PA). The slides were washed three times in phosphate-buffered saline (PBS) for 15 minutes, coverslipped using anti fading mounting

medium containing DAPI and examined under a confocal microscope (Leica TCS 4D; Lasertechnik, Heidelberg, Germany). For β tubulin III staining, the cornea was harvested and fixed in paraformaldehyde 4%, stained with anti-β tubulin III antibody (x200) (Rabbit anti–β tubulin III polyclonal antibody, Chemicon, USA) and with a secondary conjugated antibody (x200) (Donkey anti rabbit IgG FITC, Santa Cruz Biotech). Corneal whole mounts were prepared using a mounting medium. Images were taken at 400X magnification. Control incubations were done with the appropriate normal mouse, rat and rabbit, IgG at the same concentration as the primary antibody.

Real-Time PCR

RNA was isolated (RNeasy Micro Kit; Qiagen, Valencia, CA) and reverse transcribed (Superscript III Kit; Invitrogen, Carlsbad, CA). Real-time PCR was performed using a PCR mix (TaqMan Universal PCR Mastermix; Invitrogen) and preformulated primers for ABCG2 (assay ID Mm00496364_m1), p63 (assay ID Mm00495788_m1), Hes1 (assay ID Mm00468601_m1) and GAPDH (assay ID Mm99999915_gl) (all Applied Biosystems, Austin, TX). Results were analyzed by the comparative threshold cycle method and normalized to GAPDH as an internal control.

Hoechst 33342 Exclusion Assay

Freshly isolated corneal epithelial cells were resuspended at a concentration of 1 X10^6 cells/mL in Dulbecco's Modified Eagle's Medium (DMEM) containing 2% FCS and incubated with 5μg/mL Hoechst 33342 (Sigma-Aldrich) dye. To determine the effect of verapamil on the Hoechst 33342 efflux, the cells were preincubated with verapamil

(50μM; Sigma-Aldrich) before the addition of Hoechst 33342 dye. After the incubation for 60 minutes at 37°C, propidium iodide (2μg/mL) was added to exclude dead cells from the analysis, and the cells were then analyzed on a flow cytometer (LSR II; BD Biosciences). Hoechst 33342 was excited at 350 nm with a UV laser and fluorescence emission was detected through 450-nm band-pass (Hoechst blue) and 660-nm long-pass (Hoechst red) filters.

Colony-Forming Efficiency Assay

3T3 fibroblasts in DMEM containing 10% FCS were treated with MMC for 2.5 hours at 37°C and then treated with trypsin-EDTA and plated at a density of 3x 10^4 cells/well into 12 mm culture plates. Each well was seeded at 1x10^3 cells/well. The cell cultures were incubated at 37°C under 5% CO2 and 95% humidity. The cultures were incubated for 10 days. After 10 days, cultured cells were then stained with rhodamine B for 30 minutes. Colony-forming efficiency (CFE) was calculated as the percentage of colonies per number of inoculated cells.

Statistical Analysis:

Student's *t* test was used for comparison of mean between the groups. Data are presented as mean ± SEM and considered significant at $p < 0.05$.

RESULTS

Establishment of a denervated model using trigeminal stereotactic electrolysis (TSE)

We induced experimental NK in mice by means of TSE (Trigeminal Stereotactic Electrolysis). All the animals used in the experiments showed complete absence of blink reflex after 7 days. The TSE treated animals developed epithelial defects. (Fig 1A and 1B) similar to patients affected by NK. The denervation was confirmed with β tubulin III immunostaining which revealed massive disruption of the sub-basal nerve plexus after TSE (Figure 1C and 1D).

Immunostaining for Stem Cell Markers

Expression of ABCG2, p63 and hairy enhancer of split 1 (Hes1) were observed in the normal corneal limbal cells (Figure 2 A, 2C and 2E). All of these stem cell markers were decreased in the denervated eyes after 7 days (Figure 2 B, 2D and 2F). To further compare and quantify the levels of expression of these markers, we performed real-time PCR.

mRNA Expression Levels of Stem Cell markers

We analyzed the levels of ABCG2, Hes1 and p63 in the normal and denervated corneas by real-time PCR (Fig 3). Denervated corneas showed decreased mRNA expression levels of ABCG2 (5-fold reduction p=0.001), p63 (2-fold reduction p=0.059) and Hes1 (3-fold reduction p=0.006) compared to those in normal corneas.

Quantification of Stem Cells by Means of Side Population Cells

A distinct population of cells with a characteristic tail of low Hoechst 33342 blue-red fluorescence was gated using normal fresh mouse cornea epithelial cells. Side population cells could be detected by verapamil-sensitive disappearance of the tail. We compared the quantification of corneal epithelial stem cells in normal vs. denervated corneas (Fig. 4A). We repeated the experiment three times (8 eyes per experiments), and found that this population comprised only 0.42 ± 0.08% of cells in denervated corneas, compared to 1.99 ± 0.03% of cells in the normal eyes (Fig. 4B). As shown in Figure 4B, an approximately 75% reduction of SP cells was observed 7 days after denervation compared to the healthy eyes ($p<0.001$).

Analysis of Stem Cell Colony- Forming Efficiency (CFE)

We investigated the proliferative potential of corneal epithelial stem cells using the CFE assay (Fig. 5A and 5B). After 10 days of culture, the colony-forming efficiency (number of colonies/ plated cells using a 3T3 feeder layer) of epithelial cells from denervated corneas (3.0±0.4 %) was significantly reduced (~50%) compared to CFE from normal corneas (5.73±1.10%; $p<0.05$).

DISCUSSION

In this study, we used Trigeminal Stereotactic Electrolysis (TSE) to induce neurotrophic keratopathy (NK) in mice. The effectiveness of this technique was confirmed by the development of characteristic neurotrophic epithelial defects, absence of blink reflex, and massive loss of corneal nerves 7 days after TSE. Using this model, we found a significant decrease in corneal epithelial stem cell number and function. To the best of our knowledge, this is the first report showing that sensory deprivation affects stem cells homeostasis in vivo.

Mouse corneal stem cells have been characterized as side population (SP) cells by Krulova M et.al.[17] In the present study using the similar method of quantitative flow cytometry, we observed a significant (75%) decrease in SP cells in denervated eyes. In order to further characterized and quantify these cell population, we studied the expression of stem cell markers, and found 80 % reduction in ABCG2 expression in denervated corneas. Finally, we demonstrated a 50% decrease in stem cell function as tested with the colony-forming efficiency assay. In summary, our data demonstrate that stem cells are affected by denervation both quantitatively and qualitatively.

Recent studies in various animal models have shown that many nerve-secreted peptides such as substance P are important for epithelial regeneration and wound healing, and are significantly reduced in neurotrophic keratitis, which is associated with defective wound healing.[27-30] Amniotic membrane is commonly used in ocular surgery and in the cases of NK as a biological bandage to improve corneal wound healing. It has

been shown that these therapeutic effects are, at least in part, due to neurotrophic factors contained in the amniotic membrane.[31-33] Corneal stem cells have an important role in wound healing. In healthy innervated rabbit, corneal stem cells have been shown to increase five-fold; one day after a scrape injury, and return to normal levels on day two.[34] In contrast, the denervated eyes used in our experiments exhibited evident epithelial defects seven days after TSE (Fig 1A) and no increase, but rather a decrease of stem cells (75% reduction). This, together with the diminished function reflected by the CFE assay could explain why NK eyes are so prone even to minor injuries and develop unhealing ulcers.

Interestingly, a marker for corneal stem cells, ABCG2, is also expressed by neural progenitor cells, suggesting a close relationship between nerves and epithelial stem cells.[35] Although no literature exists regarding the impact of peripheral sensory innervation on epithelial stem cells, there is anecdotal evidence of defective mobilization of bone marrow stem cells in conditions such as diabetes, where peripheral nerves are severely impaired.[36] Similarly, neuro-neoplasmic synapses have also been shown to be associated with tumor stem cell migration and proliferation.[37] Regarding the eye, diabetic keratopathy may represent a paradigm for the dysfunctional interaction between corneal epithelial stem cells and nerves. Diabetic patients suffer severe peripheral neuropathy which is associated with the development of persistent corneal epithelial defects.[38-41] Interestingly, Saghizadeh et al. have recently demonstrated decreased limbal stem cells in human diabetic corneas, which supports our findings that neuropathic states are associated with stem cell dysfunction.[42] However, the high tear glucose concentration

and the protean complications of diabetes make it difficult to fully dissociate the contribution of nerve depletion versus other pathological aspects of the disease, to stem cells reduction. We suggest that our model, which selectively removes sensory innervation from the cornea represents an excellent way to study these interactions.

In conclusion, our results suggest that corneal stem cells are significantly reduced in number and function in our animal model of ocular denervation. We provide novel evidence for the critical role of innervation in maintaining corneal epithelial cells and/or the stem cell niche. It is provocative to speculate that the functional relationship between nerve and stem cells described in this paper could apply to other epithelial / non epithelial stem cells in the body. These findings contribute to our understanding of factors relevant for maintaining the stem cell niche, and suggest new ways of manipulating stem cell number and function, as more sophisticated neuroprotective strategies are developed.

REFERENCES

1. Schermer A, Galvin S, Sun TT. Differentiation-related expression of a major 64K corneal keratin in vivo and in culture suggests limbal location of corneal epithelial stem cells. *J Cell Biol.* 1986;103:49-62.

2. Cotsarelis G, Cheng SZ, Dong G, Sun TT, Lavker RM. Existence of slow cycling limbal epithelial basal cells that can be preferentially stimulated to proliferate: implications on epithelial stem cells. *Cell.* 1989;57:201-209.

3. Kinoshita S, Friend J, Thoft RA. Sex chromatin of donor corneal epithelium in rabbits. *Invest Ophthalmol Vis Sci.* 1981;21:434-441.

4. Buck RC. Measurement of centripetal migration of normal corneal epithelial cells in the mouse. *Invest Ophthalmol Vis Sci.* 1985;26:1296-1299.

5. Kruse FE. Stem cells and corneal epithelial regeneration. *Eye.*1994;8:170-183.

6. Beebe DC, Masters BR. Cell lineage and the differentiation of corneal epithelial cells. *Invest Ophthalmol Vis Sci.* 1996;37:1815-1825.

7. Nagasaki T, Zhao J. Centripetal migration of corneal epithelial cells in the normal adult mouse. *Invest Ophthalmol Vis Sci.* 2003;44:558-566.

8. Stepp MA, Zieske JD. The corneal epithelial stem cell niche. *Ocul Surf.* 2005;3:15-26.

9. Davies SB, Chui J, Madigan MC, et al. Stem cell activity in the developing human cornea. *Stem Cells.* 2009;27:2781-2792.

10. Majo F, Rochat A, Nicolas M, Jaoudé GA, Barrandon Y. Oligopotent stem cells are distributed throughout the mammalian ocular surface. *Nature.* 2008 13;456:250-254.

11. Budak MT, Alpdogan OS, Zhou M, et al. Ocular surface epithelia contain ABCG2-dependent side population cells exhibiting features associated with stem cells. *J Cell Sci*. 2005;118:1715-1724.

12. Goodell MA, Rosenzweig M, Kim H, et al. Dye efflux studies suggest that hematopoietic stem cells expressing low or undetectable levels of CD34 antigen exist in multiple species. *Nat. Med.* 1997;3:1337-1345.

13. Storms, R.W., Goodell, M.A., Fisher, A., Mulligan, R.C. and Smith, C. Hoechst dye efflux reveals a novel CD7(+)CD34(-) lymphoid progenitor in human umbilical cord blood. *Blood.* 2000;96:2125–2133.

14. Watanabe K, Nishida K, Yamato M, et al. Human limbal epithelium contains side population cells expressing the ATP-binding cassette transporter ABCG2. *FEBS Lett.* 2004;565:6–10.

15. Umemoto T, Yamato M, Nishida K, et al. Limbal epithelial side-population cells have stem cell-like properties, including quiescent state. *Stem Cells.* 2006;24:86-94.

16. Umemoto T, Yamato M, Nishida K, et al. Rat limbal epithelial side population cells exhibit a distinct expression of stem cell markers that are lacking in side population cells from the central cornea. *FEBS Lett.* 2005;579:6569-6574.

17. Krulova M, Pokorna K, Lencova A, et al. A rapid separation of two distinct populations of mouse corneal epithelial cells with limbal stem cell characteristics by centrifugation on percoll gradient. *Invest Ophthalmol Vis Sci.* 2008;49:3903-3908.

18. Nishida T. Neurotrophic mediators and corneal wound healing. *Ocul Surf.* 2005;3:194-202.

19. Goins KM. New insights into the diagnosis and treatment of neurotrophic keratopathy. *Ocul Surf.* 2005;3:96-110.

20. Li W, Hayashida Y, Chen YT, Tseng SC. Niche regulation of corneal epithelial stem cells at the limbus. *Cell Res.* 2007;17:26-36.

21. Touhami A, Grueterich M, Tseng SC. The role of NGF signaling in human limbal epithelium expanded by amniotic membrane culture. *Invest Ophthalmol Vis Sci.* 2002;43:987-994.

22. Qi H, Chuang EY, Yoon KC, et al. Patterned expression of neurotrophic factors and receptors in human limbal and corneal regions. *Mol Vis.* 2007;13:1934-1941.

23. Qi H, Li DQ, Shine HD, et al. Nerve growth factor and its receptor TrkA serve as potential markers for human corneal epithelial progenitor cells. *Exp Eye Res.* 2008;86:34-40.

24. Meyer-Blazejewska EA, Kruse FE, Bitterer K, et al. Preservation of the limbal stem cell phenotype by appropriate culture techniques. *Invest Ophthalmol Vis Sci.* 2010;51:765-774.

25. G. Ferrari, et al. *IOVS* 2010;51:ARVO E-Abstract 4787. *[Full length manuscript has been submitted to IOVS, and is currently under revision]*

26. Nakamura T, Ohtsuka T, Sekiyama E, et al. Hes1 regulates corneal development and the function of corneal epithelial stem/progenitor cells. *Stem Cells.* 2008;26:1265-1274.

27. Morishige N, Komatsubara T, Chikama T, Nishida T. Direct observation of corneal nerve fibres in neurotrophic keratopathy by confocal biomicroscopy. *Lancet.* 1999;354:1613-1614.

28. Chikama T, Fukuda K, Morishige N, Nishida T. Treatment of neurotrophic keratopathy with substance-P-derived peptide (FGLM) and insulin-like growth factor I. *Lancet.* 1998;351:1783-1784.

29. Nishida T, Chikama T, Morishige N, et al. Persistent epithelial defects due to neurotrophic keratopathy treated with a substance p-derived peptide and insulin-like growth factor 1. *Jpn J Ophthalmol.* 2007;51:442-447.

30. Araki-Sasaki K, Aizawa S, Hiramoto M, et al. Substance P-induced cadherin expression and its signal transduction in a cloned human corneal epithelial cell line. *J Cell Physiol.* 2000;182:189-195.

31. Solomon A, Meller D, Prabhasawat P, et al. Amniotic membrane grafts for nontraumatic corneal perforations, descemetoceles, and deep ulcers. *Ophthalmology.* 2002;109:694-703.

32. Chen HJ, Pires RT, Tseng SC. Amniotic membrane transplantation for severe neurotrophic corneal ulcers. *Br J Ophthalmol.* 2000;84:826-833.

33. Coassin M, Lambiase A, Micera A, et al. Nerve growth factor modulates in vitro the expression and release of TGF-beta1 by amniotic membrane. *Graefes Arch Clin Exp Ophthalmol.* 2006;244:485-491.

34. Park KS, Lim CH, Min BM, et al. The side population cells in the rabbit limbus sensitively increased in response to the central cornea wounding. *Invest Ophthalmol Vis Sci.* 2006;47:892-900.

35. Yoshida S, Shimmura S, Nagoshi N, et al. Isolation of multipotent neural crest-derived stem cells from the adult mouse cornea. *Stem Cells.* 2006;24:2714-2722.

36. Kang L, Chen Q, Wang L, et al. Decreased mobilization of endothelial progenitor cells contributes to impaired neovascularization in diabetes. *Clin Exp Pharmacol Physiol.* 2009;36:47-56.

37. Zänker KS. The neuro-neoplastic synapse: does it exist? *Prog Exp Tumor Res.* 2007;39:154-161.

38. De Cillà S, Ranno S, Carini E, et al. Corneal subbasal nerves changes in patients with diabetic retinopathy: an in vivo confocal study. *Invest Ophthalmol Vis Sci.* 2009;50:5155-5158.

39. Rosenberg ME, Tervo TM, Immonen IJ, et al. Corneal structure and sensitivity in type 1 diabetes mellitus. *Invest Ophthalmol Vis Sci.* 2000;41:2915-2921.

40. Hyndiuk RA, Kazarian EL, Schultz RO, Seideman S. Neurotrophic corneal ulcers in diabetes mellitus. *Arch Ophthalmol.* 1977;95:2193-2196.

41. Lockwood A, Hope-Ross M, Chell P. Neurotrophic keratopathy and diabetes mellitus. *Eye.* 2006;20:837-839.

42. M. Saghizadeh, et al. *IOVS* 2010;51:ARVO E-Abstract 2954.

FIGURE LEGENDS

Figure 1.

NK induced in a mouse model by means of trigeminal stereotactic electrolysis.

Representative biomicroscopy of a normal cornea (A) and of a denervated cornea after 7

days (B). Beta III tubulin immunostaining of normal and denervated corneas. (C) Normal

cornea, note regular sub-basal and epithelial nerve plexus. (D) Denervated cornea, note

massive disruption of the sub-basal nerve plexus.

Figure 2

Decreased expression of stem cell markers after denervation. Representative

immunostained micrographs of cross section of normal (A, C and E) and denervated (B,

D and F) corneas showing expression of stem cell markers. ABCG2 (B), p63 (D) and

Hes1 (F) expression were decreased in denervated eyes after 7days compared to those

in normal eyes (A, C, E).

Figure 3

Diminished mRNA expression levels of stem cell markers after denervation.

Transcript levels of ABCG2, p63 and Hes1 in the cornea are shown. ABCG2 and Hes1

were significantly decreased in denervated corneas. An approximately 2-fold reduction

of p63 was also observed, although this was not statistically significant. The dotted line

represents expression of mRNA in normal corneas. Bars represent mean ± SEM. (* p<

0.01)

Figure 4

Reduced side population (SP) cells in denervated eyes. (A) Representative flow cytometric dot plots showing analyses of the frequencies of corneal stem cells by means of SP cells. Note the disappearance of the low Hoechst 33342 blue-red fluorescence population, which represents stem cells, after verapamil addition. (B) Mean SP cells in normal and denervated corneas from three different experiments. SP cell frequencies were 1.99±0.03% and 0.42±0.08% of total epithelial cells in normal and denervated corneas, respectively. Bars represent mean ± SEM. (* p<0.001)

Figure 5.

Decreased stem cell function measured by colony-forming efficiency (CFE) assay after denervation. (A) Representative photomicrographs of CFE plates from normal and denervated corneal epithelial cells. (B) Quantification of CFE. CFE of normal corneal epithelial cells were 5.73±1.10%, whereas CFE of denervated corneal epithelial cells were 3.0±0.4 %. Bars represent mean ± SEM. (* p<0.05).
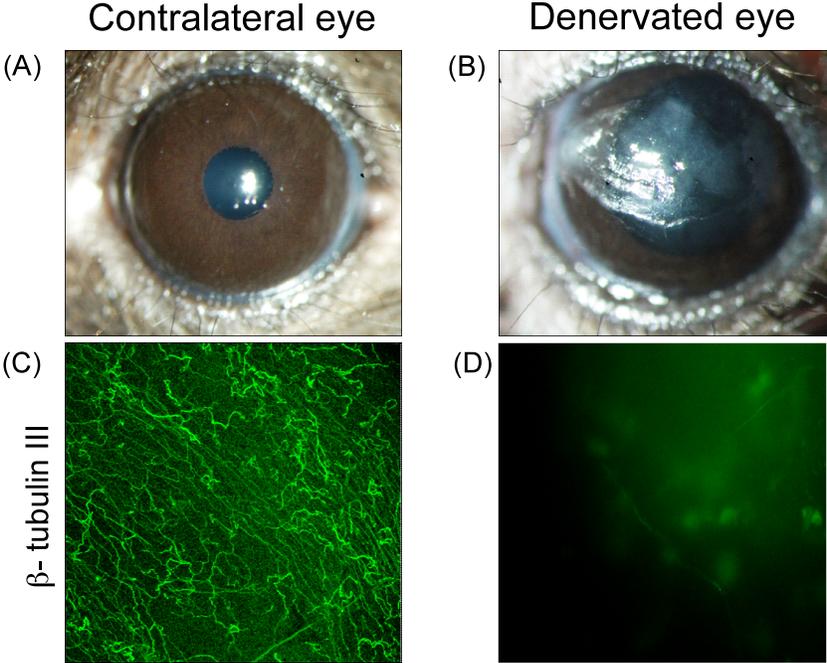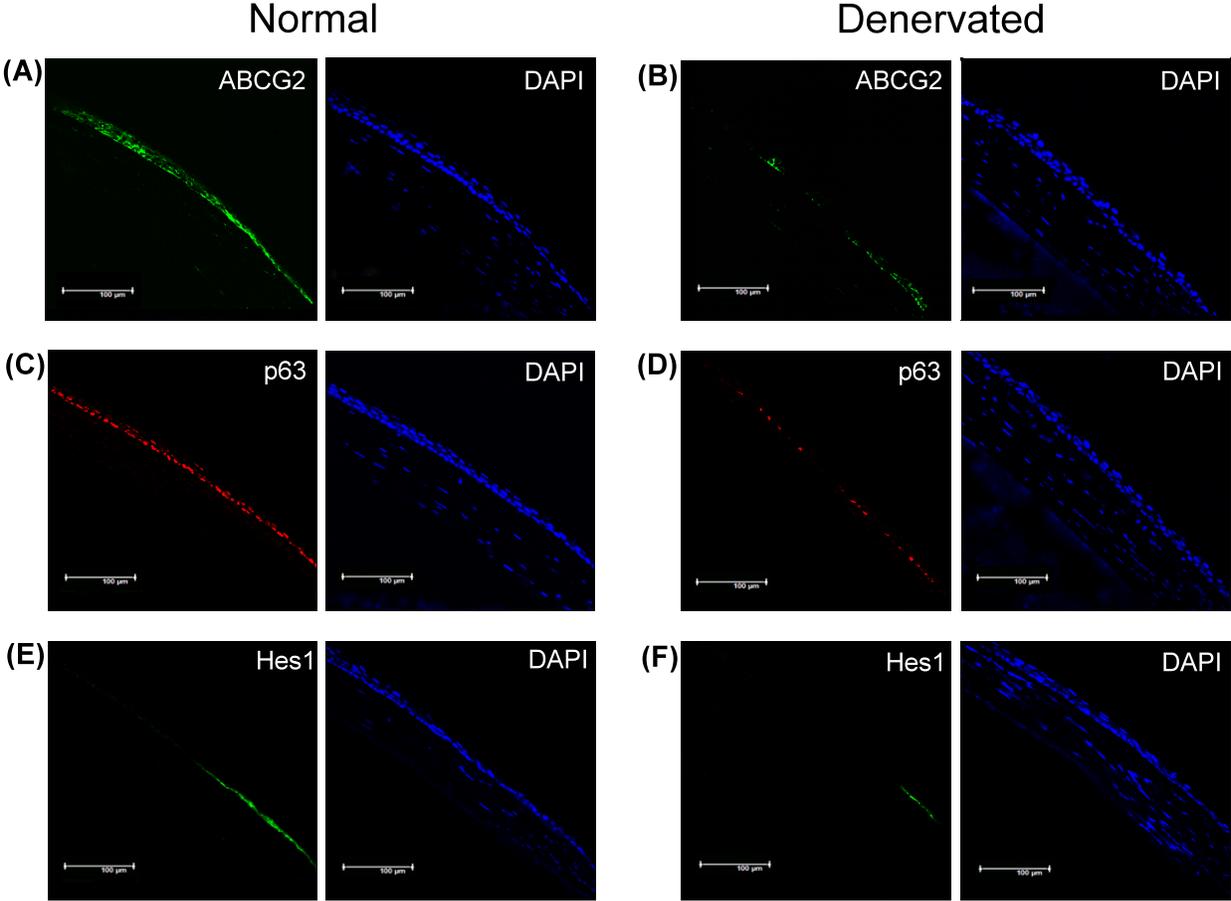
Figure 1.

Contralateral eye   Denervated eye

(A)   (B)

(C)   (D)

β- tubulin III

Figure 2.

Figure 3.

Figure 4.
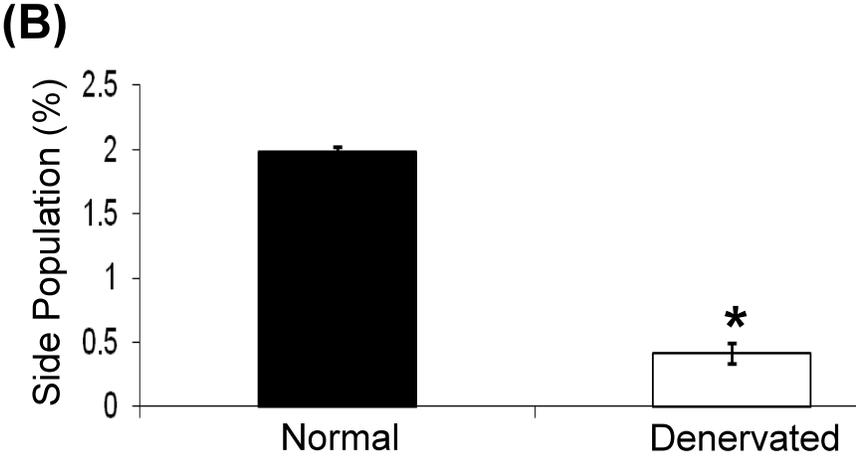
(A)

(B)

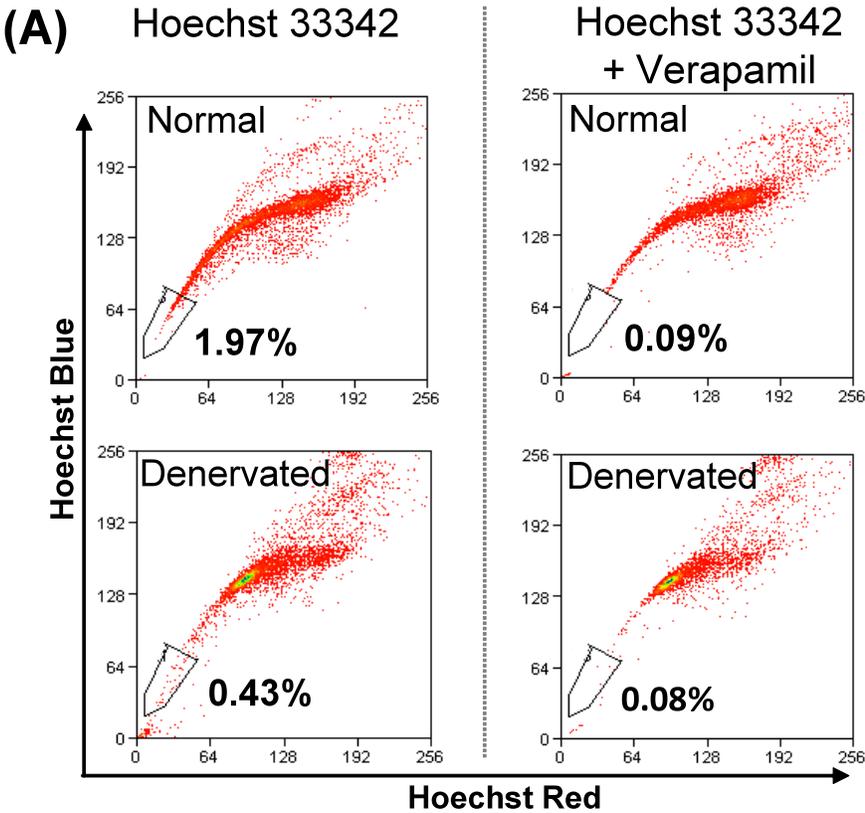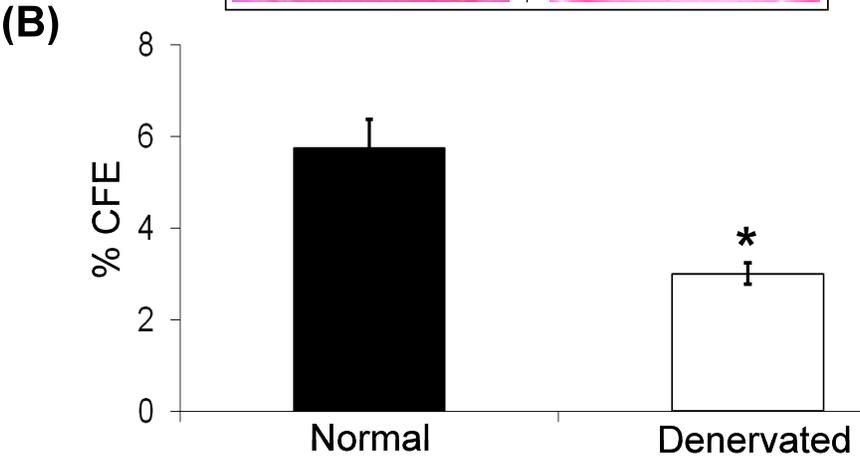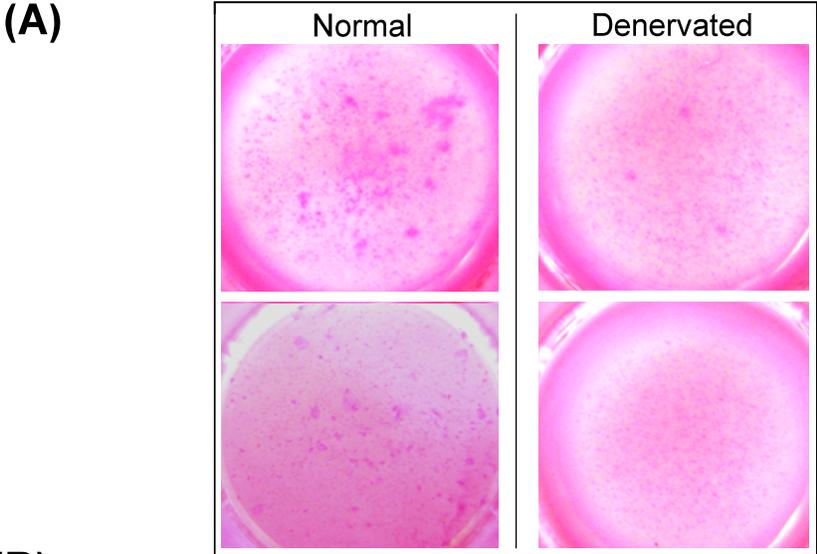**Figure 5**.

(A)

(B)
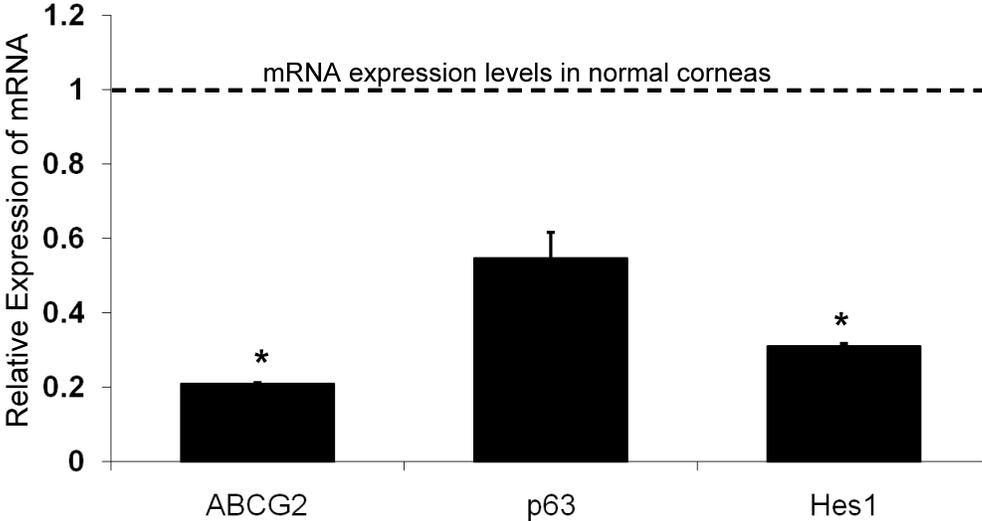
Appendix 2

Task 5
Joan Stein-Streilein, Ph.D.
Title The effect of retinal laser burn on the immunosuppressive function of retinal pigmented epithelium

Manuscript:
"Retinal laser burn disrupts immune privilege in the eye" has been published in the American Journal of Pathology 2009 Feb; 174(2): 414-22.

Cell Injury, Repair, Aging and Apoptosis

Retinal Laser Burn Disrupts Immune Privilege in the Eye

Hong Qiao, Kenyatta Lucas,
and Joan Stein-Streilein

*From the Schepens Eye Research Institute, Harvard Medical
School, Boston, Massachusetts*

**Immune privilege allows for the immune protection
of the eye in the absence of inflammation. Very few
events are capable of overcoming the immune-privi-
leged mechanisms in the eye. In this study, we report
that retinal laser burn (RLB) abrogates immune priv-
ilege in both the burned and nonburned eye. As early
as 6 hours after RLB, and as late as 56 days after RLB,
antigen inoculation into the anterior chamber of the
burned eye failed to induce peripheral tolerance. Af-
ter RLB, aqueous humor samples harvested from non-
treated eyes but not from either the burned or the
contralateral eye, down-regulated the expression of
CD40 and up-regulated interleukin-10 mRNA in peri-
toneal exudate cells, and converted peritoneal exu-
date cells into tolerogenic antigen-presenting cells
(APCs). Unlike F4/80$^+$ APCs from nontreated mice,
F4/80$^+$ APCs from RLB mice were unable to transfer
tolerance after anterior chamber inoculation of an-
tigen into naïve mice. The increased use of lasers
in both the industrial and medical fields raises the
risk of RLB-associated loss of immune regulation
and an increased risk of immune inflammation
in the eye. (Am J Pathol 2009, 174:414–422; DOI:
10.2353/ajpath.2009.080766)**

Since light amplification by stimulated emission of ra-
diation (laser) was first demonstrated in 1961,[1] the use
of lasers in the research, industrial, and military fields,
and a corresponding number of occupational eye ac-
cidents, has increased.[2,3] Many such ocular injuries
lead to retinal destruction with massive photoreceptor
loss and severe visual impairment.[4] Similarly, visual
impairment is often observed after therapeutic retinal
photocoagulation treatment, a common procedure in
clinical practice. Ophthalmic laser treatment is the
standard therapy for many sight-impairing retinal dis-
orders, such as age-related macular degeneration,
and its advanced stages of the disease, including
choroidal neovascular elements.[5] However, the laser-
treated eyes are often complicated by the immediate
visual impairment that is caused by the unavoidable
laser-induced destruction of the normal tissue adjacent
to the lesion.[6]

The eye is endowed with immune regulatory mech-
anisms (immune privilege)[7] that protect the delicate
ocular tissues from inflammatory damage. Inflamma-
tion can interfere with the visual pathways and in some
cases lead to blindness. Immune privilege is actually
thought to be an evolutionary compromise to preserve
the delicate microanatomy of the eye while maintaining
ocular immune responses. Intraocular injection of ex-
ogenous antigens induces a stereotypic alteration in
the systemic immune response termed anterior cham-
ber-associated immune deviation (ACAID).[8] ACAID re-
sults in the activation of a modified antibody response
with T-cell-mediated suppression of Th1[9] and Th2
responses.[10]

The importance of inflammation in laser injures has
been suspected but not studied in detail. There has
been no rigorous identification of either the inflamma-
tory cells that might produce damage to the retina after
laser burn or the cytokines released by these cells that
might contribute to retinal destruction. Current medical
treatment for laser injuries is systemic administration of
anti-inflammatory drugs, typically corticosteroids. The
corticosteroid treatment is believed to limit retinal in-
jury, reduce visual loss, and increase recovery.[11,12]

Understanding the extent of the inflammatory re-
sponse is a crucial step in diminishing or limiting the
extent of the laser-induced secondary retinal inflamma-
tory damage. Here we examine the postulate that laser
burn to the back of the eye affects immune privilege
throughout the eye and alters critical mechanisms in
the eye of immune regulation toward inflammation.

Materials and Methods

Mice

C57BL/6 (B6) mice were purchased from Taconic Farms (Germantown, NY). Female, 8- to 12-week-old mice were used in all experiments. EGFP transgenic female mice (B6 background)[13] were purchased from The Jackson Laboratory (Bar Harbor, ME) and also bred in our animal colony. All animals were treated humanely and in accordance with the Schepens Eye Research Institute Animal Care and Use Committee and the National Institutes of Health guidelines.

Laser Burn Model

Mice were anesthetized with ketamine (62.5 mg/kg) and xylazine (12.5 mg/kg) and pupils were dilated with 1% tropicamide. A diode laser (wave length 810 nm, diameter 200 nm, power 50 mW, duration time 50 ms) was delivered to the retina through a slit lamp microscope. The posterior pole of the retina was thus burned while a hand-held cover slide was used as a contact lens. Four spots (200 nm in diameter) were burned at the 9 o'clock position of the retina in the right eye of B6 mice. Only lesions in which a subretinal bubble or focal serous detachment of the retina developed were used for the experiments.

Histological Analysis

Eyes were enucleated at various time points (1, 4, 7, 14, 21, 56 days) after laser burn and fixed in 10% formalin for 24 hours. Tissue samples were dehydrated and embedded in paraffin. Sections (6 μm) were then prepared and subsequently stained with hematoxylin and eosin (H&E) solution to assess the histology of the laser lesion.

Retinal Pigment Epithelium (RPE)-Choroid-Scleral Flatmount

C57BL/6 mice were intravenously injected with 0.2 ml of phosphate-buffered saline (PBS) containing peritoneal exudate cells (PECs, 10^6) harvested from EGFP transgenic mice. One day later, RLB was performed. RPE-choroid-scleral flatmounts were prepared after 24 hours and evaluated. The eyes were fixed in 4% paraformaldehyde, Sigma Aldrich (3 hours). The anterior segment and neurosensory retina were removed, and peripheral choroid and sclera were dissected and flat-mounted on microscope slides for examination with a fluorescence microscope.[14] To test for blood-ocular barrier leakage, mice were deeply anesthetized 24 hours after RLB and perfused through the left ventricle with fluorescein-dextran (0.03 ml/g body weight 50 mg/ml solution of 2×10^6 molecular weight; Sigma, St. Louis, MO).

ACAID Induction and Assay for Delayed Hypersensitivity (DH)

ACAID was induced in mice by inoculating ovalbumin (OVA) [50 μg/2μl in Hanks' balanced salt solution (HBSS), Sigma Aldrich] into the anterior chamber 7 days before sensitizing, subcutaneously OVA (100 μg/ml in HBSS, 50 μl) emulsified in complete Freund's adjuvant (CFA) Sigma Aldrich (50 μl). One week later mice were tested for the development of DH by an intradermal inoculation of OVA-pulsed PECs (2×10^5 cells in 10 μl of HBSS) into the right ear pinnae. Ear swelling was measured 24 hours later with an engineer's micrometer (Mitutoyo, Paramus, NJ). Laser was performed 1, 4, 7, 14, 21, and 56 days before ACAID induction and the DH was tested by measurement of ear thickness.

Preparation of PECs

PECs were obtained from peritoneal washes of mice 3 days after they received an intraperitoneal inoculation of 2.5 ml of 3% aged thioglycolate solution (Difco, Detroit, MI). Nonadherent cells were removed from the cultures after 18 hours by three washes, and the remaining adherent cells were incubated for 1.5 hours in cold PBS (4°C) followed by vigorous pipetting to collect the cells.

Preparation of Tolerogenic Antigen-Presenting Cells (APCs)

PECs (2×10^5) were then cultured with OVA Sigma Aldrich (5 mg/ml) with or without aqueous humor (AqH) or OVA plus transforming growth factor (TGF)-β (R&D Systems, Minneapolis, MN) in 96-well culture plates. Serum-free RPMI 1640 (Cambrex Bio Science, Walkersville, MD) supplemented with 10 mmol/L HEPES, 0.1 mmol/L non-essential amino acids, 1 mmol/L sodium pyruvate, 100 U/ml penicillin, 100 mg/ml streptomycin (all from Invitrogen, Carlsbad, CA), 0.1% bovine serum albumin (Sigma Aldrich), and ITS culture supplement (BD Biosciences, San Jose, CA) were used as media.

Flow Cytometry

PECs were analyzed by flow cytometry. The following antibodies were purchased from BD Pharmingen (San Diego, CA): Fc block, phycoerythrin (PE)-CD40, PE-anti-rat IgG2a, fluorescein isothiocyanate-F4/80, and PE-Cd11b. Staining was performed in the presence of saturating concentration of Fc block (blocks FcRγII/IIIs) and PE-conjugated anti-CD40 mAb and isotype control of PE-conjugated anti-rat IgG2a. Stained cells were analyzed on an EPICS XL flow cytometry (Beckman Coulter, Miami, FL).

Aqueous Humor (AqH) Collection and Analysis

AqH was obtained from eyes of mice immediately after their euthanasia. AqH samples from panels of at least five

mice (15 eyes, 3 to 5μl/eye) at each time point were pooled and centrifuged at 200 × g for 3 minutes to sediment cells; the cell-free supernatants were cultured with 2 × 10^5 PECs.

Reverse Transcriptase-Polymerase Chain Reaction (RT-PCR)

Total cellular RNA was isolated from PECs. One hundred ng of total RNA was reverse transcribed and amplified using the Access RT-PCR system (Promega, Madison, WI) according to the manufacturer's specifications. RT-PCR products were resolved by electrophoresis in a 1.5% agarose gel containing Gel Star nucleic acid stain (Cambrex). The bands were visualized and the gels were photographed using a Molecular FX Imaging station and GelDoc (both from Bio-Rad, Hercules, CA). The primers used were as follows: murine interleukin (IL)-10, sense 5′-ACCTGGTAGAAGTGATGCCCCAGGCA-3′, antisense 5′-CTATGCAGTTGATGAAGATGTCAAA-3′; murine β-actin, sense 5′-GTGGGCCGCTCTAGGCACCAA-3′, antisense 5′-CTCTTTGATGTCACGCACGATTTC-3′.

Adherent Cells Transfer to Naïve Mice

Seven days after anterior chamber inoculation of OVA, mice were euthanized. Spleens were removed from mice and placed in HBSS. Single cell suspension was prepared by gently tapping minced spleen through a wire mesh screen. Cells were washed and resuspended in HBSS for counting and then plated at 2 × 10^6 cells/ml and incubated for 90 minutes at 37°C. Nonadherent cells were removed by gentle washing with PBS. To release adherent cells ice-cold PBS was added for 10 minutes before scraping the plates. Dissociated adherent cells were counted and resuspended to 1 × 10^6 cells/100 μl.

Statistics

Data were subjected to analysis by analysis of variance and Scheffé's test. The data are presented as mean ± SEM. An asterisk indicates a statistically significant difference between two groups. A value of $P \leq 0.05$ was considered significant.

Results

Damage Caused by the Retinal Laser Burn (RLB)

To demonstrate that the RLB causes a break in the blood ocular barrier, we injected green cells from EGFP mice into mice before delivering RLB in four separate spots to
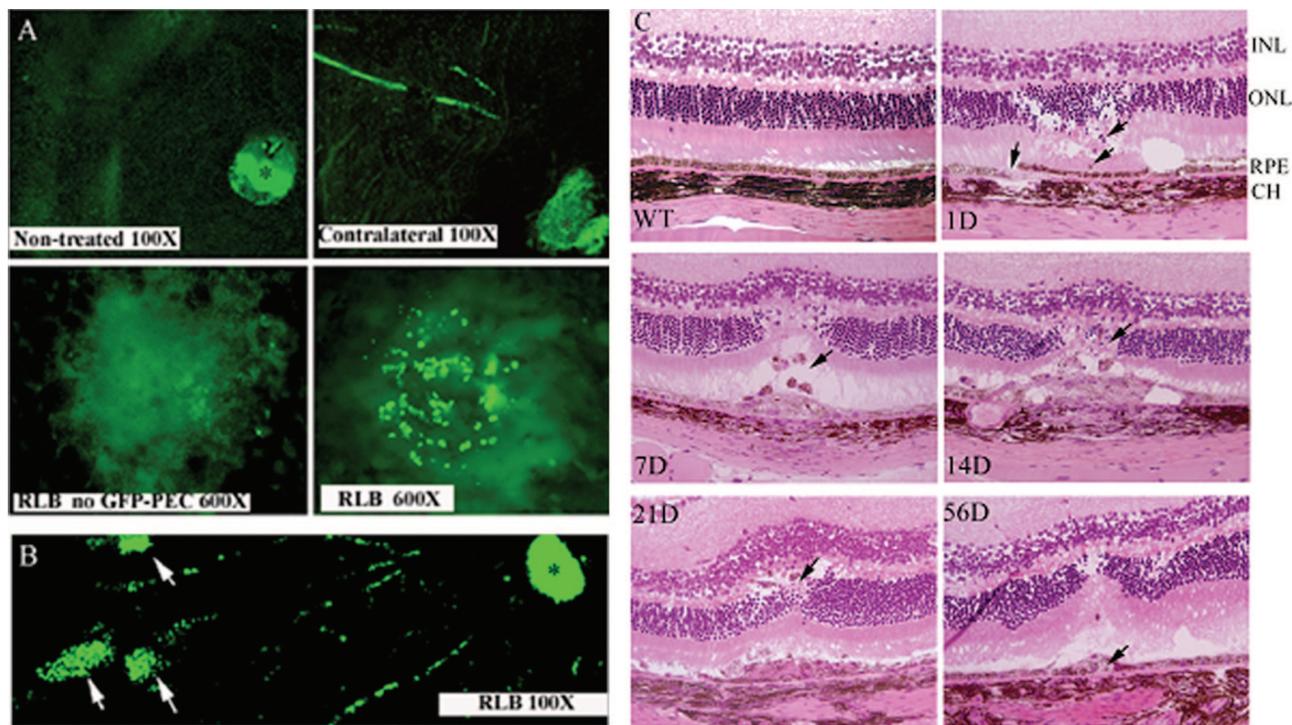

Figure 1. Photomicrographs of RPE choroid-scleral flat mounts. **A:** Photomicrograph of infiltrating green cells. GFP-PECs were injected intravenously into C57BL/6 mice 1 day before RLB treatment (**top right** and **left**, **bottom right**), or not (**bottom left**). Eyes were enucleated 1 day after RLB and the RPE-choroid-scleral flat mount was examined by fluorescence microscope. Infiltrating GFP-PECs are seen as green spots within the areas burned by the laser. Magnification as indicated in the photomicrograph. **B:** Photomicrograph of fluorescein leakage. Mice were injected intravenously with fluorescein-dextran on the same day and before receiving RLB. The eyes were excised and choroidal flat mounts were examined by fluorescence microscope. The prominent fluorescein leakage (**arrows**) indicates the breakage of Bruch's membrane and the blood-ocular barrier. **C:** Photomicrograph of paraffin-fixed slides stained with H&E of the retina of nontreated (WT) mice or RLB-treated mice. One day after laser treatment the Bruch's membrane [choroid (CH),], retinal pigment epithelium (RPE), outer nuclear layer (ONL), and photoreceptor segment were damaged. RPEs are nonpigmented and appear to migrate toward the ONL (**arrow**) at 7 to 56 days after RLB. Small lumens (**arrow**) are evident in the subretinal space and choroidal vessels are dilated at 1 to 56 days after RLB. INL, internal nuclear layer; ONL, outer nuclear layer; RPE, retinal pigment epithelium; CH, choroid. Original magnifications, ×400 (**C**).

one retina. Each laser pulse was from a diode laser. Four days before RLB, we inoculated the thioglycolate-induced PECs from EGFP C57BL/6 mice. One day after the RLB, the mice were euthanized and RPE-choroid-scleral flat mounts were prepared for examination by fluorescence microscope. Unlike the flat, mount preparations from the nontreated control mouse eye or the contralateral eye, the retina preparations from the RLB eye showed green cells within the boundaries of the burn (Figure 1A). These data are consistent with previous studies that showed F4/80-positive GFP-labeled cells infiltrated the retina in a model of laser-induced choroidal neovascular elements.[15,16] In an alternative experiment, mice were injected with fluorescein-dextran 1 day after RLB. When the RPE-choroid-scleral flat mounts of the RLB eye were examined by fluorescence microscopy, three brightly fluorescing areas (indicating the fluorescein leaked in the choroid) were observed (Figure 1B).

Other experiments examined histological changes in the tissue throughout time after RLB for evidence of RLB-induced damage. Examination of the H&E-stained section showed destruction of Bruch's membrane and RPE (Figure 1C). Although there was damage to the outer nuclear layer (ONL) and the photoreceptor segment, the inner retina was intact. The choroidal vessels are dilated suggesting an active inflammatory response was occurring. A few RPE were seen in the ONL; other RPE appeared to have lost their pigment (day 7 to day 21). Fifty-six days after laser treatment, only a few small holes remained in the subretinal space and most lesions examined appeared closed (healed) and were surrounded by RPE cells.

RLB Interferes with the Induction of ACAID

Because interference with the blood-ocular barrier may allow for unwanted inflammation, we tested the postulate that a laser burn to the retina disrupted immune privilege throughout the eye. In these experiments, groups of mice received laser burn, or not, and at various time points after, we assessed the immune-privileged status in their eyes by inducing ACAID. We observed that as early as 6 hours and as late as 56 days after RLB, the ability to induce ACAID in the eye that received the RLB was impaired (Figure 2). Thus, the induction of an inflammatory response in the back of the eye altered the immune privilege in the anterior segment of the eye and potentially throughout the eye for an extended period.

RLB Interferes with ACAID in Both RLB Eye and the Contralateral Eye

In many models of RLB, the contralateral eye is used as a control eye. To test if RLB had an effect on the contralateral eye, mice received RLB in the right eye, but the susceptibility to ACAID induction was tested by injecting antigen (anterior chamber) in the contralateral eye (left eye). Surprisingly, we were unable to induce ACAID through the contralateral eye (Figure 3). Thus, RLB to one
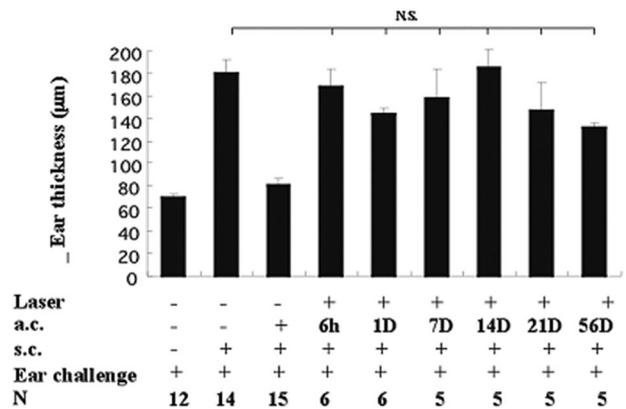
Laser	-	-	-	+	+	+	+	+	+
a.c.	-	-	+	6h	1D	7D	14D	21D	56D
s.c.	-	+	+	+	+	+	+	+	+
Ear challenge	+	+	+	+	+	+	+	+	+
N	12	14	15	6	6	5	5	5	5

Figure 2. DH assay for induction of ACAID. OVA was inoculated subcutaneously into C57BL/6 mice and a week later DH was determined after ear challenge in mice that received different treatments (indicated under abscissa and each bar). Laser = RLB treatment; a.c. = OVA inoculated into the anterior chamber; s.c. = subcutaneous immunization with OVA and CFA; ear challenge = antigen challenge into ear pinnae; (N) = number of mice in group. Ear swelling values ± SEM of each group of mice are presented on the ordinate. *Significant difference ($P \leq 0.05$) between indicated groups. N.S. indicates no significant difference. Data presented in columns 4 to 9 are representative of three experiments.

eye interferes with immune-privileged mechanisms in both eyes.

RLB Allows for Immunization via the Eye

Antigen inoculation in the anterior chamber of the eye of an unmanipulated mouse does not induce an immune response but does induce tolerance to that antigen. However, it was not clear if the inoculation of antigen into the anterior chamber of the RLB mouse was a null event or actually immunized the mouse. Thus, groups of mice received RLB, or not, 1 day before inoculation of antigen and were directly tested for immunization by challenging their ear with the same antigen a week later. Ear thick-
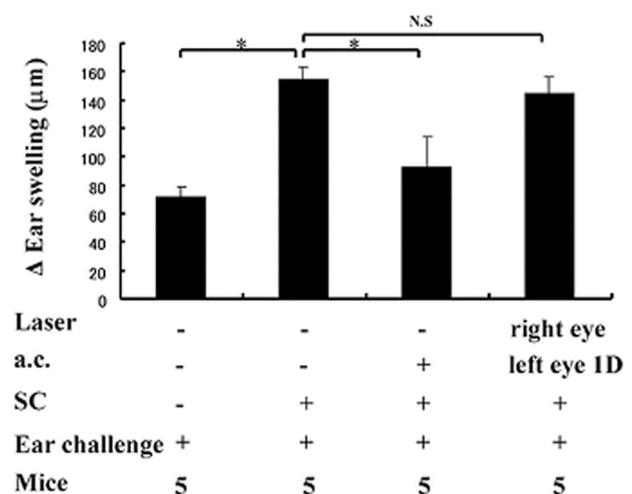
Laser	-	-	-	right eye
a.c.	-	-	+	left eye 1D
SC	-	+	+	+
Ear challenge	+	+	+	+
Mice	5	5	5	5

Figure 3. DH assay to test the effect of RLB on the ability to induce ACAID in the contralateral eye. The contralateral eye received an anterior chamber injection of OVA 1 day after laser burn; 7 days later, mice were immunized subcutaneously with OVA in CFA. Ear thickness values ± SEM of each group of five mice are presented. The treatment of the various experimental groups is indicated along the abscissa under each bar. N.S. indicates no significant difference. Significance at *$P \leq 0.05$. Data are a representative experiment from three similar experiments.
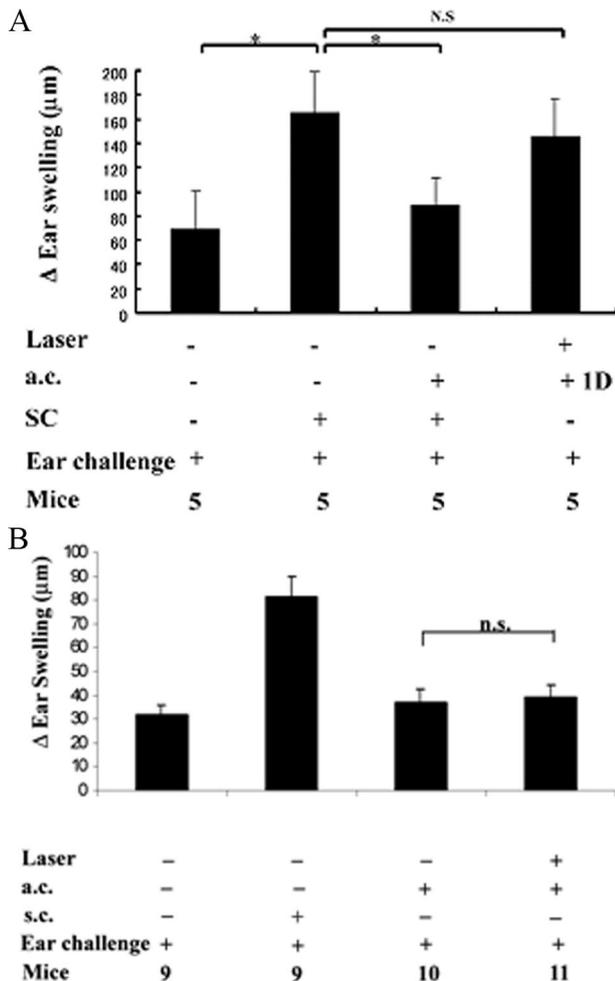
A

B

Figure 4. DH assay to test if anterior chamber inoculation immunizes after RLB. **A:** Antigen inoculation (subcutaneously) of RLB eye immunizes. First bar is negative control; second bar is positive control for DH; third bar is ACAID; fourth bar shows that when antigen is inoculated into the anterior chamber after RLB it is immunizing. The thickness of the ear is shown on the ordinate. The treatment of the experimental groups is indicated under the abscissa below each bar. Significant difference (*$P \leq 0.05$) between two groups. N.S. indicates no significant difference. The experiment was performed three times. **B:** Antigen inoculation (anterior chamber) in untreated contralateral eye of RLB mice does not immunize. Mice received RLB to the right eye. One day later, OVA was inoculated into untreated mice (third bar) or (fourth bar) the left eye of RLB mice. One week later, ears were challenged with OVA and ear thickness was a measure of DTH. Negative control, first bar; positive control, second bar; N.S. indicates no significant difference (*$P \leq 0.05$).

ness was measured 24 hours later and compared with the thickness of the ear before being challenged (Figure 4A). We observed that the mice that received RLB before the anterior chamber inoculation of antigen showed increased ear thickness when challenged locally with the antigen. Thus, the RLB not only interfered with the mechanisms that induce tolerance in the eye but also allowed the ocular route to induce an immune response.

Inoculation of Antigen into the Nonburned Eye

Since we observed that antigen inoculation into the anterior chamber of the RLB-treated eye was immunizing,

we wondered if the inoculation of antigen into the anterior chamber of the contralateral eye of RLB mice was also immunizing. To test this, groups of mice received RLB, or not, to the right eye. One day later, OVA were inoculated in the contralateral (left) eye. As before, 1 week later mice were challenged with antigen in the ear pinnae. We observed that the mice that received RLB before OVA inoculation into the contralateral eye did not show an increase of ear thickness (Figure 4B). Thus, RLB-induced mechanisms abrogate the ability to induce immune deviation (ACAID) via the anterior chamber and may be different in the burned and nonburned eye.

RLB Changes the Functional Phenotype of the Indigenous APC

It is thought that antigen that is inoculated into the anterior chamber is carried to the spleen by the indigenous F4/80[+] APCs.[17] Previously, we reported that the F4/80 protein expressed by the APCs was required for the induction of ACAID and had a correlation with the APC being tolerogenic. F4/80[+] APCs are required for both ACAID and low-dose oral tolerance.[18] Furthermore, the F4/80 marker is never found in areas of lymphoid tissue that are devoted to immune response induction. These facts suggested to us that if the anterior chamber route of antigen delivery becomes immunizing, the indigenous APCs might loose their F4/80 marker after RLB burn. Because it is difficult to monitor the cells within the eye, we collected peripheral blood cells or spleen cells to evaluate changes in F4/80 expression after anterior chamber inoculation in RLB-treated and nontreated mice. Knowing that F4/80^{+} cells increased in both the peripheral blood and the spleens of anterior chamber inoculated mice,[19] we determined if the F4/80[+] APC population increased in RLB mice after anterior chamber inoculation of antigen (Figure 5, A and B). We observed that unlike the naive mice, RLB mice showed no increase in F4/80^{+} cells 3 days after anterior chamber inoculation of antigen. The CD11b^{+} + APCs were less affected by the RLB but did not increase as much as they did in the anterior chamber-inoculated mice. Because it is known that F4/80^{+} cells from peripheral blood or spleen of ACAID mice transfer ACAID,[17,19] other studies were done to show that splenic adherent cells harvested from untreated (but not mice that received RLB) mice that were inoculated with OVA in the anterior chamber were able to transfer tolerance (Figure 5C).

AqH Is No Longer Immunosuppressive after RLB

AqH is known to be immunosuppressive, to contain TGF-β, and to contribute to the maintenance of the immune-privileged environment of the eye.[20–22] Because RLB allows for inflammation within the eye, we postulated that RLB induced major changes in the composition of AqH. Wilbanks and colleagues[26] showed that AqH treatment of APC, in the presence of antigen *in vitro*, altered
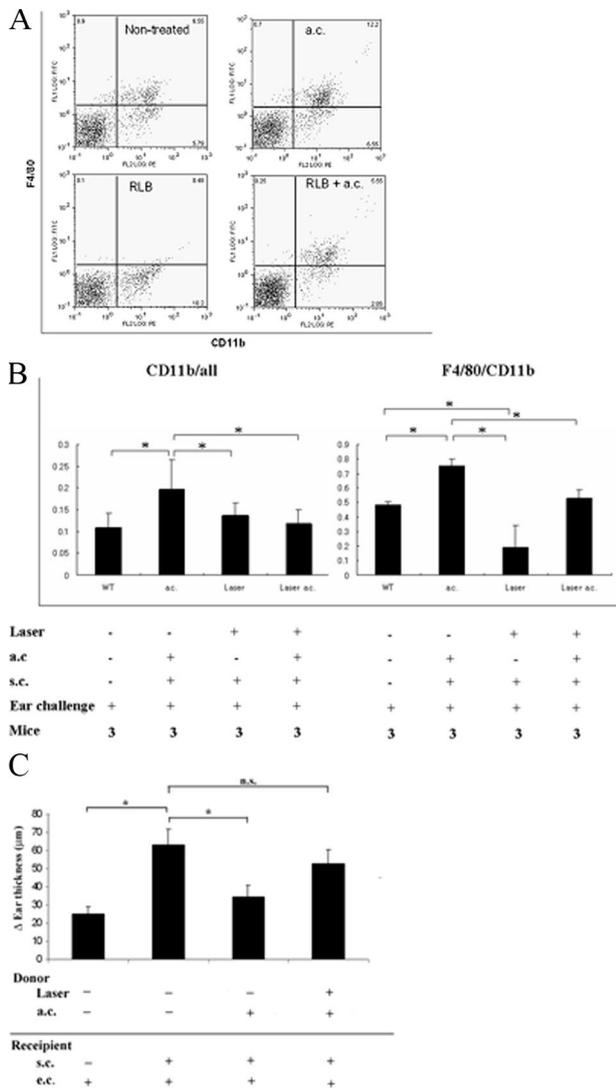
Figure 6. Capacity of AqH to induce tolerogenic PECs. Thioglycolate-induced PECs were cultured for 18 hours with AqH collected from experimental and control animals. **A:** Flow cytometry analyses of APC activation marker, CD40. Treatment of the PECs is given within each panel. **Top:** Expression of CD40 in the PECs under various control conditions. The last panel in top row shows that TGF-β is capable of down-regulating CD40, *in vitro*. **Bottom:** The effect of various samples of AqH collected from wild-type (WT) and RLB mice on CD40 expression. Percentage of cells that are positive for CD40 is indicated above the population marker in each block. **B:** RT-PCR analyses of IL-10 mRNA expression. PECs cultured with AqH were examined by RT-PCR. Treatment of the cells before mRNA analysis is indicated under the abscissa. *In vitro* imaging of gel is lined up with the densitometry reading (ordinate) of IL-10β:actin ratio.

Figure 5. DH assay to test if APC from anterior chamber inoculated mice transfer tolerance. **A:** Flow cytometry analysis of F4/80^{+} and CD11b^{+} cells in peripheral blood mononuclear cells after anterior chamber inoculation of nontreated or RLB mice. Peripheral blood mononuclear cells were collected (3 days after anterior chamber) from mice that were previously splenectomized so that cells remained in circulation. Splenectomized mice received RLB or not. Percentage of positive cells is shown in each panel. **B:** Ratio of cells with markers in peripheral blood mononuclear cells from RLB and untreated mice. Ratio of markers is shown above each panel. Treatment of the mice from which the cells were harvested is indicated under the abscissa below each bar. **C:** Peripheral APCs from mice that received RLB do not transfer tolerance. APCs were transferred intravenously from mice that received RLB before ACAID induction by anterior chamber injection of antigen. Six days later, spleens were removed and cells dissociated and incubated on plastic for 90 minutes. Adherent cells were collected and transferred intravenously to naïve mice. Recipient mice were immunized a week before antigen challenge into the ear pinnae. Ear thickness (ordinate) was measured as an indication of DH. Significance; N.S. indicates no significant difference. (*$P \leq 0.05$).

their antigen-presenting ability in such a way they acquired the ability to induce tolerance instead of immunity to that antigen.[23–26] To test the immunoregulating function of AqH, the fluid was collected from 15 eyes of nontreated mice, 15 RLB treated eyes, and 15 contralateral eyes, then separately co-cultured with OVA-pulsed PECs. Unlike AqH from eyes of naïve mice, *in vitro* analyses of the AqH samples harvested 24 hours after RLB
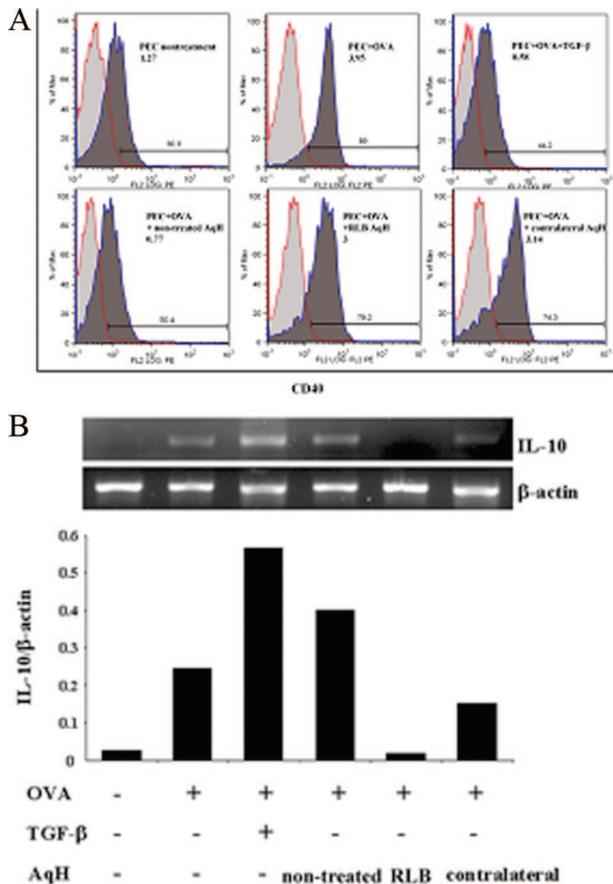
from either the RLB or contralateral eye were unable to modulate the antigen-presenting ability of OVA-pulsed PECs as assessed by their expression of CD40, a critical co-receptor for immune activation (Figure 6A).

Because APC-derived IL-10 is essential for ACAID induction,[27] other experiments tested if AqH from RLB mice was able to induce the production of IL-10 in the co-cultured APCs (Figure 6B). OVA pulsed PECs were cultured (24 hours) with AqH from naïve, RLB-treated, or RLB contralateral eyes and assessed for IL-10 mRNA by RT-PCR. We observed that IL-10 mRNA expression was increased in APCs that were cultured with AqH from nontreated eyes but not increased in APCs cultured with AqH collected from either eye of mice that received RLB to only one eye. These data support the postulate that RLB alters the characteristics of AqH so that it is no longer able to induce tolerogenic changes in the APCs.

Discussion

Although the eye is an immune-privileged site and has mechanisms to interfere with the development of immune inflammation, under certain pathological conditions, ocular immune privilege is terminated and vigorous inflammation occurs.[8,28] This process contributes to the pathogenesis of many eye diseases. Understanding mechanisms that abrogate immune privilege may lead to novel therapies to restore immune regulatory mechanisms in the eye and other sites of autoimmunity.[29]

Here we report that mechanisms that contribute to immune privilege are disrupted in the eye when the retinal pigment epithelial cells are damaged by laser burn. Surprisingly, damage to the retina in one eye had altering effects on immune privilege in the nontreated eye. There is general agreement that immune privilege is a constitutive feature of the anterior chamber in normal eyes, and there is a general expectation that when inflammation occurs in the anterior segment of the eye immune privilege will be lost.[30] Although we were surprised that laser damage to the back of the eye affected immune privilege of mechanisms in the front of the eye, studies using experimental uveitis models of ocular inflammation had shown that posterior inflammation disturbed the anterior chamber and robbed it of its capacity to support ACAID induction.[31,32] However in all these cases, unlike our RLB model, the loss of ACAID was transient.[33] Moreover the conclusion from the effects of uveitis on immune privilege was that immune privilege is surprisingly resistant to abolition by intraocular inflammation.[33] Additionally, unlike uveitis models that were explored previously, in the RLB models only one eye is inflamed yet immune privilege is breached in both. Therefore, a new immune-privileged mechanism maybe revealed by studying this model.

Immune privilege is mediated by both active and passive mechanisms.[8] The eye is privileged in part because of the blood ocular barriers that include the iris, ciliary body, and retinal pigment epithelium as well as the retinal microvasculature. Local immunosuppression is provided by immunomodulatory and anti-inflammatory factors in ocular fluids,[34] and on parenchymal cell surfaces.[35,36] Constitutive expression of FasL on intraocular cells provides protection by inducing apoptosis of activated lymphocytes and neutrophils that transgress the borders and might damage ocular tissues.[37] Systemic factors also contribute to immune privilege in that eye-derived APCs carry antigens to the spleen where they induce antigen-specific T-regulatory cells that affect both local and peripheral tolerance to the eye-derived antigens.

Thus, with the overlapping mechanisms that contribute to immune privilege, inoculation into the anterior chamber is a route that consistently leads to tolerance. Thus, when we observed that RLB interfered with development of tolerance in the ACAID model we thought is was a null event. However, we noted the inoculation of antigen into the anterior chamber of the burned eye led to immunization and a DH response. This is remarkable in that we did not add adjuvant, a substance that is absolutely necessary even if immunization is through the skin.[38,39] This may suggest that the RLB leads to release of local mol-

ecules (maybe stress proteins) that act as adjuvants. This notion raises new questions about regulation of immune privilege.

To explain the loss of ACAID in the burned eye after RLB, we postulated that the quality of the AqH was altered by the break in the barrier and subsequent infiltration of inflammatory cells caused by the burn. It is known that soluble factors within the AqH, such as macrophage-derived migration inhibitory factor (MIF),[34] TGF-β,[20] and neuropeptides,[22,40] all contribute to the immune privilege of the eye[8] through their immunosuppressive and anti-inflammatory effects.

Because our focus was to extend previous studies and understanding of immune privilege, we chose to examine the functional affects of AqH on APCs. Similar to other factors found in AqH, TGF-β is produced locally within the eye, and is thought to be the most important agent responsible for modulating APC toward tolerance induction.[23,41–43] Here, we observed that AqH from eyes of nontreated mice converted APCs into tolerogenic APCs unlike the AqH from either eye of mice that had received RLB in one eye. Furthermore APCs collected from the spleen after anterior chamber inoculation of antigen in mice receiving RLB were unable to transfer tolerance. These observations suggest that RLB induces changes in AqH that affect the tolerogenic function of the indigenous APC in the eye.

It is easier to explain the abrogation of ACAID phenomenon in the burned eye than in the contralateral eye, because inflammatory cells enter the eye through the break in the blood ocular barrier caused by the burn. Inflammatory cells by definition release inflammatory cytokines that then alter the composition of the AqH[44] and its capacity to induce tolerance. But, because the barrier is apparently intact in the contralateral eye, we pose that the mechanisms that caused the change in tolerogenic capacity of the AqH collected from the non-burned eye are different and unrelated to the presence of inflammatory cytokines produced by recruited cells in the burned eye.

Neuronal signals from the laser-damaged RPE cells of the treated eye may have a modifying influence on the contralateral eye. It is known that RPE cells produce neural messages[45,46] that are able to travel between eyes via the nerves. Thus, the possibility is raised that laser burn damage to the RPE initiates a process that spreads to nearby undamaged RPE cells as well as to the RPE in the contralateral eye. Therefore, tolerogenic neural messages could be lost between the eyes and lead to the loss of an ability to develop ACAID in the contralateral eye. Such an idea raises concerns about the safety of laser treatment even if it is targeted to selected RPE cells.[47,48]

Because RPE cells also make immunosuppressive cytokines another idea that is unveiled by this model is that the RLB damage to the RPE may interfere with nonneuronal immunosuppressive factors[49] and the posterior eye (RPE) may be a major source of the immunosuppressive factors found throughout the AqH in both eyes.[50] We

suspect that if the mechanisms that led to the RLB-associated abrogation of immune privilege were understood it might be possible to restore immune privilege to the inflamed eye. Even though RLB is commonly used as treatment in inflammatory disease of the eye, few studies have been done to determine whether the immune privilege is altered by such therapeutic measures. This may be a mute point, however, because an eye that warrants laser burn treatment may already have its immune-privileged mechanisms compromised. Then the question becomes, "Is the additional interference of immune privilege by laser burn helping or hindering the restoration of immune stability in the eye?"

Understanding how to restore immune regulation in the face of immune inflammation might lead to novel therapeutic strategies for immediate intervention in patients with accidental laser burn or trauma to an eye and may prevent the appearance of sympathetic ophthalmia. Sympathetic ophthalmia is a condition in which trauma to one eye leads to immune inflammation and potentially blindness in the nontraumatized eye[51,52] because of a loss of its immune privilege. At the very least this puzzling situation might benefit from future studies exploiting RLB model as a model for sympathetic ophthalmia.

Acknowledgments

References

1. Solon LR, Aronson R, Gould G: Physiological implications of laser beams. Science 1961, 134:1506–1508
2. Fowler BJ: Accidental industrial laser burn of macula. Ann Ophthalmol 1983, 15:481–483
3. Wolbarsht ML, Welch AJ: Evaluation of ocular protection filters in field situations. Health Phys 1989, 56:729–739
4. Warner J, Boulton M, Mellerio J, Eysteinsson T, Marshall J: Temporal variations in the ionic transport across rabbit retinal pigment epithelium. Curr Eye Res 1991, 10:513–522
5. Curcio CA, Medeiros NE, Millican CL: Photoreceptor loss in age-related macular degeneration. Invest Ophthalmol Vis Sci 1996, 37:1236–1249
6. Solberg Y, Dubinski G, Tchirkov M, Belkin M, Rosner M: Methylprednisolone therapy for retinal laser injury. Surv Ophthalmol 1999, 44(Suppl 1):S85–S92
7. Medawar PB: Immunity to homologous grafted skin; the fate of skin homografts transplanted to the brain, to subcutaneous tissue and to the anterior chamber of the eye. Br J Exp Pathol 1948, 29:58–69
8. Streilein JW: Ocular immune privilege: therapeutic opportunities from an experiment of nature. Nat Rev Immunol 2003, 3:879–889
9. Kaplan HJ, Streilein JW, Stevens TR: Transplantation immunology of the anterior chamber of the eye. II. Immune response to allogeneic cells. J Immunol 1975, 115:805–810
10. Katagiri K, Zhang-Hoover J, Mo JS, Stein-Streilein J, Streilein JW: Using tolerance induced via the anterior chamber of the eye to inhibit Th2-dependent pulmonary pathology. J Immunol 2002, 169:84–89
11. Lam TT, Takahashi K, Fu J, Tso MO: Methylprednisolone therapy in laser injury of the retina. Graefes Arch Clin Exp Ophthalmol 1993, 231:729–736
12. Wilson JW, Djukanovic R, Howarth P, Holgate ST: Lymphocyte activation in bronchoalveolar lavage and peripheral blood in atopic asthma. Am Rev Respir Dis 1992, 145:958–960
13. Okabe M, Ikawa M, Kominami K, Nakanishi T, Nishimune Y: 'Green mice' as a source of ubiquitous green cells. FEBS Lett 1997, 407:313–319
14. Tsutsumi C, Sonoda KH, Egashira K, Qiao H, Hisatomi T, Nakao S, Ishibashi M, Charo IF, Sakamoto T, Murata T, Ishibashi T: The critical role of ocular-infiltrating macrophages in the development of choroidal neovascularization. J Leukoc Biol 2003, 74:25–32
15. Caicedo A, Espinosa-Heidmann DG, Pina Y, Hernandez EP, Cousins SW: Blood-derived macrophages infiltrate the retina and activate Muller glial cells under experimental choroidal neovascularization. Exp Eye Res 2005, 81:38–47
16. Espinosa-Heidmann DG, Reinoso MA, Pina Y, Csaky KG, Caicedo A, Cousins SW: Quantitative enumeration of vascular smooth muscle cells and endothelial cells derived from bone marrow precursors in experimental choroidal neovascularization. Exp Eye Res 2005, 80:369–378
17. Wilbanks GA, Streilein JW: Macrophages capable of inducing anterior chamber associated immune deviation demonstrate spleen-seeking migratory properties. Reg Immunol 1992, 4:130–137
18. Lin HH, Faunce DE, Stacey M, Terajewicz A, Nakamura T, Zhang-Hoover J, Kerley M, Mucenski ML, Gordon S, Stein-Streilein J: The macrophage F4/80 receptor is required for the induction of antigen-specific efferent regulatory T cells in peripheral tolerance. J Exp Med 2005, 201:1615–1625
19. Faunce DE, Sonoda KH, Stein-Streilein J: MIP-2 recruits NKT cells to the spleen during tolerance induction. J Immunol 2001, 166:313–321
20. Cousins SW, McCabe MM, Danielpour D, Streilein JW: Identification of transforming growth factor-beta as an immunosuppressive factor in aqueous humor. Invest Ophthalmol Vis Sci 1991, 32:2201–2211
21. Cousins SW, Trattler WB, Streilein JW: Immune privilege and suppression of immunogenic inflammation in the anterior chamber of the eye. Curr Eye Res 1991, 10:287–297
22. Taylor AW: Ocular immunosuppressive microenvironment. Chem Immunol 1999, 73:72–89
23. Granstein RD, Staszewski R, Knisely TL, Zeira E, Nazareno R, Latina M, Albert DM: Aqueous humor contains transforming growth factor-β and a small (<3500 daltons) inhibitor of thymocyte proliferation. J Immunol 1990, 144:3021–3027
24. Kaiser CJ, Ksander BR, Streilein JW: Inhibition of lymphocyte proliferation by aqueous humor. Reg Immunol 1989, 2:42–49
25. Hara Y, Caspi RR, Wiggert B, Dorf M, Streilein JW: Analysis of an in vitro-generated signal that induces systemic immune deviation similar to that elicited by antigen injected into the anterior chamber of the eye. J Immunol 1992, 149:1531–1538
26. Wilbanks GA, Mammolenti M, Streilein JW: Studies on the induction of anterior chamber-associated immune deviation (ACAID) III. Induction of ACAID depends upon intraocular transforming growth factor-beta. Eur J Immunol 1992, 22:165–173
27. D'Orazio TJ, Niederkorn JY: A novel role for TGF-beta and IL-10 in the induction of immune privilege. J Immunol 1998, 160:2089–2098
28. Niederkorn JY: See no evil, hear no evil, do no evil: the lessons of immune privilege. Nat Immunol 2006, 7:354–359
29. Zhang-Hoover J, Stein-Streilein J: Therapies based on principles of ocular immune privilege. Chem Immunol Allergy 2007, 92:317–327
30. Gery I, Streilein JW: Autoimmunity in the eye and its regulation. Curr Opin Immunol 1994, 6:938–945
31. Ohta K, Wiggert B, Taylor AW, Streilein JW: Effects of experimental ocular inflammation on ocular immune privilege. Invest Ophthalmol Vis Sci 1999, 40:2010–2018
32. Ohta K, Yamagami S, Taylor AW, Streilein JW: IL-6 antagonizes TGF-beta and abolishes immune privilege in eyes with endotoxin-induced uveitis. Invest Ophthalmol Vis Sci 2000, 41:2591–2599
33. Streilein JW, Ohta K, Mo JS, Taylor AW: Ocular immune privilege and the impact of intraocular inflammation. DNA Cell Biol 2002, 21:453–459
34. Apte RS, Sinha D, Mayhew E, Wistow GJ, Niederkorn JY: Role of macrophage migration inhibitory factor in inhibiting NK cell activity and preserving immune privilege. J Immunol 1998, 160:5693–5696

35. Niederkorn JY: Immune privilege in the anterior chamber of the eye. Crit Rev Immunol 2002, 22:13–46

36. Ferguson TA, Griffith TS: The role of Fas ligand and TNF-related apoptosis-inducing ligand (TRAIL) in the ocular immune response. Chem Immunol Allergy 2007, 92:140–154

37. Griffith TS, Brunner T, Fletcher SM, Green DR, Ferguson TA: Fas ligand-induced apoptosis as a mechanism of immune privilege. Science 1995, 270:1189–1192

38. Matzinger P: An innate sense of danger. Semin Immunol 1996, 10:399–415

39. Matzinger P: The danger model: a renewed sense of self. Science 2002, 296:301–305

40. Taylor AW, Streilein JW, Cousins SW: Identification of alpha-melanocyte stimulating hormone as a potential immunosuppressive factor in aqueous humor. Curr Eye Res 1992, 11:1199–1206

41. Streilein JW, Ksander BR, Taylor AW: Immune deviation in relation to ocular immune privilege. J Immunol 1997, 158:3557–3560

42. Taylor AW, Alard P, Yee DG, Streilein JW: Aqueous humor induces transforming growth factor-beta (TGF-beta)-producing regulatory T-cells. Curr Eye Res 1997, 16:900–908

43. Kriegel MA, Li MO, Sanjabi S, Wan YY, Flavell RA: Transforming growth factor beta: recent advances on its role in immune tolerance. Curr Rheumatol Rep 2006, 8:138–144

44. Li Y, Reca RG, Atmaca-Sonmez P, Ratajczak MZ, Ildstad ST, Kaplan HJ, Enzmann V: Retinal pigment epithelium damage enhances expression of chemoattractants and migration of bone marrow-derived stem cells. Invest Ophthalmol Vis Sci 2006, 47:1646–1652

45. Bazan NG, Marcheselli VL, Cole-Edwards K: Brain response to injury and neurodegeneration: endogenous neuroprotective signaling. Ann NY Acad Sci 2005, 1053:137–147

46. Bronzetti E, Artico M, Kovacs I, Felici LM, Magliulo G, Vignone D, D'Ambrosio A, Forte F, Di Liddo R, Feher J: Expression of neurotransmitters and neurotrophins in neurogenic inflammation of the rat retina. Eur J Histochem 2007, 51:251–260

47. Song Q, Risco R, Latina M, Berthiaume F, Nahmias Y, Yarmush ML: Selective targeting of pigmented retinal pigment epithelial (RPE) cells by a single pulsed laser irradiation: an in vitro study. Opt Express 2008, 16:10518–10528

48. Brinkmann R, Koop N, Ozdemir M, Alt C, Schule G, Lin CP, Birngruber R: Targeting of the retinal pigment epithelium (RPE) by means of a rapidly scanned continuous wave (CW) laser beam. Lasers Surg Med 2003, 32:252–264

49. Sugita S, Futagami Y, Smith SB, Naggar H, Mochizuki M: Retinal and ciliary body pigment epithelium suppress activation of T lymphocytes via transforming growth factor beta. Exp Eye Res 2006, 83: 1459–1471

50. Zamiri P, Masli S, Streilein JW, Taylor AW: Pigment epithelial growth factor suppresses inflammation by modulating macrophage activation. Invest Ophthalmol Vis Sci 2006, 47:3912–3918

51. Damico FM, Kiss S, Young LH: Sympathetic ophthalmia. Semin Ophthalmol 2005, 20:191–197

52. Subedi S: Sympathetic ophthalmia: a blinding complication of ocular injury. JNMA J Nepal Med Assoc 2005, 44:57–59

Appendix 3

Task 5
Joan Stein-Streilein, Ph.D.
Title The effect of retinal laser burn on the immunosuppressive function of retinal pigmented epithelium

Abstract:
Abstract by Dr. Kenyatta Lucas presented as Poster at the ARVO 2011 meeting in Fort Lauderdale.

Retinal Laser Burn induces Substance P dependent loss of Immune Privilege

Kenyatta Lucas and Joan Stein-Streilein
Schepens Eye Research Institute,Department of Ophthalmology,Harvard Medical School,
Boston, MA, 02114

Purpose: Immune inflammation in the eye is tightly regulated by multiple processes that contribute to ocular immune privilege. Many studies have shown that it is very difficult to abrogate immune privileged mechanisms including anterior chamber immune deviation (ACAID). Previously we showed that Retinal Laser Burn (RLB) abrogated ACAID, bilaterally. The purpose of our studies is to understand how RLB to one eye induces the loss of immune privilege in the non-burned eye. Here we tested the role of a neuroinflammatory peptide(substance P) in the RLB induced abrogation of ACAID.

Methods: RLB was caused by delivering four (200nm) laser spots to the right eye of mice. ACAID was induced in wild type (C57BL/6) or Substance P KO mice (B6.Cg-Tac1tm1Bbm/J). To block the activity of Substance P, the antagonist for Substance P receptor [Neurokinin 1 receptor (NK1-R)], Spantide I, was injected into the anterior chamber simultaneously with ovalbumin at various times post RLB treatment. The expression of NK1-R in the retina was assessed by histological examination of immunostained frozen tissue slides. Eyes were removed from mice that received RLB treatment, 6h, 24h and 72h earlier. Cryosections of the eyes were stained with Anti-NK1-R (Millipore Billerica, MA), and DAPI (Vector Lab, Burlingame, CA). Images were taken using a Leica TCS-SP5 confocal microscope (Leica Microsystems, Bannockburn, IL).

Results: WT mice lost ACAID bilaterally post RLB but Substance P KO mice. Spantide I treated WT mice retained their ability to develop ACAID when given early (24h) post RLB treatment. Histologically we observed an increase of NK1-R in the retina of both eyes of mice at 6h, 24h, and 72h post RLB.

Conclusion: While RLB induced the loss of immune privilege (ACAID) in both eyes, blocking Substance P signaling prevented RLB induced loss of ACAID. In addition the central role of Substance P signaling in disregulating immune regulation in the eye was supported by an increase in the NK1-R early(6 h) post RLB. Substance P is a neuronal signal that contributes to the loss of ACAID in the contralateral eye thus explaining a pathway that may cause the loss of immune regulation in the absence of a break in the blood ocular barrier or recruitment of inflammatory cells. The possibility is raised that inhibitors of Substance P may provide therapeutic maintenance of immune regulation in patients with posttraumatic injuries to the CNS or eye. This work was supported in part by grants to JSS: NIH EY11983 and DOD W81XWH; KL: F32 EY018983.

Appendix 4

Task 8
Patricia D'Amore, Ph.D.
Title: Regeneration of bruch's membrane in vitro and in vivo

Manuscript:
"Heat treatment of retinal pigment epithelium induces production of elastic lamina components and anti-angiogenic activity." Submitted to FASEB J.

Heat treatment of retinal pigment epithelium induces production of elastic lamina components and anti-angiogenic activity.

Eiichi Sekiyama [1, 2], Magali Saint-Geniez [1, 2], Kazuhito Yoneda [4], Toshio Hisatomi [5], Shintaro Nakao [5], Tony E. Walshe [1, 2], Kazuichi Maruyama [1, 4], Ali Hafezi-Moghadam [5], Joan W. Miller [5], Shigeru Kinoshita [4], and Patricia A. D'Amore[1, 2, 3,]

[1] Schepens Eye Research Institute, Harvard Medical School, Boston, Massachusetts, USA.
[2] Department of Ophthalmology, Harvard Medical School, Boston, Massachusetts, USA.
[3] Department of Pathology, Harvard Medical School, Boston, Massachusetts, USA.
[4] Department of Ophthalmology, Kyoto prefectural University of Medicine, Graduate School of Medicine, Kyoto, Japan.
[5] Angiogenesis Laboratory, Massachusetts Eye and Ear, Harvard Medical School, Boston, Massachusetts, USA.

Corresponding author:
Patricia A D'Amore
20 Staniford Street, Boston, MA 02114
tel   617-912-2559
fax   617-912-0128
patricia.damore@schepens.harvard.edu

Short title:
Heat induces RPE production of elastic lamina components

Abstract

Age related macular degeneration (AMD) is the leading cause of blindness in the western world. In advanced AMD, new vessels from choriocapillaris (CC) invade through the Bruch's membrane (BrM) into the retina forming choroidal neovascularization (CNV). BrM, an elastic lamina that is located between the RPE and CC, is thought to act as a physical and functional barrier against CNV. The BrM of patients with early AMD are characterized by decreased levels of anti-angiogenic factors, including endostatin, thrombospondin-1 (TSP-1), and pigment epithelium derived factor (PEDF) as well as by degeneration of elastic layer. Motivated by a previous report that heat increases elastin expression in the human skin, we examined the effect of heat on human ARPE-19 cells production of BrM components. Heat treatment stimulated the production of BrM components, including TSP-1, PEDF, and tropoelastin in vitro and increased the anti-angiogenic activity of RPE measured in a mouse corneal pocket assay. The effect of heat on experimental CNV was investigated by pretreating the retina with heat via infrared diode laser (IDL) prior to the induction of CNV. Heat treatment blocked the development of experimental CNV in vivo. These findings suggest that heat treatment may restore BrM integrity and barrier function against new vessel growth.

Key words: choroidal neovascularization, transpupillary thermotherapy, endostatin, thrombospondin-1, pigment epithelium derived factor, elastin

Introduction

Age-related macular degeneration (AMD), the leading cause of blindness in the

elderly population in the Western world (1), is classified as either wet AMD or dry macular

degeneration. In contrast to the patients with dry AMD in whom impairment of vision is

gradual, wet AMD has rapid and devastating visual effects. The clinical and histopathologic

features of wet AMD involve the dysfunction of retinal pigment epithelium (RPE), Bruch's

membrane (BrM) and the choriocapillaris (CC). In wet AMD, new vessels from CC invade

through the BrM into the retina resulting in choroidal neovascularization (CNV). Early AMD is

distinguished by subretinal deposits and atrophic changes in the RPE, which are not

associated with changes in visual acuity. However, once new blood vessels develop and

invade the retinal space, vision is lost. Thus, strategies that could prevent the progression to

wet AMD would be valuable.

BrM, a thin elastic lamina located between RPE and CC, is composed of five distinct

layers: a central elastic layer, bounded on both sides by collagenous layers and bordered

externally by the basal laminas of the RPE and CC. The basement membranes underlying

the RPE and the CC endothelial cells contain collagen IV, laminin, and decorin. Many of

these molecules have reported effects on the proliferation and/or survival of vascular

endothelium. Collagen IV alpha 2 chain has been reported to induce apoptosis of vascular

endothelial cells (2), and alpha 3 chain has been shown to inhibit the vascular endothelial

proliferation and block tube formation in vitro (3). The collagenous layers of BrM include

collagens I, III, and XVIII, and fibronectin. Collagen I is reported to down regulate

VEGF-mediated VEGFR2 activation (4) and to bind thrombospondin-1 (TSP-1), a major

anti-angiogenic factor (5). Through cleavage by enzymes, including cathepsin B and MMP-7,

collagen XVIII produces endostatin, a well-described endogenous anti-angiogenic factor,

which has been shown to regulate CNV (6). The elastic layer, which is formed by the cross

linking of tropoelastin on microfibrils of fibrillin-1 and -2 molecules, is believed to act as

physical barrier against new vessel growth (7, 8). Interestingly, BrM from patients with early

AMD have been reported to have decreased levels of anti-angiogenic molecules including

endostatin, TSP-1, and pigment epithelium derived factor (PEDF) (9, 10, 11) as well as

degeneration of the elastic layer (8).Taken together, these observations indicate that the BrM

functions as a physical and functional barrier against the growth of new blood vessel from the

CC.

Previous reports have demonstrated that heat induces elastin expression in the

human skin (12) and that the expression of heat shock protein increases the levels of

endostatin and TSP-1 in tumors (13). With a goal of identifying a mean to restore BrM, we

investigated the effect of mild heat treatment on human RPE-production of BrM components.

Additionally, we tested the effect of heat on the retina in vivo using topical heat treatment with

IDL. Results of these studies suggest that heat treatment can induce the expression of

components of BrM and thus might be useful in preventing the progression to neovascular

AMD.

Materials & Methods

ARPE-19 cell cultures

ARPE-19 cells obtained from American Type Culture Collection (Manassas, VA) were used between passages 21 and 25. Transwells (0.4 µm pore size, 12 mm or 24 mm diameter; Corning/Costar) were coated with laminin and approximately 1.7×10^5 cells/cm^2 ARPE-19 cells were seeded in DMEM/F-12 culture medium, supplemented with 100 U/mL penicillin-streptomycin and 1% FBS. The medium was changed twice a week. Cells were cultured for at least four weeks to form differentiated monolayers. RNAs were isolated from cells after one, two, three, and four weeks of culture.

For heat treatment, ARPE-19 cells grown for four weeks on the transwells were cultured at 43°C for 30 min. RNA was isolated 15 min, one, two, and four hr after heat treatment and cell associated proteins were examined in cell lysates collected two and four hr after heat treatment. Proteins secreted into the culture media were collected four hr after heat treatment and analyzed.

RNA isolation and real-time PCR analysis

Total RNA was extracted (RNAqueousTM-4PCR kit; Ambion Inc., Austin, TX), according to the manufacturer's instructions. Residual DNA was removed by treatment with 1

unit DNase I (Ambion) at 37°C for 20 min. One microgram of RNA was reverse-transcribed

and one twentieth of the total cDNA was used in each amplification reaction. Each gene was

quantified (Prism 9700 Sequence Detection System; Applied Biosystems, Inc. (ABI, Foster

City, CA) according to the manufacturer's instructions (Table 1). Reactions were performed in

25 µl with 0.3 µM primers and master mix (SYBR Green Master mix; ABI). PCR cycles

consisted of an initial denaturation step at 95°C for 10 min, followed by 40 cycles at 95°C for

15 sec and at 60°C for 60 sec. To confirm amplification specificity, PCR products from each

primer pair were subjected to a melting curve analysis. Amplification of the GAPDH was

performed on each sample as a control for sample loading and to allow normalization

between samples. Each sample was run in duplicate and each experiment was conducted at

least three times.

Western blot analysis

ARPE-19 cells were collected in lysis buffer (10 mM Tris-HCl, pH 7.4, 5 mM EDTA,

50 mM NaCl, 1% Triton X-100, 50 mM NaF, 1 mM phenylmethylsulfonyl fluoride, 2 mM

Na_3VO_4, and 20 mg/ml aprotinin) and protein concentrations were quantified using the

NanoDrop (Scrum, Tokyo, Japan). Medium conditioned by ARPE-19 cells was concentrated

10-fold with a centrifugal filter with a molecular size cutoff of 10 kDa (Amicon Ultra; Millipore,

Bedford, MA) and an equal volumes of samples were analyzed. Proteins from cell lysates and

conditioned media were separated by SDS-PAGE. Cell lysates were probed with rabbit polyclonal anti-human tropoelastin (1:300, Elastin Products Company Inc., Owensville, Missouri) and mouse monoclonal anti-human TSP-1 (1:400, Abcam, Cambridge, MA). Concentrated media were probed with mouse monoclonal anti-human endostatin (1:100, Oncogene, San Diego, CA) and mouse monoclonal anti-human PEDF (1:1000, Millipore). Binding was detected with the appropriate HRP-conjugated secondary antibody (1:1000, Amersham Biosciences, Piscataway, NJ) and ECL-Plus Western Blotting Detection System (GE Healthcare, Waukesha, WI). The intensity of western blot bands was quantified by densitometric analysis using NIH Image J (n=3).

TUNEL assay

ARPE-19 cell apoptosis was evaluated using the *In Situ* Cell Death Detection Kit (TMR red; Roche, Germany), according to the manufacturer's instructions. Briefly, cells were fixed with 4% paraformaldehyde for 1 hr at room temperature and then permeabilized with 0.1% TritonX-100 in 0.1% sodium citrate for 2 min on ice. After the incubation with TUNEL reaction mixture and DAPI for 60 min at 37°C in the dark, cells were observed. Three wells were analyzed by counting apoptotic cells in four randomly chosen fields.

Transmission electron microscopy

Monolayers of ARPE-19 cells cultured on transwells for three days and four weeks were fixed with half-strength Karnovsky's fixative, followed by 2% osmium tetroxide and stained en block stain with 0.5% uranyl acetate. After dehydration and embedding, ultra-thin sections were visualized using a transmission electron microscope (model 410; Phillips).

Effect of media conditioned by heat-treated ARPE-19 on endothelial cell wound closure assay and proliferation

Media were collected after four hr of conditioning by heat-treated ARPE-19 cells, unconditioned media served as a control. The media were mixed with an equal volume of endothelial basal medium (EBM-2) supplemented with SingleQuots, 20% FBS, and 1 X glutamine-penicillin-streptomycin and tested for their effect on the closure of scratch wounds by human umbilical vein cell (HUVEC). Monolayers of confluent HUVEC in 24-well plates (Corning/Costar) were scratch-wounded using the p1000 pipette tips. Two scratches were made per well (n=4). The progress of wound closure was photographed with an inverted microscope equipped with a digital camera (SPOT; Diagnostic Imaging, Sterling Heights, MI) immediately after injury and at 16 hr after wounding. The width of the wound was measured using NIH image J software. Three random measurements were taken of each wound and their average was taken as the width of each wound.

For the assay of proliferation, HUVEC were seeded at 2×10^4 cells/well in triplicates onto 12-well plates (Corning/Costar). Three days later, cell proliferation was evaluated by direct cell count of trypsin-detached cells with a hemocytometer (n=3).

Corneal micropocket assay

Rodent studies were approved by the Animal Care Committee of the Massachusetts Eye and Ear Infirmary. BALB/c mice were anesthetized by intraperitoneal injection of ketamine at 100 mg/kg and xylazine at 10 mg/kg. Hydron pellets (0.3 μl) containing 200 ng of human VEGF (201-LB; R&D Systems, Minneapolis, MN) were prepared. Heat-treated (n=6) or control untreated (n=10) ARPE-19 cells cultured on the transwells were dissected into 0.3 μm square pieces and implanted into the corneas with VEGF containing pellet. The pellets and tissues were positioned 1 mm from the corneal limbus as described previously (14). Implanted eyes were treated topically with bacitracin ophthalmic ointment (E. Fougera & Co., Melville, NY). Six days after implantation, digital images of the corneal vessels were obtained and recorded using OpenLab software, version 2.2.5 (Improvision Inc.) with standardized illumination and contrast. Quantification of neovascularization in the mouse corneas was performed using NIH Image J software.

Effect of elastin on endothelial cell migration

Transwells (3.0 μm pore size, 6.5 mm diameter; Corning/Costar) were coated

overnight at 4 °C with soluble elastin (Elastin Products Company Inc.) diluted in PBS (0, 10,

100, or 1000 μg/ml). Approximately 2.5 x10^5 cells/well HUVEC were seeded on the

elastin-coated transwells in EBM-2 supplemented 20% FBS, 1 X

glutamine-penicillin-streptomycin, and SingleQuots. Two hr later, the culture media were

replaced and the number of unattached cells was counted with a hemocytometer to

determine plating efficiency. Fourteen hr after plating, the cells from the upper side of the filter

were removed with a cotton swab and the cells that had migrated through the pores to the

opposite side of the membrane were stained with hematoxylin and eosin. The filter was gently

cut from the chamber and the cells that had migrated were counted in 4 high-power fields per

insert. For each migration condition, three replicates were performed.

Heat treatment of mouse retina

These mouse studies were approved by the Committee on the Ethics of Animal

Experiments at the Kyoto Prefectural University of Medicine. C57BL/B6J mice were

anesthetized by intraperitoneal injection of 100mg/kg ketamine and 10mg/kg xylazine. Pupils

were dilated with 1% tropicamide. Heat from an IDL was delivered through a slit lamp (model

30 SL-M; Carl Zeiss Meditec, Oberkochen, Germany) by a trimode IDK emitting at 810 nm

(Iris Medical Instrument, Inc., Mountain View, CA) at a power setting of 50 mW and a beam

diameter of 1.2 mm for 60 sec. A series of four laser spots were delivered to the posterior

pole of each retina at two disc-diameters from the optic nerve.

Fourteen days after heat treatment, eyes were enucleated and dissected into 0.8 μm

sections, which were stained with hematoxylin and eosin.

Induction of CNV in heat-treated mouse retina

One day following the heat treatment, mice were anesthetized as above and fixed on

a rack connected to the slit lamp delivery system. To induce CNV, an argon laser

photocoagulation burn was placed in the center of the IDL heat treatment area at a power

setting of 300mW and a beam diameter of 50 μm for 0.05 sec to induce CNV. Only eyes in

which a subretinal bubble was formed following each burn were included in the study. Seven

days following argon photocoagulation, mice were perfused with concanavalin A lectin (20

μg/ml in PBS)(Vector Laboratories, Burlingame, CA), then the eyes were enucleated and

fixed in 2% paraformaldehyde. The RPE-choroid-sclera complex was flat mounted and was

imaged using a Zeiss fluorescence microscope (Univision, Carl Zeiss Meditec). The

neovascular area was measured using Scion Image software (version 4.0.2; Scion Corp.).

Statistical analysis

Values are expressed as mean ± SE; statistical analysis was performed using the

Mann-Whitney U test.

Results

ARPE-19 cells secrete a BrM-like matrix

The matrix produced by ARPE-19 cells cultured on transwells for three days and four weeks was examined by transmission electron microscopy. Cells cultured for three days had deposited little matrix, however, after culture for four week, a 0.3-0.4μm thick matrix had accumulated under the basal surface of the cells (Fig. 1A).

ARPE-19 cells cultured for one, two, three and four week were assessed for the levels of mRNA of the BrM components, including collagen I, collagen IV, collagen XVIII, decorin, fibronectin, laminin, tropoelastin, fibrillin-1, TSP-1, PEDF, MMP-7, and cathepsin B. The expression of collagen IV and I peaked at week two where that of decorin and fibronectin begun to increase after two weeks in culture. Of the angiogenesis-related proteins, TSP-1 was maximally expressed at week three whereas PEDF and cathepsin B peaked at week four. Collagen XVIII, tropoelastin, fibrillin-1, and MMP-7 showed constant expression during the four week of culture (Fig. 1B and C).

Heat treatment increases ARPE-19 expression of endostatin, TSP-1, and PEDF

Heat treatment at 43°C for 30 min did not affect the viability of the ARPE-19 cells as detected by immunostaining for markers of apoptosis (Fig. 2). The effect of heat treatment on the levels of TSP-1, PEDF, and endostatin mRNA and protein were examined by real-time

PCR and western blot analysis. TSP-1 mRNA levels were increased significantly 120 min after heat treatment and PEDF mRNA levels were elevated significantly as early as 60 min after heat treatment. Collagen XVIII mRNA levels were unchanged after heat treatment, but the mRNA expression of MMP-7, which cleaves the C-terminal of collagen XVIII to yield endostatin was increased significantly at 15, 60, and 120 min following heat treatment (Fig.3A). The levels of cell-associated protein TSP-1 were increased at 240 min after heat treatment as was the secretion of PEDF and endostatin (Fig. 3B).

Heat treated ARPE-19 cells suppress VEGF induced corneal angiogenesis

RNA and western blot analysis indicated that heat treatment of ARPE-19 cells induced an increase in the production of anti-angiogenic molecules. To investigate whether heat treatment led ARPE-19 cells to become functionally anti-angiogenic, we assayed the effect of heat-treated and control ARPE-19 cells on VEGF-induced angiogenesis using the corneal micropocket assay. The presence of untreated ARPE-19 cells did not affect VEGF-induced corneal angiogenesis; however, the inclusion of heat-treated ARPE-19 cells along with the VEGF pellet in the micropocket led to a nearly 70% reduction in VEGF-induced corneal angiogenesis (Fig.4A).

Media conditioned by heat-treated ARPE-19 suppresses HUVEC migration and proliferation

I   Incubation of HUVEC in media conditioned by untreated ARPE-19 cells led the

endothelial cells to close almost 90 % of a scratch wound in 16 hr.   In constrast, HUVEC

treated with media conditioned by heat-treated ARPE-19 cells closed just over 25 % of the

wound (Fig. 4B). Treatment of HUVEC with media conditioned by heat-treated ARPE-19 cells

led to a modest but statistically significant reduction in HUVEC proliferation relative to cells

treated with media conditioned by untreated ARPE-19 (Fig. 4C).

Heat treatment increased tropoelastin expression by ARPE-19 cells

The effect of heat treatment on the levels of tropoelastin mRNA and protein were

examined by real-time PCR and western blot analysis of cell lysates. Tropoelastin mRNA

levels were increased by 180% at 15 min after heat treatment and the protein levels

increased by 170% at 120 min after heat treatment (Fig. 5A and B).

Elastin suppressed HUVEC migration in a dose dependent manner

Elastin coating did not affect the attachment of HUVECs onto the transwells;

however, HUVEC migration was reduced by about 20 % and 27 % when the transwells were

coated using 100 and 1000 μg/ml of elastin, respectively (Fig. 5C).

Pre-treatment with heat reduced the laser induced CNV

To determine whether pre-treatment with heat would affects laser-induced CNV, the retinas of mice were heated by delivering a series of four IDL spots to the posterior pole of each retina at two disc diameters from the optic nerve, followed placement of a photocoagulation burn in the center of the heat treatment. Laser-induced CNV was visualized and measured in choroidal flat mounts. The mean size of neovascular areas in heat-treated mice was only 15 % of control mice (Fig. 6A).

To determine if heat treatment has any effect on normal retina, IDL irradiated retinal tissues were dissected and examined. The area that had been irradiated by IDL showed no visible structural abnormalities including atrophic change or fibrosis of neural retina, or recruitment of inflammatory cells (Fig. 6B).

Discussion

In mouse, the BrM begins to develop around the 17th day of gestation (15), well after the differentiation of the RPE and the formation of the CC. During the development of BrM, the basement membranes of the RPE and the CC are laid down first, followed by the collagenous layers and finally the inner elastic lamina (15). Studies of human adult BrM reveal no fibroblasts or other cells, except in the extreme periphery (16). These findings suggest that BrM is produced by RPE and/or CC; however, there have been no studies to assess these possibilities.

In this study, we used ARPE-19 cells to determine if RPE can synthesize the various components of BrM. ARPE-19 cells are a well-established line of cells that forms differentiated and polarized monolayers after prolonged (four week) culture on transwells (17). The apical surface of the ARPE-19 cells represents the retina-facing domain, whereas the basal aspect would be the side that apposes the CC. Using these cells, we have demonstrated that RPE cells produce most of the constituents of BrM and that, after four weeks in culture, a significant amount of matrix material is deposited basally. In spite of the fact that the RPE produce a number of specific BrM components, such as tropoelastin and fibrillin, the matrix that was deposited did not display any structure that would be considered characteristic of pentalaminar BrM. We speculate that the appropriate organization of BrM requires the combined contribution of both the RPE and CC, a notion supported by the recent

observation of a lack of a defined BrM in a model of transgenic mice that lack a proper

choriocapillaris network (18).

BrM represents both a functional and structural barrier to growth of new blood vessels

from the CC into the retinal space. Interestingly, the structure of BrM beneath the macula

differs from that under the rest of the retina. Rather than a continuous central elastic layer that

is found under most of the retina, the elastic layer under the macula is discontinuous (8).

Although this specialization presumably facilitates diffusion of oxygen and nutrients to the

metabolically active overlying neural retina it also renders the macula particularly vulnerable

to the development of pathology. The BrM of the patients with early AMD have been

documented to contain decreased levels of endostatin, TSP-1, and PEDF (9, 10, 11), and as

well as fragmentation of elastic layer (8). A comparison of the BrM proteome profile over the

course of AMD revealed that a decreased levels of collagen I alpha1 and fibronectin

precursor (19). A breach in the structural integrity of BrM is permissive for the formation of

new blood vessels. Patients with hypermyopia who suffer lacquer cracks (breaks in outer

retinal layers of macula) frequently develop CNV and a break in BrM always precedes the

development of neovascularization in wet AMD (20). Thus, restoration of the biochemical and

structural integrity of BrM could slow or prevent the progression of CNV.

Motivated by observations that heat treatment of skin can induce the production of

elastin (12), we investigated the possibility that heat treatment of RPE might stimulate their

production of BrM components. Incubation of ARPE-19 at 43°C for 30 min led to the increased expression of endostatin, TSP-1, PEDF, and tropoelastin mRNA and protein. As well as mRNA levels of collagen I alpha 1 and fibronectin (data not shown). Cells exposed to high temperatures (44°C for 4 hr) develop a transient thermal resistance that protects them by inducing or enhancing the synthesis of a set of heat shock proteins (HSPs) (21). HSP70 and HSP27 have been detected in the RPE, and HSP70 is reported to have an important regulatory role in the protein turnover of human RPE cells (22, 23). Thus, induction of HSP may mediate some of the observed effects of heat on ARPE-19 cells.

Induction of ARPE-19 cells that had been treated with heat blocked VEGF-induced angiogenesis in the corneal pocket assay whereas the presence of untreated ARPE-19 cells had no effect. Similarly, media conditioned by heat-treated ARPE-19 cells significantly blocked endothelial cell migration in a wound closure assay. Among the anti-angiogenic agents that were examined, endostatin showed the most prominent heat-induced increase. This observation is consistent with a report that the anti-angiogenic effects of endostatin are likely due to its potent inhibition of migration (24).

Motivated by the results of our in vitro studies, we tested the effect of heat treatment on new vessel growth in the retina by subjecting the retina to topical heat treatment with IDL. IDL has been previously examined for the treatment of AMD by targeting new vessels as a transpupillary thermotherapy (TTT). Although its safety was proven and there were some

reports of positive effect, results of a multicenter TTT4CNV trial did not show benefit (25). TTT

has also been previously used in early AMD with the goal of activating RPE phagocytosis of

drusen. However, this approach did not reduce progression to wet AMD (26). The treatment

regime used in these prior studies includes 48 shots of TTT with a beam diameter of 125 µm

and with power settings of 50 mW or more for 0.1 sec. The treatment utilized here consisted

of four applications of laser light (modified TTT) with a beam diameter of 1.2mm and with

power setting of 50mW for 60sec. Though the previous studies used a similar power level,

the spot diameter was one-tenth the size. With a smaller diameter, the energy per unit area

increases, very likely destroying the RPE and causing acute inflammation. Such tissue

damage does not occur with the treatment protocol employed in our study. In contrast to

these early applications where new vessels themselves were targeted and/or very high levels

of treatment were applied, our goal was to use pretreatment with heat to restore/increase BrM

barrier functions by using mild heat to stimulate RPE cells to produce components of BrM.

Our results revealed that pretreatment with heat, or modified TTT, blocked the formation of

laser-induced CNV.

Though it is clear that the normal BrM provides a biochemical and physical barrier

against CNV, there have been no reports regarding the regeneration of BrM as an approach

for the management for AMD. Results of our in vitro and in vivo observations demonstrate

that heat treatment may provide a means to restore BrM integrity and its barrier functions

against CNV and suggest that a form of TTT may be used to prevent the development of

CNV in patients who are at high risk, such those as with neovascular AMD in a fellow eye.

References

1. West S.K. (2000) Looking forward to 20/20: a focus on the epidemiology of eye diseases. *Epidemiol Rev*. 22, 64-70

2. Roth J.M., Akalu A., Zelmanovich A., Policarpio D., Ng B., MacDonald S., Formenti S., Liebes L., Brooks P.C. (2005) Recombinant alpha2(IV)NC1 domain inhibits tumor cell-extracellular matrix interactions, induces cellular senescence, and inhibits tumor growth in vivo. *Am J Pathol*. 166, 901-911.

3. Maeshima Y., Colorado P.C., Torre A., Holthaus K.A., Grunkemeyer J.A., Ericksen M.B., Hopfer H., Xiao Y., Stillman I.E., Kalluri R. (2005) Distinct antitumor properties of a type IV collagen domain derived from basement membrane. *J Biol Chem*. 275, 21340-21348.

4. Mitola S., Brenchio B., Piccinini M., Tertoolen L., Zammataro L., Breier G., Rinaudo M.T., den Hertog J., Arese M., Bussolino F. (2006) Circulation Res. Type I collagen limits VEGFR-2 signaling by a SHP2 protein-tyrosine phosphatase-dependent mechanism 1. *Circ Res*. 98, 45-54.

5. Cockburn C.G., Barnes M.J. (1991) Characterization of thrombospondin binding to collagen (type I) fibres: role of collagen telopeptides. *Matrix*. 11, 168-176.

6. Marneros A.G., She H., Zambarakji H., Hashizume H., Connolly E.J., Kim I., Gragoudas E.S., Miller J.W., Olsen B.R. (2007) Endogenous endostatin inhibits

choroidal neovascularization. *FASEB J*. 21, 3809-3818.

7. Yu H.G., Liu X., Kiss S., Connolly E., Gragoudas E.S., Michaud N.A., Bulgakov O.V., Adamian M., DeAngelis M.M., Miller J.W., Li T., Kim I.K. (2008) Increased choroidal neovascularization following laser induction in mice lacking lysyl oxidase-like 1. *Invest Ophthalmol Vis Sci*. 49, 2599-2605.

8. Chong N.H, Keonin J., Luthert P.J., Frennesson C.I., Weingeist D.M., Wolf R.L., Mullins R.F., Hageman G.S. (2005) Decreased thickness and integrity of the macular elastic layer of Bruch's membrane correspond to the distribution of lesions associated with age-related macular degeneration. *Am J Pathol*. 166, 241-251.

9. Bhutto I.A., Uno K., Merges C., Zhang L., McLeod D.S., Lutty G.A. (2008) Reduction of endogenous angiogenesis inhibitors in Bruch's membrane of the submacular region in eyes with age-related macular degeneration. *Arch Ophthalmol*. 126, 670-678.

10. Bhutto I.A., Kim S.Y., McLeod D.S., Merges C., Fukai N., Olsen B.R., Lutty G.A. (2004) Localization of collagen XVIII and the endostatin portion of collagen XVIII in aged human control eyes and eyes with age-related macular degeneration. *Invest Ophthalmol Vis Sci*. 45, 1544-1552.

11. Uno K., Bhutto I.A., McLeod D.S., Merges C., Lutty G.A. (2006) Impaired

expression of thrombospondin-1 in eyes with age related macular degeneration.

Br J Ophtalmol. 90, 48-54.

12. Chen Z., Seo J.Y., Kim Y.K., Lee S.R., Kim K.H., Cho K.H., Eun H.C., Chung J.H.

(2005) Heat modulation of tropoelastin, fibrillin-1, and matrix metalloproteinase-12

in human skin in vivo. *Invest Dermatol*. 124, 70-78.

13. Kang J.H., Kim S.A., Hong K.J. (2006) Induction of TSP1 gene expression by heat

shock is mediated via an increase in mRNA stability. *FASEB Lett*. 580,

510-516.

14. Nakao S., Hata Y., Mimura M., Noda K., Kimura Y.N., Kawahara S., Kita T.,

Hisatomi T., Nakazawa T., Jin Y., Dana M.R., Kuwano M., Ono M., Ishibashi T.,

Hafezi-Moghadam A. (2007) Dexamethasone inhibits interleukin-1beta-induced

corneal neovascularization: role of nuclear factor-kappaB-activated stromal cells

in inflammatory angiogenesis. *Am J Pathol*. 171, 10581065.

15. Hirabayashi Y., Fujimori O., Shimizu S. (2003) Bruch's membrane of the

brachymorphic mouse. *Med Electron Microsc*. 36, 139-146.

16. Wolter J.R. (1955) Histologic character of connection between Bruch's membrane

and choriocapillaris of human eye; a study with silver carbonate technique. *AMA

Arch Ophthalmol*. 53, 208-210.

17. Dunn K.C., Aotaki-Keen A.E., Putkey F.R., Hjelmeland L.M. (1996) ARPE-19, a human retinal pigment epithelial cell line with differentiated properties. *Exp Eye Res*. 62, 155-169.

18. Marneros A.G., Fan J., Yokoyama Y., Gerber H.P., Ferrara N., Crouch R.K., Olsen B.R. (2005) Vascular endothelial growth factor expression in the retinal pigment epithelium is essential for choriocapillaris development and visual function. *Am J Pathol*. 167. 1451-1459.

19. School S., Bode E., Tezel T.H. (2008) Bruch's membrane proteome reveals specific changes in age-related macular degeneration (AMD). *Invest Ophthalmol Vis Sci.* 49, E-Abstract 1750.

20. Avila M.P., Weiter J.J., Jalkh A.E., Trempe C.L., Pruett R.C., Schepens C.L. (1984) Natural history of choroidal neovascularization in degenerative myopia. Ophthalmology. 91. 1573-1581.

21. Landry J., Chrétien P., Lambert H., Hickey E., Weber L.A. (1989) Heat shock resistance conferred by expression of the human HSP27 gene in rodent cells. *J Cell Biol*. 109, 7-15.

22. Ryhänen T., Hyttinen J.M., Kopitz J., Rilla K., Kuusisto E., Mannermaa E., Viiri J., Holmberg CI., Immonen I., Meri S., Parkkinen J., Eskelinen E.L., Uusitalo H., Salminen A., Kaarniranta K.   (2008) Crosstalk between Hsp70 molecular

chaperone, lysosomes and proteasomes in autophagy-mediated proteolysis in human retinal pigment epithelial cells. *J Cell Mol Med*. Epub ahead of print.

23. Strunnikova N., Baffi J., Gonzalez A., Silk W., Cousins S.W., Csaky K.G. (2001) Regulated heat shock protein 27 expression in human retinal pigment epithelium. *Invest Ophthalmol Vis Sci.* 42, 2130-2138.

24. Taddei L., Chiarugi P., Brogelli L., Cirri P., Magnelli L., Raugei G., Ziche M., Granger H.J., Chiarugi V., Ramponi G. (1999) Inhibitory effect of full-length human endostatin on in vitro angiogenesis. *Biochem Biophys Res Commun*. 263, 340-345.

25. Reichel E., Musch D.C., Blodi B.A., Mainster M.A., and TTT4CNV Study Group. (2005) Results From the TTT4CNV Clinical Trial *Invest Ophthalmol Vis Sci*. 46, E-Abstract 2311

26. Owens S.L., Bunce C., Brannon A.J., Xing W., Chisholm I.H., Gross M., Guymer R.H., Holz F.G., Bird A.C., and Drusen Laser Study Group. (2006) Prophylactic laser treatment hastens choroidal neovascularization in unilateral age-related maculopathy: final results of the drusen laser study. *Am J Ophthalmol.* 141, 276-281.

A
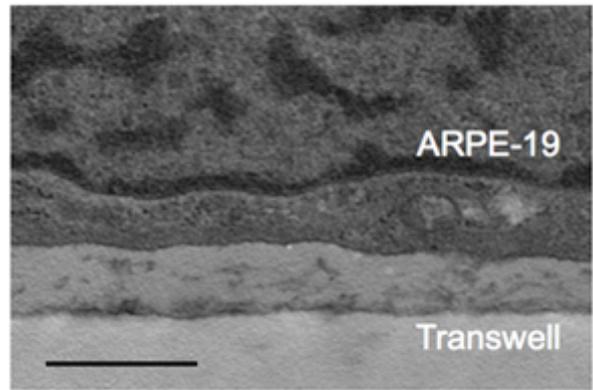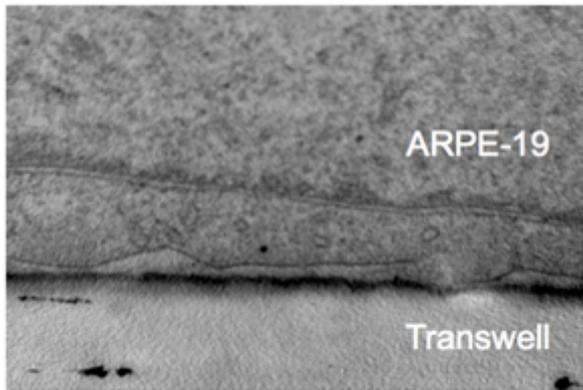
B
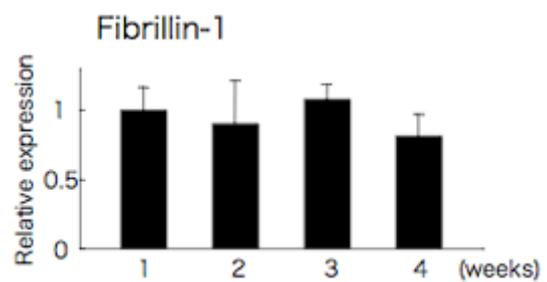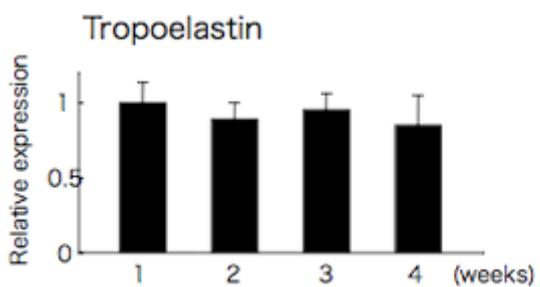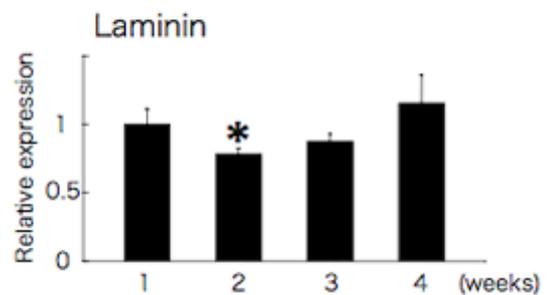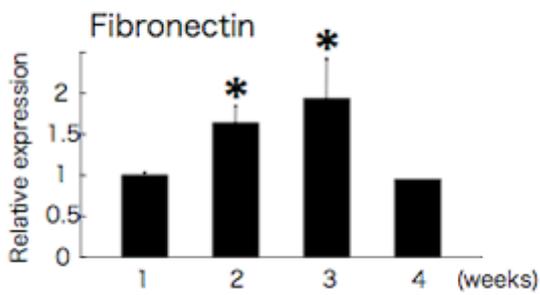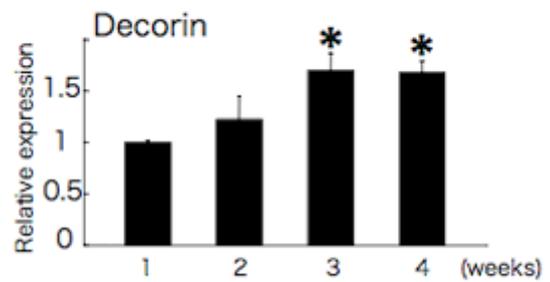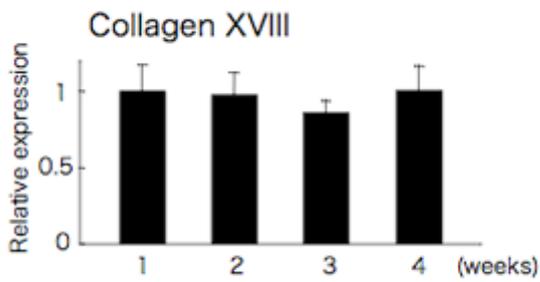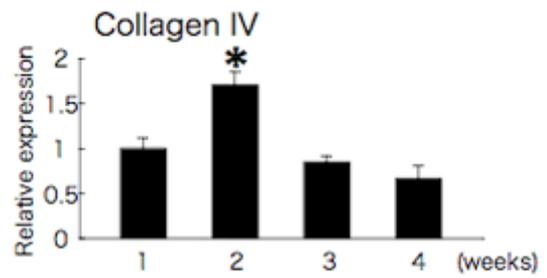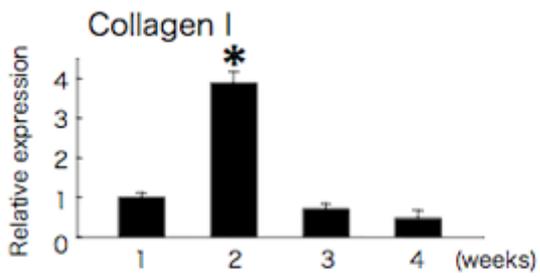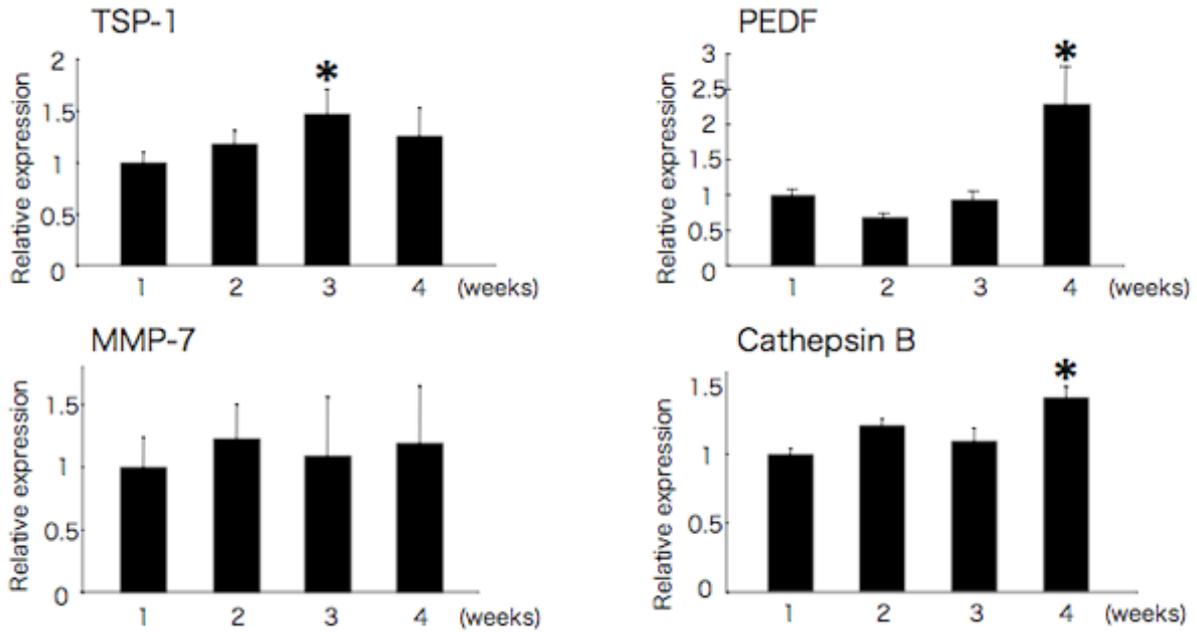
Figure 1. Differentiated ARPE-19 cells secrete components of the BrM.

(A) Transmission electron microscopic examination of ARPE-19 cells after three days and four weeks of culture. Dashed white dash line shows the accumulation of extracellular matrix under the cells. Scale bar = 0.5µm. (B) Real-time PCR analysis of BrM components during ARPE-19 cell differentiation. (C) Real-time PCR analysis of angiogenesis related factors during ARPE-19 cell differentiation. Values are means ± SE (n=3).
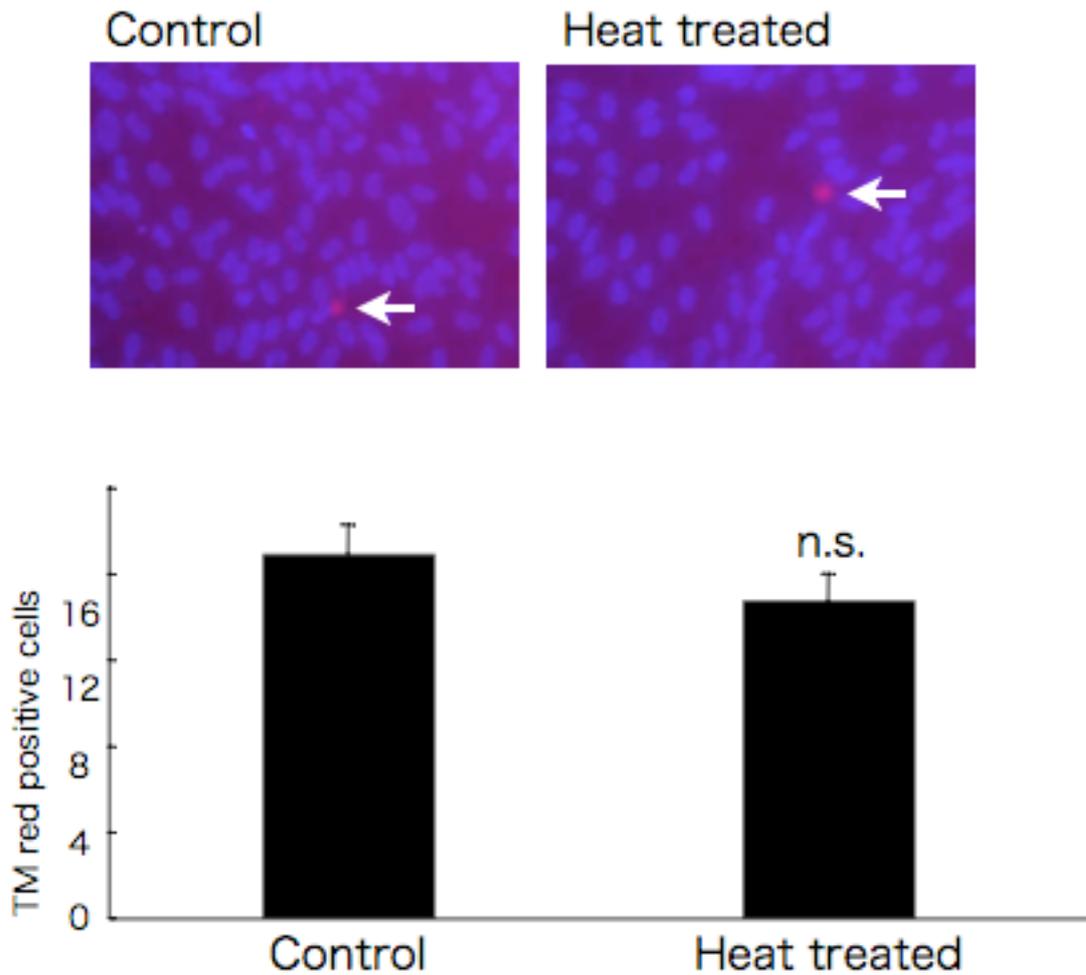
Figure 2. Heat treatment does not affect the viability of ARPE-19 cells.

(A) Representative micrographs of untreated and heat-treated ARPE-19 cells three days after heat treatment at 43°C for 30 min. White arrows indicate apoptotic bodies stained with TMR red. (B) Quantification of the number of apoptotic bodies. Values are means ± SE. Four random fields were chosen from three culture wells.
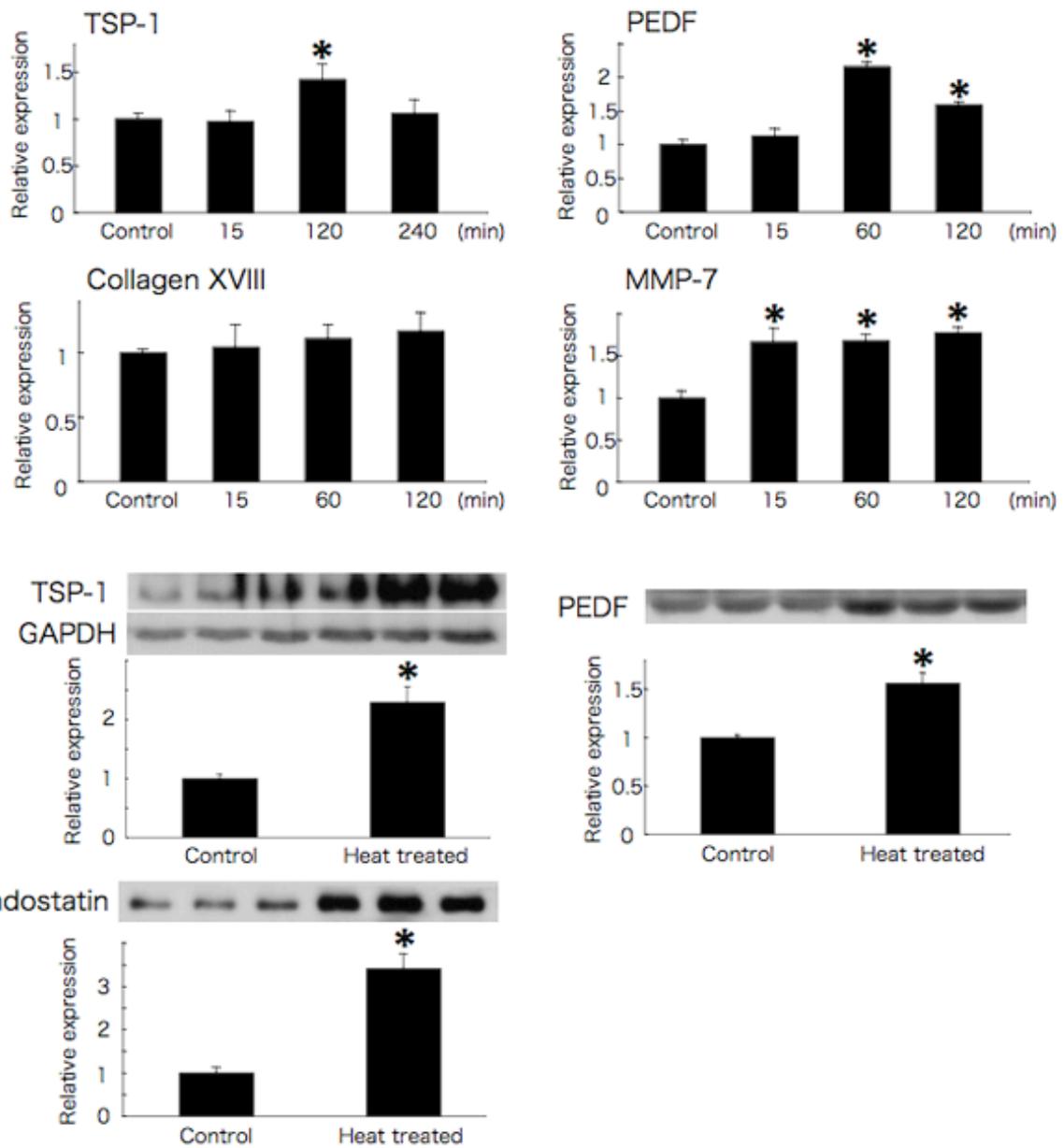
Figure 3. Heat treatment increases TSP-1, PEDF, and endostatin expression by ARPE-19 cells.

(A) Expression of TSP-1, PEDF, collagen XVIII, and MMP-7 mRNA by ARPE-19 cells at 15, 60, 120, and 240 min after heat treatment at 43°C for 30 min. (B) Expression of TSP-1, PEDF, and endostatin protein at 240 min after heat treatment at 43°C for 30 min. Values are means ± SE (n=3).

A
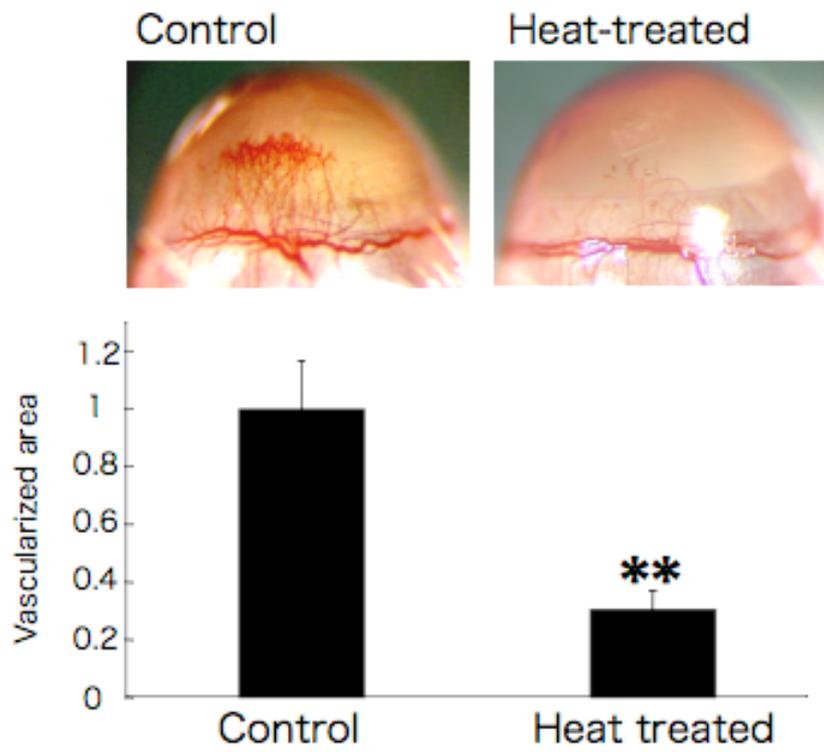
B
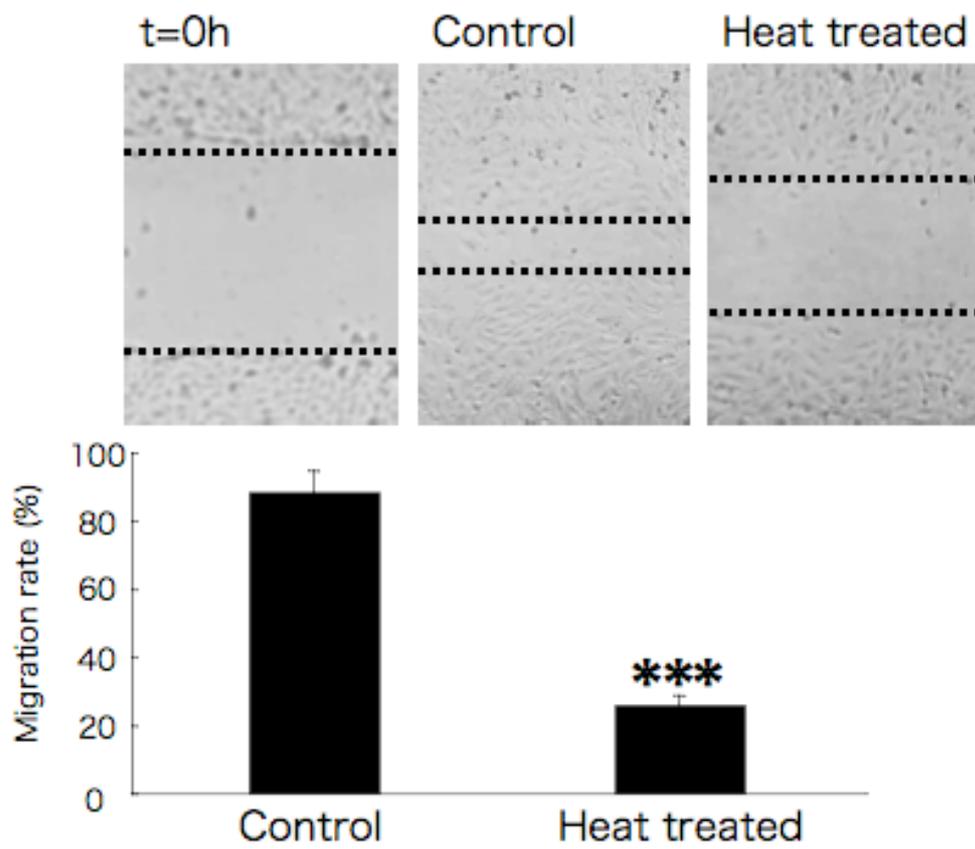
C
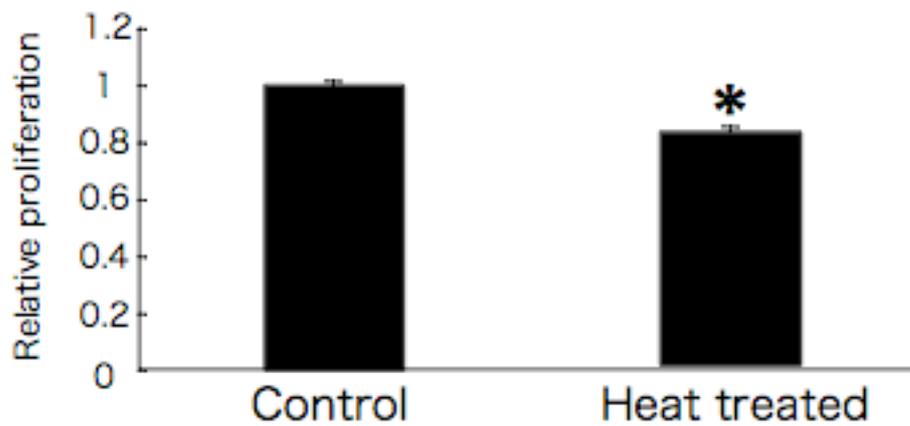
Figure 4. Heat treatment induces ARPE-19 cells to become anti-angiogenic.

(A) Representative micrographs of corneal neovascularization taken six days after implantation of untreated or heat-treated ARPE-19 cells with VEGF containing pellet. Vascularized area was measured and quantified. Values are means ± SE (n=6 and 10, respectively). (B) Representative micrographs of HUVECs taken sixteen hr after a scratch wound. Cells were cultured with the media conditioned by untreated or heat-treated ARPE-19 cells. The width of the wound was measured and quantified as a measure of HUVECs migration. Values are means ± SE. (C) Proliferation of HUVECs cultured with the media conditioned by untreated or heat-treated ARPE-19 cells. HUVECs were cultured for three days and proliferation was evaluated by direct cell count on trypsin-detached cells with a hemocytometer. Values are means ± SE (n=3).
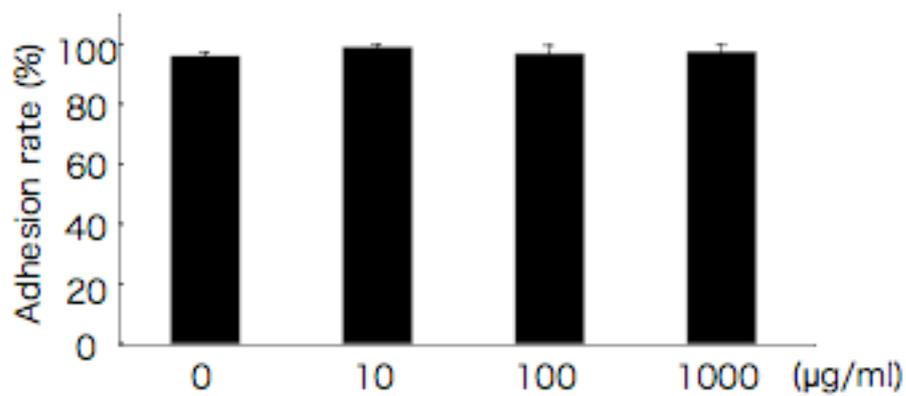
A

Tropoelastin

B
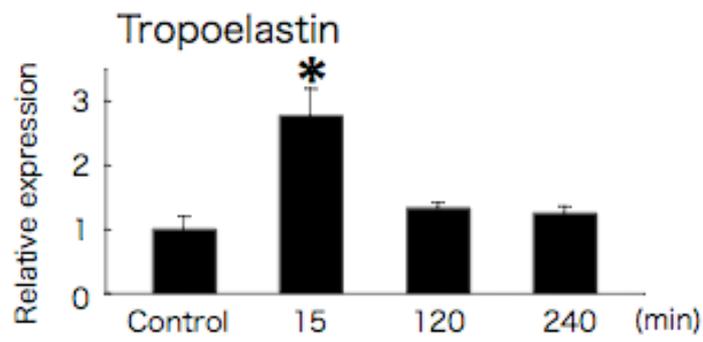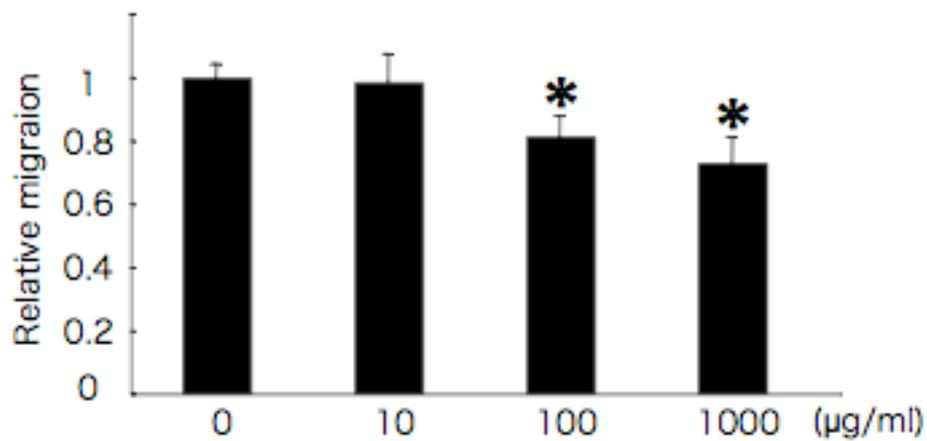
Tropoelastin
GAPDH
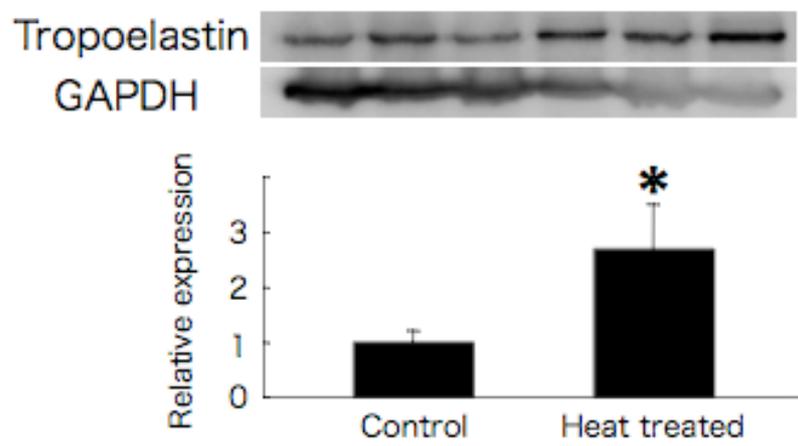
C

D

Figure 5. Heat treatment increases tropoelastin expression by ARPE-19 cells.

(A) Expression of tropoelastin mRNA by ARPE-19 cells 15, 120, and 240 min after heat treatment at 43°C for 30 min. (B) Expression of tropoelastin protein 120 min after treatment at 43°C for 30 min. Values are means ± SE (n=3). (C) Adhesion of HUVECs seeded on the elastin-coated transwells. Two hr after cell plating, the adhesion of HUVECs was determined by counting the number of unattached cells with a hemocytometer. Values are means ± SE (n=3). (D) Effect of elastin on migration of HUVECs. Fourteen hr after cell plating, cells that had not migrated were removed by gentle scraping and those that had migrated through to the bottom of the transwell were counted. Values are means ± SE (n=3).
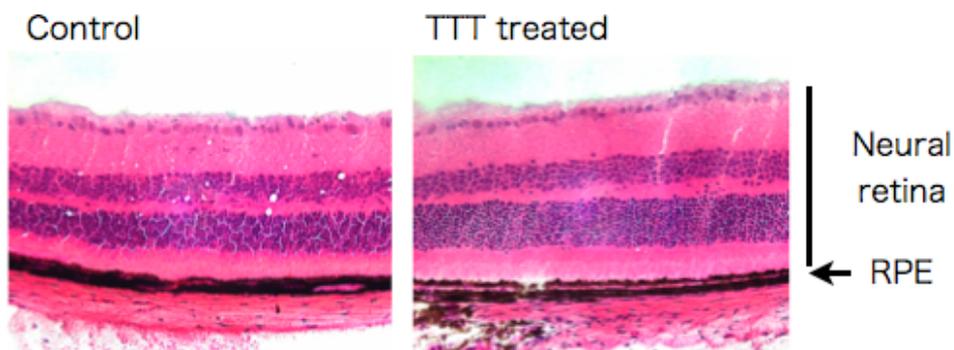
A
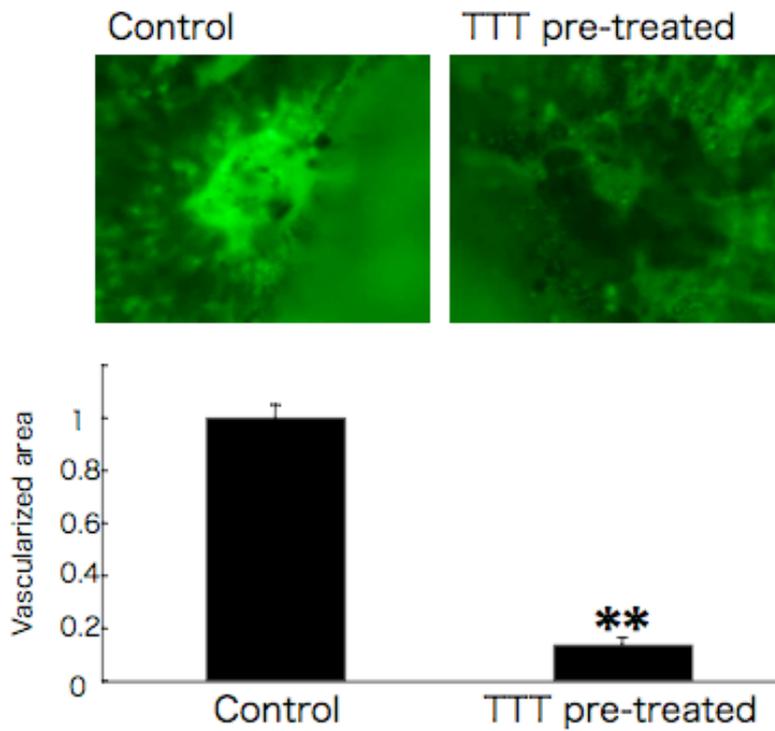
B

Figure 6. Pretreatment of the retina with heat reduced CNV in vivo without causing tissue damage.

(A) Representative micrographs of PC-induced CNV in retinas with no pretreatment and in retina that had been pretreated with TTT. CNV was visualized in choroidal flat mounts by fluorescein angiography. Hyperfluorescent areas were quantified. Values are means ± SE (n=6). (B) Untreated and TTT treated mouse retina. Fourteen days after TTT treatment, mouse retina was sectioned, and stained with hematoxylin and eosin